12-18-2016

Design and Realization of a Nonlinear Vibration Energy Harvester for Cost Effective Additive Manufacturing

Rodrigo Barriuso de Juan
Grand Valley State University

Design and realization of a nonlinear vibration energy harvester for cost effective additive manufacturing

Rodrigo Barriuso de Juan

A Thesis Submitted to the Graduate Faculty of

GRAND VALLEY STATE UNIVERSITY

In

Partial Fulfillment of the Requirements

For the Degree of

Master of Science in Engineering

School of Engineering

December 2016

Acknowledgements

This thesis work is the result of a hard year's work. The positive outcome of this effort wouldn`t have been possible without the continuous help, tips, and corrections from my advisor Dr. Nael Barakat. Thanking you is the least I can do for all your support and assistance. Whenever I became lost or frustrated along the way you were always there to get me back on the correct path. I would also like to thank Dr. Eihab Abdel-Rahman for letting me test his prototype of vibration energy harvesting and for his immense experience regarding energy harvesting. Without his technical help this thesis would be just numbers and letters without connection. I would also like to thank Dr. Jiao for becoming a member of my thesis committee. The realization of this thesis work also would not have been possible without the aid of Ryan Aldridge and his incommensurable experience with 3D printing. Together we have learnt and improved our knowledge of 3D printing materials and techniques. I would finally like to thank all the professors at Grand Valley because all of them have in greater or lesser manner been involved in this thesis, with opinions, ideas, and support.

Abstract

Environmental energy harvesting has always been an attractive solution to the search for sustainable energy sources. Combined with the miniaturization and power consumption reduction of sensors and portable electronic devices, the possibility of powering using environmental energy, like vibration energy, instead of conventional batteries increases exponentially. Vibrational energy harvesting can be achieved using devices based on different physical phenomena. Electromagnetic based devices seem to be among the most effective when considering the power output levels within low frequency applications. However, these devices have always had inherent challenges including size and manufacturing cost reduction as well as limitations on the range of effective harvesting frequencies. The purpose of this thesis is to improve the design and manufacturing of an existing electromagnetic energy harvester, while maintaining comparable output power and range of effective harvesting frequency of the new harvester. The improved harvester is designed to maintain functionality based on nonlinear dynamics of an impact oscillator, which increases the effective range of harvesting frequency. This harvester is also designed to be manufactured using additive manufacturing techniques, which reduces the manufacturing cost and time significantly.

To achieve this purpose, the design of a fully metallic vibration energy harvester made by a partner group in the University of Waterloo was used as the starting point. The new harvester was redesigned for manufacturing using 3D printing technology as the rapid prototyping manufacturing process. This technology was implemented using the most cost effective material and equipment possible. Three consecutive iterations of the new harvester were produced including multiple versions of each iteration. These iterations presented the

gradual improvement in design and manufacturing of the new harvester to overcome technical challenges while maintaining comparable performance levels. Iteration 1 was the baseline, process verification iteration, which included replacing the base of the original harvester with a redesigned and 3D printed base. In the second iteration the mechanism used to obtain the linear displacement of the seismic mass with respect to a fixed structure of the harvester was redesigned and 3D printed. The final iteration produced a fully 3D printed electromagnetic energy harvester for the first time. This new harvester was founded on the same displacement and generation nonlinear dynamic principles as the original metallic harvester with improvements in the design and material of the structure, as well as the selected components and mass of the harvester.

In spite of all the manufacturing challenges, iteration number 1 achieved a maximum output voltage of 138mV using a 76g metallic seismic mass, which was considered as the baseline for performance measurements. The price of the harvester base was reduced from $111.26 considering a metallic base to $28.16 with a 3D printed base. Iteration number 2 achieved a 78% output voltage compared to iteration number 1 with a cost reduction of 18.84%. Iteration number 3 achieved almost 50% maximum output voltage compared to iteration number 1 with a cost reduction of around 73% but remarkably with a seismic mass reduction of 65%.

The consecutive reductions of mass and cost of the springless vibration energy harvester with less proportional reduction in produced energy brings closer the possibility of further implementation of energy harvesters in daily applications including consumer products and education applications. The reduction in output voltage is linked to the type and quality of material used in 3D printing causing higher friction rates beside the reduction in

seismic mass. Understanding these factors opens many possibilities for future work to improve the output of 3D printed magnetic-based energy harvesters even farther.

Table of Contents

List of Figures

List of Tables

1. Introduction

Energy harvesting, or energy scavenging, is the process of collection and transformation of environmental energy into electrical energy for storage or direct use. There are several types of environmental energy that can be harvested such as wind, solar, electromagnetic, chemical, hydraulic, thermal and vibrational energy.

Energy harvesting is an important technological development that can replace existing non-sustainable sources, with a sustainable source of energy, particularly in applications where the amount of power required is small and where the accessibility for battery replacement is difficult or impossible. In summary there are three main advantages, among many others, of energy harvesters compared to batteries, which are [1]:

1. No need for replacement (finite battery life).
2. Clean life cycle, no pollution.
3. Disposal, no recycling needed.

Vibrational energy, or energy present in mechanical vibrations, is a viable source for harvesting that is associated with any type of motion. Examples where mechanical vibrations are usually present include vehicle suspension systems [2] or engines [3, 4], ocean waves [5], buildings [6] (vibrations generated by wind or earthquakes), bridges [7, 8] (vibrations induced by wind or traffic), roads (vibrations generated by traffic), offshore structures (vibrations generated by waves), human body (walking and running [9], arm or hand shaking [10, 11] or breathing [12]), and windmills.

2. Problem Statement

This applied research aims at toggling two major challenges related to electromagnetic based, vibration energy harvesting devices. The first challenge stems from the inherent limitation on the range of effective vibration frequency for energy harvesting. Literature shows that energy can be effectively harvested when ambient vibrations are in match with the resonance vibration of the harvesting device. This inherent property results in significant limitations on the effectiveness of vibration energy harvesters. This applied research work aims at implementing the nonlinear phenomenon of impact oscillators to expand the effective frequency band for energy harvesting, beyond a single resonance frequency.

The second challenge stems from the fact that implementing nonlinear vibration energy harvesters is still in its early development stages resulting in high cost and manufacturing challenges. This work aims at designing a nonlinear vibration energy harvester for additive manufacturing using cost effective means. Namely, 3D printing is implemented using a low-end printer and commonly available material to toggle this part of the problem.

3. Literature Review

3.1. Vibration Energy Harvesting Method Classification

Vibration energy harvesting can be classified based on the energy transformation methodology from mechanical (vibrations) to electrical energy. Recent studies have also attempted investigating the possibility of using hybrid mechanisms such as the combination of more than one of these methods [13, 14]. There are four principal methods for vibration energy harvesting as follows:

1. Electromagnetic: Electromagnetic energy harvesting is based upon Faraday's law. This law establishes that "an electrical current will be induced in any closed circuit when the magnetic flux through a surface bounded by the conductor changes". In this type of harvesters a magnetic mass normally displaces around a conductor coil modifying the magnetic flux and therefore generating electrical current. This method has become very interesting because of the possibility of harvesting in the low frequency range [15, 16].
2. Piezoelectric: Piezoelectric harvesters use the intrinsic properties of piezoelectric materials to transform mechanical strains into electrical currents. Generally used piezoelectric materials are crystals such as Quartz (SiO_2) and piezoceramics such as Lead Zirconate Titanate (PZT). These harvesters normally present one or multiple cantilever beams with a layer of piezoelectric material on top of it. The vibrations of the beam (produced by ambient vibrations) generate an electrical current in the piezoelectric material that can be used a posteriori [17].
3. Electrostatic: Electrostatic harvesters produce energy when two conductive plates are moving relative to each other in the presence of an electrically isolated medium forming a

capacitor. The two ways of converting energy from an electrostatic energy harvester are referred to as either charge (of the capacitor) constrained or voltage constrained [17].

4. Magnetostrictive: This type of harvesters uses the special properties of magnetostrictive materials (small ferromagnets of iron, nickel or cobalt, Terfenol-D and Metglass [18]). The application of a mechanical force in a magnetostrictive material generates an electromagnetic field that can be transformed into electrical energy with the presence of a conductive coil.

A comparison between these methods outlining their advantages and disadvantages is presented in Table 1 [19, 20].

Table 1: Comparison showing the advantages and disadvantages of vibrations energy harvesting methods [19, 20]

Method	Advantages	Disadvantages
Electromagnetic	• Large output current • High output power • High energy conversion efficiency • Low frequency energy conversion • Multiple architectural options • MEMS manufacturing compatible processes for planar coil/planar spring • Relatively low output impedance	• Large volume of magnetic circuits • Small working air-gap magnetic field strength • Extra components • Low output voltage levels • Voltage rectification required
Piezoelectric	• MEMS manufacturing compatible processes • High output voltage levels • Easy voltage rectification	• Few device architecture options (normally cantilever beams) • Piezoelectric materials are stiff and brittle. • Piezoelectric materials limit the application to low g environments • Relatively low energy conversion efficiency • High output impedance • Low output electrical current levels
Electrostatic	• High output voltage • Easy voltage rectification • MEMS manufacturing compatible processes	• External voltage source needed • High resonance frequencies • High output impedance • Low output electrical current levels
Magnetostrictive	• High energy conversion efficiency • Suited to high frequency vibration	• Difficult to integrate with MEMS • Non-linear effect

3.2. Vibration Energy Harvesting Applications

Vibration energy harvesters (VEH) have multiple applications and their use continues to expand. However, they all share the common factor of being low consumption applications. This characteristic might be one of the most limiting aspects of energy harvesting in general and an impediment to globally implement this technology as the energy source of the future. In general, the amount of energy that can be obtained with these devices fluctuates in between the orders of magnitude of mW and μW. Table 2 presents several vibration energy harvesters reported in the literature and their power output [21].

Table 2: Vibration energy harvesters and power output

References	Volume (cm^3)	Frequency (Hz)	Amplitude (m/s^2)	Power (W)	Power density (W/cm^3)
Glynne-Jones et al. (2000)	0.84	322	2.7	1.80E−04	2.14E−04
Williams et al. (2001)	0.0054	4,400	382	3.00E−07	5.56E−05
Ching et al. (2002)	1	110	95.5	8.30E−04	8.30E−04
Beeby et al. (2007)	0.15	52	0.589	4.60E−05	3.07E−04
Wang et al. (2009)	3.15	280	10	1.72E−05	5.46E−06
Domme (2008)	112	16	3.74	5.50E−03	4.91E−05
Saha et al. (2008)	12.5	8	0.38	1.50E−03	1.20E−04
Hoffmann et al. (2009)	0.68	390	88.29	5.00E−06	7.35E−06
Hadas et al. (2010)	100.9	17	4.9	5.00E−03	4.96E−05

Even with this impediment, applications are broadening everyday and will continue growing in the future in consonance with the trends of constant reduction of power consumption and the miniaturization in sensors and electric components using micro electromechanical systems (MEMS) technology. These aspects combined with the evolution of “The Internet of Things”, “Smart Things” and “Smart Cities” has pushed energy harvesting towards a new era. Economic viability will also play a significant role in advancing this technology, as manufacturing harvesters and bringing them in the hands of consumers becomes affordable to the point of competing with disposable batteries

Some applications of vibration energy harvesters include mainly the powering sensors, actuators, low energy consumption devices, and Wireless Sensors Networks (WSNs). A WSN consists of multiple stations called sensor nodes that can both transmit and receive information related to the type of sensor that they include. The communication between the sensor nodes and a central computer is done wirelessly and powered by a battery or an energy harvester.

Other applications for VEHs include:

- Biomedical implantable devices: hearing aid [21], body implants, pacemakers, defibrillators [21] and medical remote sensing.
- Portable electronics: portable phones, smart watches [10, 11], personal health bracelets and portable music players.
- Rotating objects: hydroelectric generators, steam driven generators or air driven turbines [3, 22].
- Inside liquids: plastic or concrete structures [3].
- Home automation systems: environment control in offices and homes, home appliances [20].
- Structural health monitoring: bridges [7, 8], roads, wind turbine blades [22], buildings and plant machinery.
- Transportation: tire pressure monitoring [23], engine temperature, driving aid systems, suspension systems [2] or GPS.
- Environmental monitoring: pollution in fields and forest fires [24].
- Data transmission: WSNs [13] and radio.
- Security and surveillance: microrobotic drones [1].

- Military and aerospace: aircraft [25], satellite or missiles health monitoring and energy harvesting in space applications (International Space Station, ISS).
- Sensors and actuators: temperature, accelerometers [26], mass dampers [6].

Table 3 presents a list of sensors including their power consumption. Notice that due to their low power consumption, they are all in the range of microwatts, so they could be powered using a vibration energy harvester.

Table 3: Commercial sensors and power consumption

Sensor type	Company	Model type	Voltage (V)	Current (μA)	Standby current (μA)	Calculated power (P = VI) (μW)
Pressure	Measurement Specialties	MS5607-B	1.8	1	0.15	1.8
	BOSCH	BMPO85	1.8	3	n.r.	5.4
	VIT Technologies	SCP1000	2.4	3.5	0.2	8.4
	Sensonor	SP300 (pressure mode)	2.1	4	n.r.	8.4
Temperature	Sensonor	SP300 (temperature mode)	2.1	0.9	n.r.	1.89
	STMicroelectronics	STLM20	2.4	4.8	0.02	11.52
	Fairchild Semiconductor	FM20	2.4	9	n.r.	21.6
	Andigilog sensors Inc.	TS10	2.4	12	n.r.	28.8
	Andigilog sensors Inc.	aSM121 (SiMISTOR ™)	2.7	14	n.r.	37.8
Acceleration (3-axis)	STMicroelectronics	LIS331DLH (0.5 Hz to 1 kHz)	2.16	10	1	21.6
	Analog Devices Inc.	ADXL346 (0.1 Hz–3.2 kHz)	1.7	23	0.2	39.1
	VTI Technologies	CMA3000-D01 (340–460 Hz)	1.7	70	4	119
	Kionix Inc.	KXSD9-1026 (15 Hz to 2 kHz)	1.8	120	0.3	216
	VTI Technologies	SCA3000-E05 (7–100 Hz)	2.5	120	n.r.	300
	Analog Devices Inc.	ADXL330 (0.5 Hz–1.6 kHz)	1.8	180	n.r.	324

n.r. not reported in the data sheet provided by the manufacturer

3.3. Common Problems in Energy Harvesting

Vibration energy harvesters can scavenge a high amount of energy when the ambient vibrations have frequencies matching the resonance frequency of the harvester. However, with minor deviations away from this resonance frequency, the energy that can be harvested is critically reduced rendering the harvester ineffective. This is one of the biggest limits of this technology and also one of the topics under constant improvement. Multiple solutions have been suggested to solve this problem including:

1. Modifying the resonance frequency of the harvester in-situ (active or passive tuning). This method can be divided into three categories: mechanical, magnetic and piezoelectric [27]. The main objective of this technique is to modify the stiffness of the system, and therefore the resonance frequency. Different methods of tuning include electrical tuning using a generalized load (a capacitance in parallel with a resistance) [16], load resistance adjustment [28], power electronics [29] or a rotatable spring (to adjust the spring constant) [30]. The inconvenience of these methods is that active tuning normally requires the presence of an external power source while passive tuning is not self-implementable requiring re-adjustment after every test.
2. Increasing the range of resonance frequencies of the harvester. To increase the number of resonance frequencies of a harvester (multimodal energy harvesting), solutions suggesting multiple cantilever beams with different resonance frequencies or exploiting multiple bending modes of a continuous beam have been proposed. If the multiple resonance frequencies are all in a close range, this method would allow obtaining a quasi-continuous frequency harvesting. If on the other hand the resonance frequencies are disperse, they can be tuned to the multiple resonance frequencies of the application. This improvement in the amount of resonance frequencies negatively affects the system complexity [27].
3. Increasing the frequencies at which a considerable amount of energy is obtained, which is also known as increasing the usable frequency range or bandwidth. To widen the harvesting bandwidth, nonlinear energy harvesting is proposed as potential solution. The nonlinearities of the system are employed as desired characteristics that allow harvesting energy in wider intervals of frequency and not only around the

resonance frequency of the application. There are two types of nonlinearities known as hardening [31] and softening [32]. The first is characterized by output improvement when the device resonance approaches a higher frequency (the resonance curve shifts towards the right). The second will show an output improvement when the device resonance approaches a lower frequency (the resonance curve shifts towards the left). Figure 1 shows the general frequency response curve shape in both hardening and softening effects.

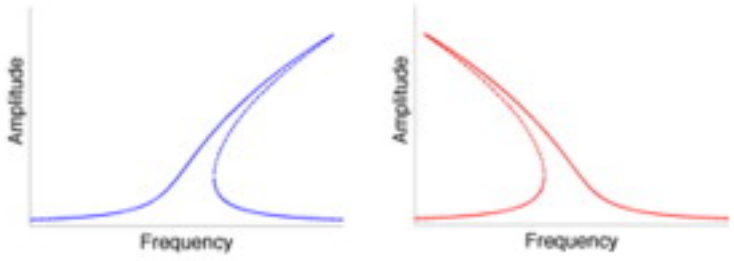

Figure 1: Hardening (left) and softening (right) nonlinearities [33]

Adding nonlinearities to a system can cause vital improvement in applications with unknown resonance frequencies and a small frequency interval like human body vibrations (range of frequencies from 1 to 10Hz and aperiodic). Nonlinearities can be generated using different methods including: mechanical stoppers [32], nonlinear springs [34], and nonlinear magnetic springs [10, 35].

3.4. Electromagnetic Vibration Energy Harvesting Evolution

Throughout the historical evolution of the electromagnetic vibration energy harvesters (EVEH), numerous shapes and sizes have been proposed to overcome their main challenge of being bulky and relatively requiring space. The current tendency is moving towards the miniaturization of harvesters and so multiple recent studies have concentrated on planar

EVEH [31, 36, 37, 38], cubic [39], cylindrical [21] and spherical forms with the purpose of reducing the size while at the same time increasing the harvested power density. Smaller harvesters with higher energy levels would proliferate the possible application for these devices, whereas high scale EVEH would present lesser uses.

As a consequence, manufacturing processes of these harvesters have evolved in parallel with the size drop. Micro Electromechanical Systems (MEMS) manufacturing methods have been increasingly applied [31, 36, 37], as well as processes like: 3D printing [24], Printed Circuit Board (PCB) [13], Flexible Printed Circuit (FPC) [39], and D-RIE (deep reactive ion etching) technologies [40]. These new processes can improve the repeatability and batch or mass production and save enormous manufacturing costs. The materials used in these manufacturing processes have also changed and adapted to the non-conventional manufacturing processes, as in the example of FR4 [23, 41] manufacturing.

Not only the shapes and materials used in the harvesters themselves but also the ones used in the other components of the harvesters (magnets and springs for example) have evolved. Magnets are progressing from the traditional rectangular shape to cylindrical [13], or spherical. The most common material used in magnets is Neodymium Iron Boron (NdFeB) [15, 36, 37, 39], which presents the highest magnetic properties per volume unit [3]. Other choices are Neodymium (Nd) [42], Samarium Cobalt (SmCo) [43], useful for its high temperature operation, and electroplated Cobalt Nickel Manganese Phosphorus (CoNiMnP) [38]. Stainless steel and music wire springs are being replaced in some cases by silicon springs [44], electroplated copper planar springs [36], MEMS technology nickel planar springs [37], laser cutting FR4 springs [16], and micro-machined Si springs [40].

The use of Halbach Arrays is another field of study that is proliferating in EVEHs [15, 45, 46]. Halbach Arrays consist of an array of permanent magnets that can concentrate the magnetic field on one side while canceling out the magnetic field on the other side. The increase of magnetic field strength combined with a reduction of device volume enhances the output power and energy density harvested [15].

3.5. 3D Printing of Vibration Energy Harvesters

Additive manufacturing using 3D printing is a rapid prototyping manufacturing process that allows substantial reductions in time and cost when compared to traditional manufacturing. Although the idea of including 3D printed components in vibration energy harvesters has been previously considered [24, 33], the possibility of generating fully 3D printed harvesters is completely new. The use of 3D printing to manufacture vibration energy harvesters introduces all the advantages associated with the 3D printing process, which are more critically needed in the development phase. These advantages include: time and cost savings, rapid production with allowance of quick minor modifications, and high possibility of scalability to mass production with minor changes.

The technology of 3D printing comes with some of its own challenges, especially the idea of using a low-cost general-purpose material to produce complex precise parts, similar to those within a vibration energy harvester. The solution to this problem is usually to adopt an iterative process of design, manufacture, and testing of the 3D printed parts. Other challenges are related to the proportional relation between printing time and increased quality as well as the total unexpected outcomes when changing the printing material, particularly with tight tolerances in the printed parts.

To produce a 3D printed part, several different materials, each one with unlike density, frictional properties, viscosity or price, are available in the market for the printing process. Table 4 shows some of these 3D printing materials that could be used in vibration energy harvesting and their characteristics.

Table 4: 3D printing materials considered in vibration energy harvesting and properties

	Material Name				
	High Impact Polystyrene	Acrylonitrile butadiene styrene	Polylactic Acid	PolyEthylene Terephthalate	Acrylonitrile butadiene styrene
Material Abbreviation	HIPS	ABS Blue	PLA	PET	ABS Green
Material Heating Temperature (C)	240	240	205	245	240
Material Bed Temperature (C)	110	100	50	70	100
Filament Spool Price ($)	24.95	29	48	48	19.47
Filament Spool Mass (Kg)	1	1	1	1	1

As an example of the variation between these materials, material bed temperature has a 100% difference between two types of these available materials, which is one of two parameters influencing output part quality. The material heating temperature and bed temperature are two important printing parameters that need to be set-up in the printer before the manufacturing process begins.

4. Theoretical Background

The theoretical foundation of the proposed nonlinear, electromagnetic, vibration energy harvester starts from the known Faraday law, which states that a change in the magnetic flux will generate an electric current in a circuit exposed to this flux change. In the proposed application, this change in the magnetic flux is produced via relative displacement of a cart built with magnetic materials and a fixed structure where the magnetic coil is set. The relative displacement will periodically modify the magnetic flux and therefore an electric current will be produced in the coil. If N loops of coil are considered in the electromagnetic harvester, the voltage obtained can be calculated as [33]:

$$\boldsymbol{V = N\frac{d\emptyset}{dt} = N\frac{d}{dt}(BAcos\theta)} \qquad (4.1)$$

Where N is the number of loops of the coil, $\emptyset$ is the linkage magnetic field, B is the magnetic flux density vector, A is the area vector and $\boldsymbol{\theta}$ is the angle between the magnetic flux density vector and the area vector.

In this thesis, the number of loops in the harvester's coil, N, is considered fixed at 40. The magnetic flux density vector (B), the area vector (A), and the angle between the magnetic flux density vector and the area vector ($\boldsymbol{\theta}$), are considered fixed for the harvester particular geometry and type of magnets. From equation 4.1 it is noted that the coil size N is proportional to the output voltage. Also, increasing the size of the magnets would increase B, and so would the harvester output voltage. Assuming that $\boldsymbol{\theta}$ is selected as zero in order to maximize B, the equation becomes:

$$\boldsymbol{V = NB\frac{dA}{dt} = NBl\frac{dx}{dt}} \quad (4.2)$$

Where l is the length of the coil (in the direction perpendicular to the movement of the magnetic cart) and x is the length of the coil affected by the magnetic field.

Linear harvesters are designed to harvest energy near the resonance frequency of the harvester. This means that the resonance frequency of the harvester is chosen as the frequency at which the environment, system or application vibrates most of the time. The inconvenience of this practice is that out of this specific resonance frequency the amount of energy harvested is greatly reduced. To overcome this inherent problem the range of frequencies where energy can be harvested should be increased to accommodate more than just the resonance frequency. This would be closer to the practical situation where natural systems vibrate either in multiple frequencies, or in a range around a targeted frequency. Knowing that hardening and softening nonlinearities tend to increase the bandwidth around the resonance frequency, as seen in Figure 1, such nonlinearities are added to the harvester. A specific type of nonlinearity that provides such effect is the springless vibration energy harvester, which is based on modifying the stiffness of the harvester by means of stoppers. These stoppers are springs attached to a fixed part of the harvester´s structure but that are not connected to the moving part (seismic mass) of the harvester. This is also known as the impact oscillation. In this type of harvester, two different movements need to be considered. Figure 2 presents a free body diagram of the harvester including the two different movements.

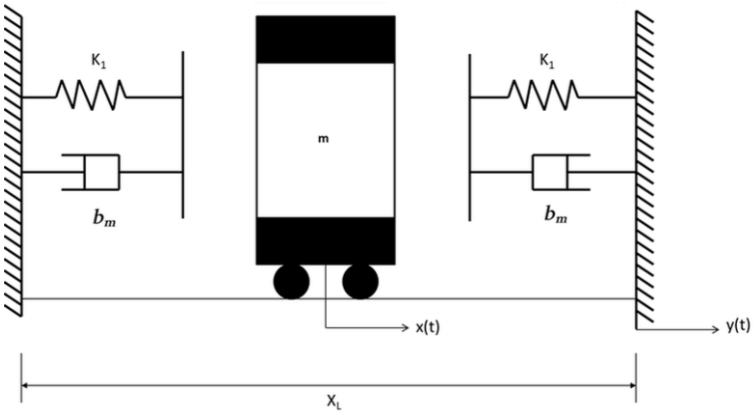

Figure 2: Free body diagram of the proposed nonlinear harvester [33]

The first movement is associated with the displacement of the environment, system or application where the harvester is installed. This displacement can be consider as absolute (y(t)) and is coincident with the displacement of the fixed part of the harvester's structure. This absolute displacement can be expressed in terms of frequency and time as:

$$\boldsymbol{y(t) = y_0 cos(w_0 t) = y_0 cos(2\pi f_0 t)} \qquad (4.3)$$

The second movement is associated with the displacement of the cart or moving part of the harvester's structure. It can be considered as relative displacement (x(t)) between the cart and the outer body of the harvester. The equation that describes the movement of this electromagnetic harvester attached to an external system is:

$$\boldsymbol{m\ddot{x} + b_m\dot{x} + f_n(x,\dot{x}) + F_e + F_{st}(x) + mgsin\theta = -m\ddot{y}} \qquad (4.4)$$

Where m is the mass of the moving part of the harvester (magnetic cart), x is the relative displacement of the harvester, y is the displacement of the system where the harvester is

installed, b_m is the mechanical damping coefficient, F_e is the electromagnetic force ($\boldsymbol{F_e} = \boldsymbol{b_e\dot{x}}$, with b_e being the electromagnetic damping coefficient), g is the gravity, $\boldsymbol{\theta}$ is the angle of the movement with respect to the horizontal, f_n is the non-linear damping due to energy loses ($\boldsymbol{f_n} = \boldsymbol{b_n\dot{x}x^2}$, with b_n being the non-linear damping coefficient) and F_{st} is the equation that considers the changes in stiffness of the system due to nonlinearities.

For a horizontal harvester$\boldsymbol{\theta} = \mathbf{0}$, which renders the equation to be solved as:

$$\boldsymbol{m\ddot{x} + (b_m + b_e)\dot{x} + b_n\dot{x}x^2 + F_{st}(x) = -m\ddot{y}} \qquad (4.5)$$

To understand the factors that affect the previous equation, the mechanical and electromagnetic damping factors need to be calculated. This calculation is explained in detail in the following sections.

Mechanical damping

The mechanical damping in an energy harvester can be related to its mechanical quality factor (Q_m) [33], with the mechanical quality factor defined as:

$$\boldsymbol{Q_m = \frac{f_0}{\Delta f} = \frac{f_0}{f_2 - f_1} = \frac{\sqrt{km}}{b_m} = \frac{2\pi f_0 m}{b_m} \Longrightarrow b_m = \frac{2\pi f_0 m}{Q_m}} \qquad (4.6)$$

Where b_m is the mechanical damping factor, m is the mass of the harvester, f_0 is the central frequency at which the system resonates, k is the stiffness of the harvester and $\boldsymbol{\Delta f}$ is the difference between the two half-power cut-off frequencies (f_1 and f_2) surrounding the range of useful frequencies to harvest energy.

Electromagnetic damping

When a mass moves insides a magnetic field, the current induced, due to Faraday's law, generates a magnetic field that opposes the moving magnetic field (back electromagnetic force (emf)). The interaction between both magnetic fields can be considered as an electromagnetic damping or electromagnetic resistance force. The electromagnetic power generated by the electromagnetic force during this interaction is dissipated in the harvester by both its coil and internal load.

$$\mathbf{P_{emf} = F_e\dot{x} = b_e\dot{x}^2 = P_{diss} = \frac{V^2}{R_p+R_L+j\omega L}} \quad (4.7)$$

Where P_{emf} is the generated electromagnetic power, P_{diss} is the dissipated power, V is the voltage, R_p is the parasitic resistance of the coil, R_L is the parasitic resistance of the load and L is the inductance of the coil.

Assuming that the coil inductance (L) can be neglected compared to the parasitic resistance of both load and coil, the electromagnetic damping can be expressed as:

$$\mathbf{b_e = \frac{V^2}{R_p+R_L}\frac{1}{\dot{x}^2} = \frac{1}{R_p+R_L}\frac{V^2}{\dot{x}^2} = \frac{1}{R_p+R_L}\left(\frac{d\phi}{dx}\right)^2 = \frac{(Bl)^2}{R_p+R_L}} \quad (4.8)$$

Substituting the damping coefficients and the absolute displacement in the equation of displacement of the harvester we obtain:

$$\mathbf{m\ddot{x} + \left(\frac{2\pi f_0 m}{Q_m} + \frac{(Bl)^2}{R_p + R_L}\right)\dot{x} + b_n \dot{x} x^2 + F_{st}(x) = -mA_0 \cos(2\pi f_0 t)} \quad (4.9)$$

Where x is also a function of time, x=x (t).

Focusing on equation 4.9, increasing the mass of the magnetic cart of the harvester would increase the harvester output voltage. This is because it reduces all the terms representing damping in the equation. The same behavior can be obtained by increasing the frequency of the application, until a certain value when the magnetic cart displacement becomes uncontrolled. This theoretical performance can be extracted from the frequency response curve of a typical vibration energy harvester (see Figure 6).

As previously mentioned, F_{st} is the piecewise function that describes the changes of stiffness of the springs depending on the bouncing of the moving cart against them. It can be described in intervals depending whether the cart is contacting the springs or not and how much compression there is:

$$\boldsymbol{F_{st} = 0,\ -x_s \le x \le x_s,\ \text{No contact with springs}} \quad (4.10)$$

$$\boldsymbol{F_{st} = k_1(x - x_s),\ x_s \le x \le x_c,\ \text{Contact with springs}} \quad (4.11)$$

$$\boldsymbol{F_{st} = k_2(x - x_c) + k_1(x_c - x_s),} \qquad \boldsymbol{x_c \le x \le \frac{L}{2},}$$

$$\textbf{Contact and springs totally compressed} \quad (4.12)$$

$$\boldsymbol{F_{st} = k_1(x + x_s),} \qquad \boldsymbol{-x_c \le x \le -x_s,} \quad \textbf{Contact with springs} \quad (4.13)$$

$$F_{st} = k_2(x + x_c) + k_1(x_s - x_c), \qquad \frac{L}{2} \leq x \leq -x_c,$$

Contact and springs totally compressed (4.14)

Where k_1 is the stiffness of the springs when they are partially compressed, k_2 is the stiffness of the springs when they are totally compressed, x_s is half of the displacement of the cart between compressed springs and x_c is half of the displacement of the cart between uncompressed springs.

Equations 4.10 to 4.14 add the relationship relating the harvester performance to the type of springs included in it. However, this relationship between the spring stiffness, k, and the performance of the harvester is not easy to determine. Nevertheless, it can be generally concluded from these theoretical equations that: on the one hand, a very stiff spring would produce violent impact of the seismic mass and reduce the output voltage while increasing the harvesting bandwidth frequency. On the other hand, a less stiff spring would increase the output voltage as far as it is able to stop the seismic mass without deforming out of shape and misaligning the carriage with respect to its linear movement.

5. Experimental Setup

To test the proposed harvester performance, an experimental setup was constructed as presented by Figure 3. The main equipment used in this setup included: the shaker, with its controlling unit, the data collection unit, and a mechanical base to hold the harvester with a feedback accelerometer in place. Table 5 includes specifications of the used equipment.

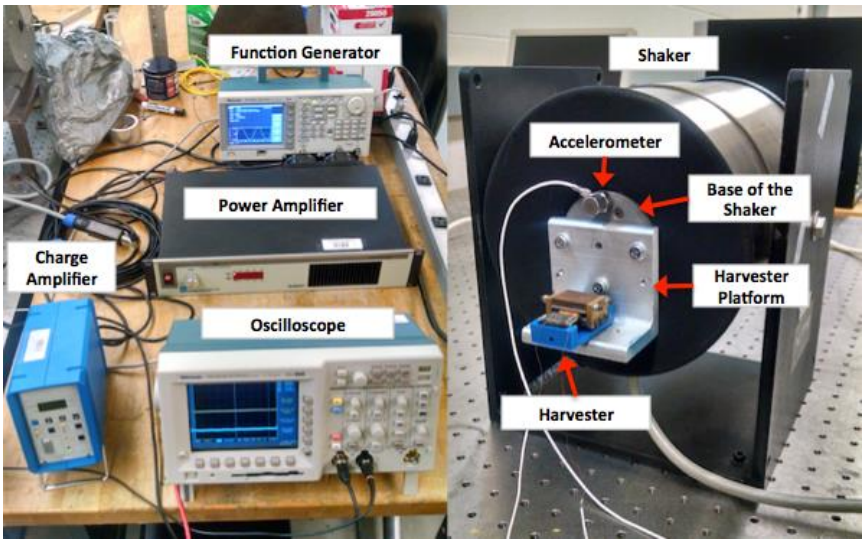

Figure 3: Experimental setup

Table 5: Electronic equipment specifications

Electronic Component	Model
Function Generator	Tektronic AFG 3021
Power Amplifier	MB dynamics SL500VCF
Shaker	VTS VG100-6
Accelerometer	Kistler 8702B50
Charge Amplifier	Kistler 5010B
Oscilloscope	Tektronic TDS 3012

Figure 4 shows the control block diagram of the experimental setup. The configuration is in an open loop since there is no direct feedback line from the accelerometer output to the function generator or power amplifier. This is because of the limited capabilities of the available equipment. Sweeping the frequency input up and down was carried out manually,

in the same setting, in a consistent and sequential manner to avoid any possible interruptions and changes compared to an automated sweep. The manual setting was also necessary to ensure maintaining a constant level of acceleration input to the harvester.

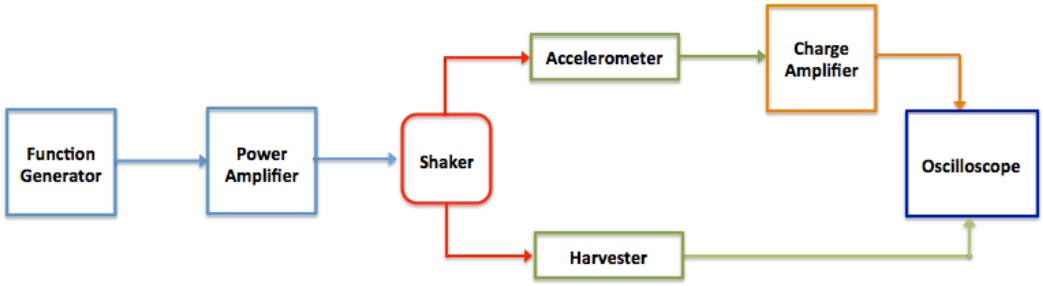

Figure 4: Control block diagram of the experimental setup

The function generator was set to produce a sinusoidal wave that is amplified at the next step to be able to run the shaker. Both the accelerometer and the harvester are attached to the base of the shaker; the first one is connected directly and the second one via an additional platform. The output of the accelerometer is connected to a charge amplifier that allows displaying its results using the oscilloscope. The output of the harvester is also plugged to the oscilloscope and showing as a second signal collected through a separate channel.

The input signal settings were as listed in Table 6.

Table 6: Input signal settings for testing the proposed harvester

Input signal settings
Sinusoidal wave to simulate periodic environmental vibrations
Frequencies from 5 to 25Hz
Constant acceleration of 0.5g to mimic real application conditions

Sinusoidal waves are typical in repetitive environmental applications and are normally considered to be the closest representation of the natural situation in energy harvesting [15,

39]. There exist some applications that present other type of spectrum such as human body vibrations, which are aperiodic [47], but those were out of the scope of this work.

The accelerometer attached to the base of the shaker measures the acceleration that both the shaker and the harvester are experiencing. Kistler 8702B50 is a low impedance piezoelectric accelerometer with acceleration range from -50g to 50g and sensitivity of 100mV/g. Due to the low signal power at its output, it needs to be connected to a charge amplifier that provides constant current power to sensors.

Kistler 5010B is a dual mode charge amplifier; this means that it can amplify both in voltage (used for low impedance sensors) and charge modes (used for high impedance sensors). Apart from selecting the mode (depending of the type of sensor used), the values of the sensor sensitivity (100mV/g) and a scale value need to be input into the charge amplifier. The scale value refers to the amount of volts or millivolts that are displayed in the oscilloscope per acceleration unit value. This is, if a scale value of 1V/g is selected, when the oscilloscope shows a voltage value of 1V, an acceleration of 1g is present in the test. To fulfill the requirements of the experiment a value of 0.5g is needed, and so for a scale value of 1V/g, 500mV are needed throughout the whole interval of frequencies.

A platform was designed and built to connect the harvester to the shaker, while simultaneously hosting a connected accelerometer for feedback to the data acquisition system. The rational for selecting this platform design is detailed in Appendix 2. The final design of this platform and its assembly to the shaker are presented in Figure 5.

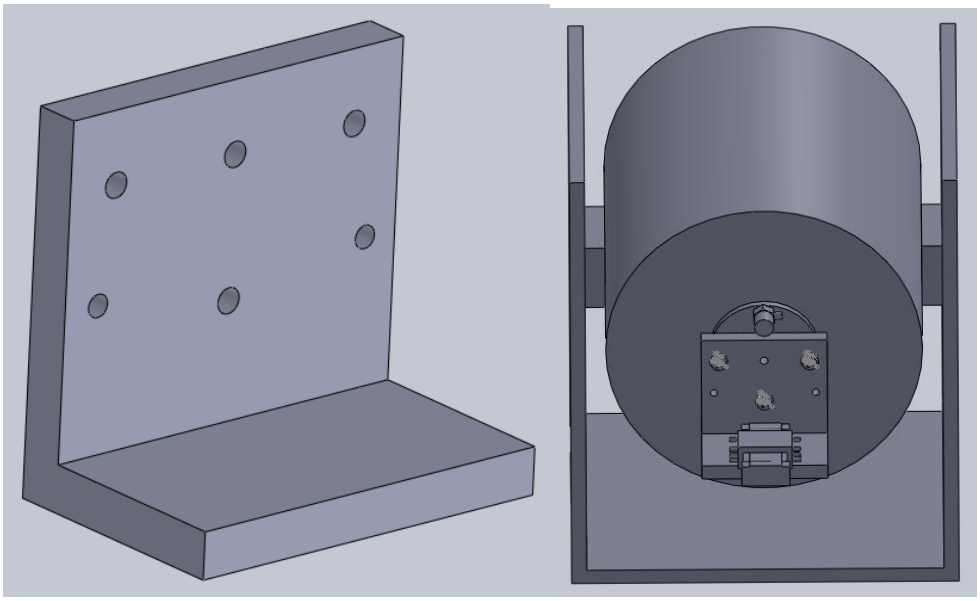

Figure 5: Harvester platform used in experimental setup

6. Springless Vibration Energy Harvester

An electromagnetic harvester built using traditional manual manufacturing methods at the University of Waterloo was used during this thesis work as an initial baseline to redesign for additive manufacturing and nonlinear functionality, 3D print, and test. This harvester was denominated Springless Electromagnetic Vibration Energy Harvester because of the fact that the springs in it are not attached to the seismic mass [33]. This arrangement makes this harvester a nonlinear device. For comparison, a typical sketch of a linear vibration harvester and its resonance phenomena are presented in Figure 6.

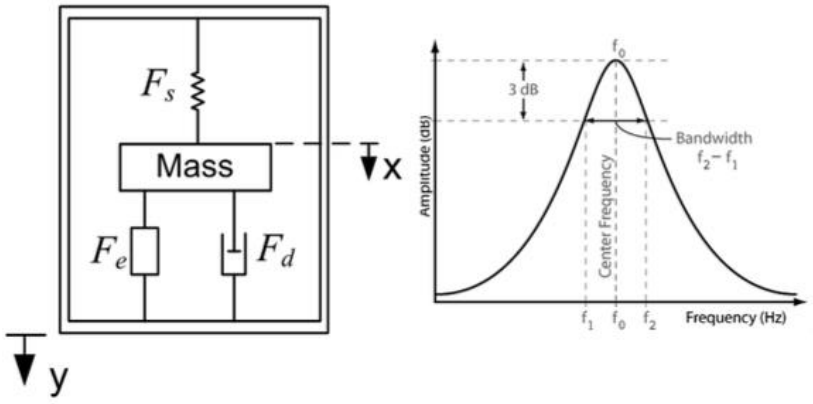

Figure 6: Vibration harvester and resonance phenomena

In the springless vibration energy harvester the springs are attached to the fixed structure of the harvester (metallic base), and the moving mass, also denominated magnetic cart, bounces against them. These springs act as stoppers and generate nonlinearities in the system, consequently widening the efficient harvesting frequency bandwidth. Figure 7 presents this original springless vibration energy harvester [33].

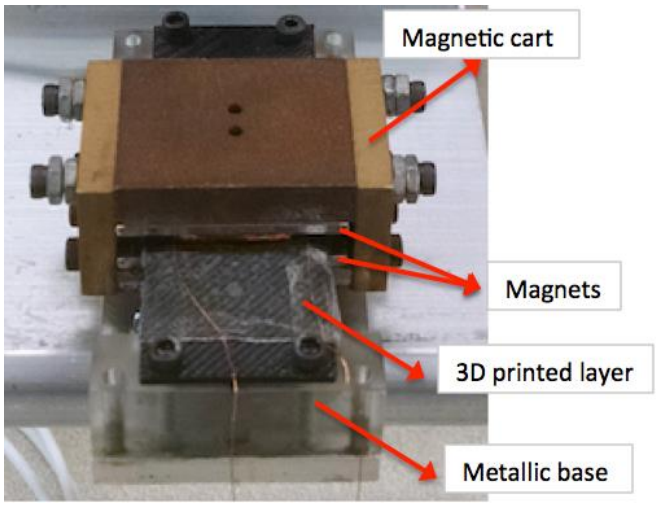

Figure 7: Springless vibration energy harvester

The magnetic cart of this harvester linearly moves through a metallic rail (attached to the fixed structure) and a metallic linear guide (attached to the magnetic cart). The combination of the rail and linear guide is called miniature linear guide. The variation in magnetic field is generated by the magnets included in the magnetic cart that move on the upper and lower sides of a 3D printed layer which includes a certain number of loops of coil (N). Apart from the magnets, the magnetic cart is formed by: a big steel plate (located in the upper side of the magnetic cart), a small steel plate (located in the lower side of the magnetic cart), and two lateral copper plates. For more information regarding the components and dimensions of the springless vibration energy harvester see Appendix 1.

The characteristic frequency response curve of the springless vibration energy harvester can be seen in Figure 8 from 5Hz to 15Hz for both up sweep and down sweep of input frequency.

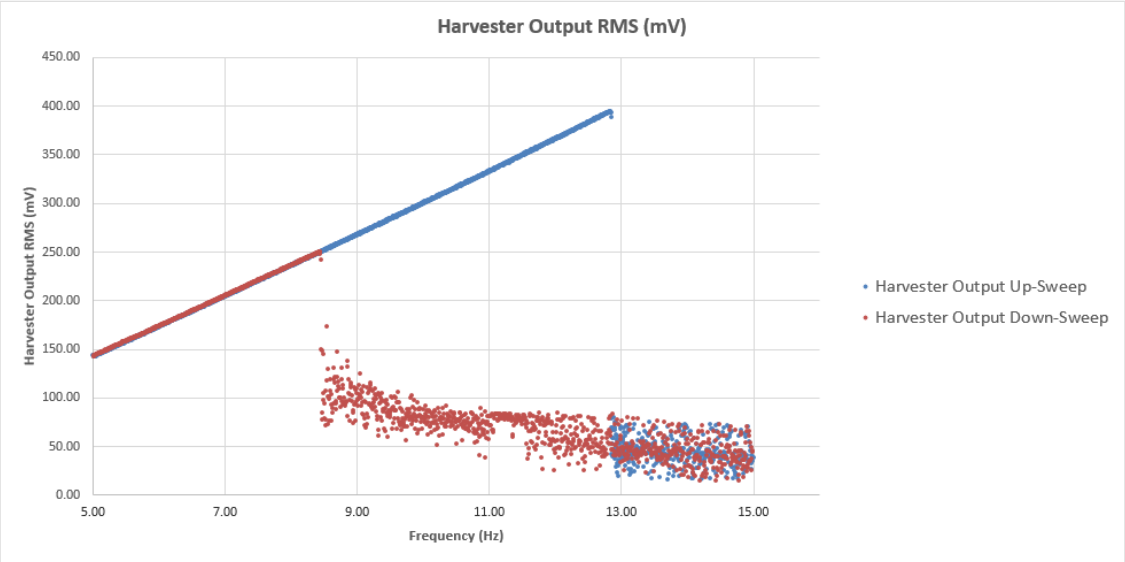

Figure 8: Springless vibration energy harvester frequency response curve

A maximum voltage output of 394mV was obtained at 12.84Hz input using an automated closed loop that maintains an acceleration level of 0.5g throughout the test. In spite of the hysteresis between the up sweep and down sweep results, the voltage output values from 5Hz to 8.47Hz are similar in both sweeps.

The voltage values obtained for this harvester are illustrative of an automated closed loop, and can't be considered as the thesis baseline because they were obtained using a far more advanced setup than the one presented in chapter 5. These values are added here as a reference to show how the experimental setup can greatly influence the harvester results.

7. Results and Discussion

Based on the conceptual design of the springless harvester mentioned in section 6, a new harvester was proposed to be designed for cost effective additive manufacturing. In particular, 3D printing using general-purpose material and a low-end printer were to be used in producing the new nonlinear vibration energy harvester. The strategy of the work included attempting gradual changes and modifications to the springless harvester design until arriving at a fully 3D printed harvester while testing harvester performance along the way. Three iterations were generated as the work progressed:

1) Iteration 1: The metallic base used in the original springless vibration energy harvester was replaced with a 3D manufactured base. The new harvester was tested and results were considered the baseline for any further developments in the harvester. This step was critical to test and verify the 3D printing capabilities selected for manufacturing while introducing the least modifications to the original design.
2) Iteration 2: The majority of the harvester design was modified for manufacturing and 3D printed. The produced harvester was denominated low cost harvester. This new low cost harvester was obtained through modifying the initial design and 3D printing of the base of the harvester, the rail and guide that form the miniature linear guide, and the external structure of the magnetic cart. Its only metallic parts left were installed inside the magnetic cart consisting of 2 steel plates. It is to be noted here that the springs, bolts, and magnets of the harvester are not considered reproducible using 3D printing techniques, and so they are excluded from the metallic components category. This new low cost harvester

was tested for power generation in comparison to the first iteration harvester results.

3) Iteration 3: The harvester was fully 3D printed and multiple versions were produced and tested.

Following are the details of the design and manufacturing challenges, as well as the results and relevant discussion of each iteration.

7.1. First Iteration: Springless Vibration Energy Harvester With 3D Printed Base

The first iteration of the nonlinear harvester included the introduction of a 3D printed base to the fully metallic harvester. The base is a supporting element that does not influence the functionality of the core pieces of the harvester. However, it provides the general dimensions of the harvester and an opportunity to test 3D printing effects in action. This iteration included the iterative design and production of 9 versions of bases to use with the harvester. A detailed description of each of these versions can be found in Appendix 4. Following is a detailed discussion of the experience and challenges in manufacturing the first iteration.

7.1.1. Manufacturing the New Base of the Springless Vibration Energy Harvester

The initial 3D printed model of the harvester base, or harvester base v1.0, is presented by Figure 9. This base was 3D printed as described in section 3.5. It included 4 holes to attach the 3D printed layer, five holes and a lateral slot to bolt the rail of the miniature linear guide to it, and four lateral holes to fix the springs to the base.

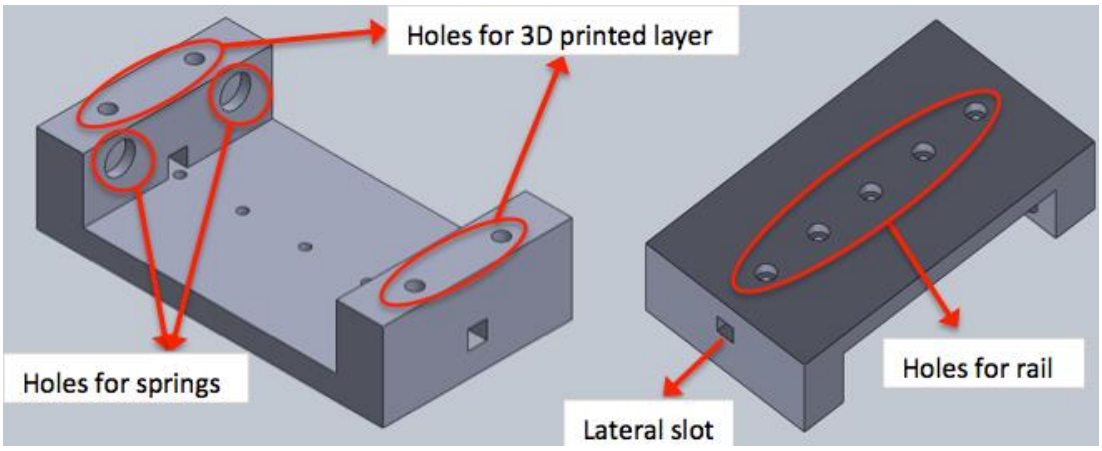

Figure 9: Model and attributes of 3D printed harvester base v1.0

The global dimensions of harvester v1.0 can be seen in Figure 10.

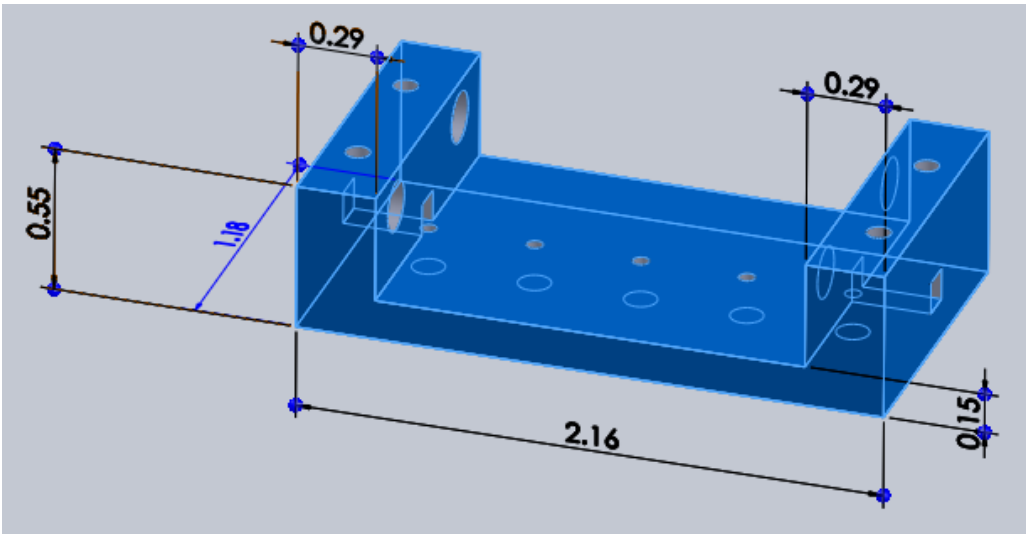

Figure 10: Global dimensions (in inches) of harvester base v1.0

Harvester base v1.0 did not match the specifications to fit the rest of the harvester due to minor design defects as well as manufacturing defects. These defects are mainly related to selecting tolerances related to the 3D printing process, which are different than what would be selected to produce a metallic base. This version was redesigned and manufactured evolving until base v1.4 was obtained through 8 versions. In between these 8 versions, base v1.2.4 was the first base to fit the assembly of the harvester but improvement was still

required because of new design defects being observed in the harvester functionality. In specific, continuous contact between the magnets and the springs was observed due to some minor attraction between them. Figure 11 shows one of the areas where magnetic attraction between springs and magnets occurred.

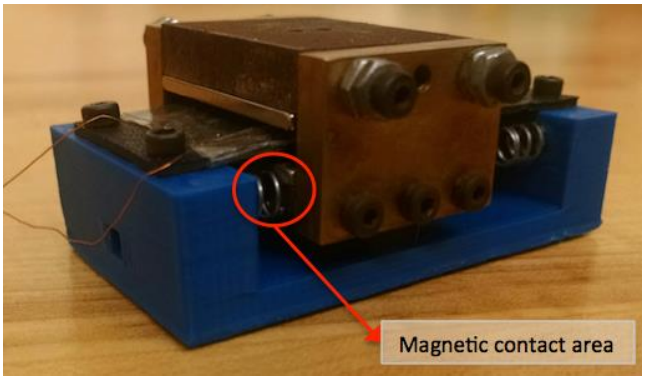

Figure 11: Attraction between springs and magnets in the harvester base v1.2.4

After correcting more of these defects, v1.4, which is the 9th version in this process, was the first version used for energy harvesting testing. Table 7 presents the different design and manufacturing challenges and defects in all versions of the 3D printed harvester bases.

Table 7: Design defects in all versions of 3D printed harvester bases

Harvester Base Version	Design and Manufacturing Defects
v1.0	• Tolerance of lateral slots too small (0.12”x0.12”) • Wrong distance between holes for 3D printed layer
v1.1	• Tolerance of lateral slots too big(0.136”x0.125”)
v1.2	• Dimensions of lateral slot 0.128”x0.1225”
v1.2.1	• Dimensions of lateral slot 0.128”x0.1225”
v1.2.2	• Dimensions of lateral slot 0.128”x0.1225”
v1.2.3	• Dimensions of lateral slot 0.128”x0.1225”
v1.2.4	• Wrong tolerance in the top holes of the harvester’s base • Incorrect depth of the holes of the base • Wrong height of spring holes causing spring-magnet contact
v1.3	• Wrong tolerance in the top holes of the harvester’s base • Incorrect height of the holes of the base • Minimum spring-magnet contact
v1.4	• None

Multiple testing of equipment and material was carried out to solve the manufacturing defects in 3D printing. Three different 3D printers (Makerbot replicator 2, Makerbot replicator 5th generation, and Lulzbot TAZ 5), as well as three different materials (HIPS, PLA, and ABS) were tested. The printing quality was also adjusted in the 3D printers to achieve the best possible performance, shifting from low quality to high detail. Finally, two additional adjustments were also included in some of the 3D printed components, a brim and a raft. A raft is an initial 3D printed sheet that is not a part of the model and that serves as structural support of the harvester base to reduce the buckling due to thermal effects. A brim is a single layer of extra material surrounding the 3D printed part, which is also useful to reduce buckling and separation of the component from the printer bed.

During this testing, several types of manufacturing defects were observed through the 3D printing process including:

1. Layering gaps as shown by the example in Figure 12 obtained for v1.0.
2. Filling of holes.
3. Lateral displacement of initial material layers.
4. Raft melted to the harvester base as shown in Figure 13 obtained from v 1.2.1.
5. Buckling as shown by Figure 14 of v1.3.

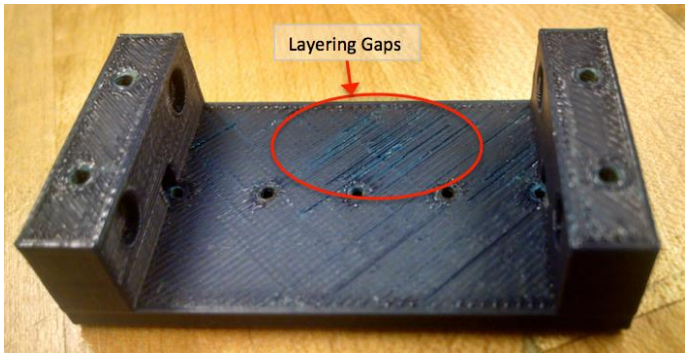

Figure 12: Layering defects in harvester base v1.0

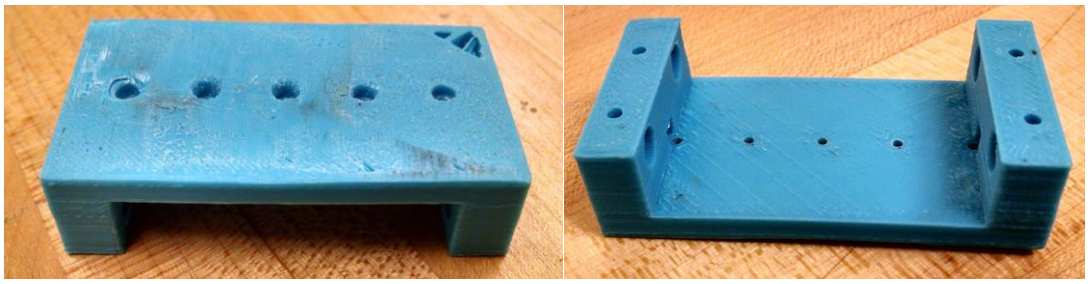

Figure 13: Consequences of raft melted in harvester base v1.2.1

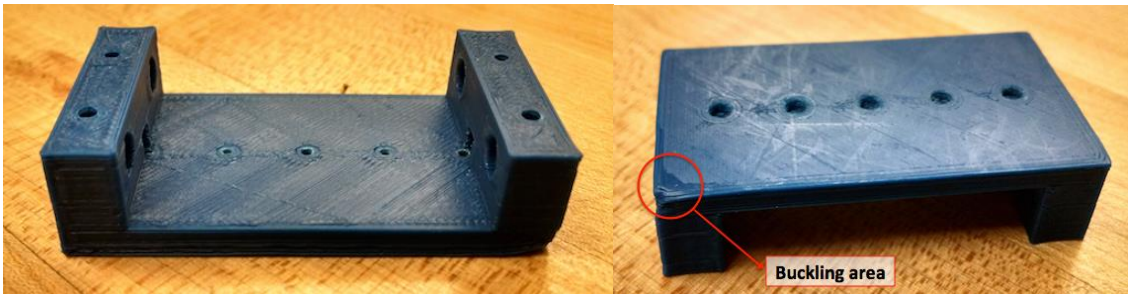

Figure 14: Buckling in harvester base v1.3

The final harvester base in v1.4 which was the one used in the functional harvester is shown in Figure 15. This version was produced using the Lulzbot TAZ 5 printer, the blue ABS as the 3D printing material, and a brim to avoid twisting and buckling of the produced part.

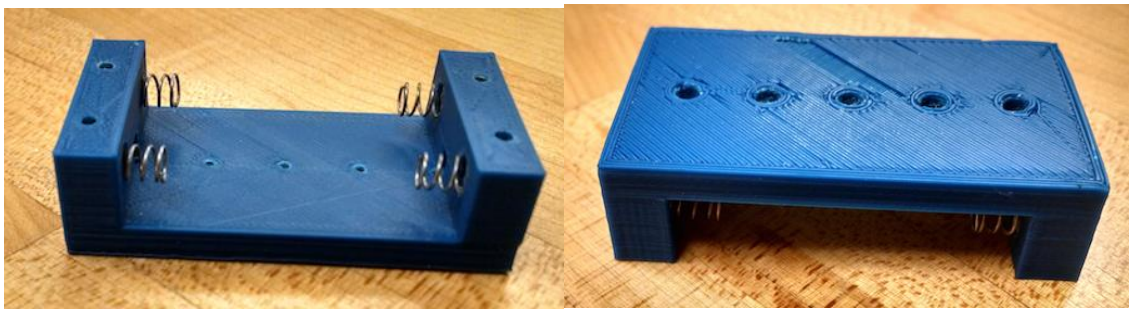

Figure 15: 3D printed harvester base v1.4 with springs attached to it

Table 8 presents the details of the printing specifications of base v1.4.

Table 8: Harvester base v1.4 3D printing specifications

Printing Features	Harvester base v1.4
3D printer model	Lulzbot TAZ 5
3D printer cost ($)	2200
Printing mass including raft or brim (g)	9
Additional components (raft of brim)	Brim
Final mass (g)	7
Material	Blue ABS
Material cost ($/Kg)	29
Total cost ($)	0.26
Printing quality	High Detail
Design defects	• None
First component set-up time (min)	8
Printing time (min)	76
Total time (min)	84
Manufacturing defects	• None

The total time for the manufacturing process to take place as presented in Table 8 includes time for printing the part and set-up time of the component. The total cost of the part is calculated as:

$$\textbf{Total cost } (\$) = \frac{\textbf{Total weight (gr)} \times \textbf{Material Cost } (\$/\textbf{kg})}{\textbf{1000}} \qquad (7.1)$$

This base was used to establish the baseline harvester in terms of manufacturing and performance benchmarking. Precision and care was invested in producing this part as it allows the installation of the other components of the harvester, including springs, 3D printed layer and miniature linear guide, on a base with least defects and errors possible to influence the following iterations.

7.1.2. Composition and Assembly of the Springless Vibration Energy Harvester With a 3D Printed Base

New springs were selected and installed in the 3D printed base. The specifications of this new type of springs, denominated v1, are provided in Table 9.

Table 9: Specifications of the new springs installed in the first iteration harvester

	Outside Diameter (inch)	Wire Diameter (inch)	Total Length (inch)	Rate (lbs/inch)	Material
Springs v1	0.18	0.018	0.25	13.5	Music wire

Also the dimensions of the magnets that are installed in the magnetic cart of this harvester can be seen in Table 10.

Table 10: Dimensions of small magnets installed in the first iteration harvester

	Length (inch)	Width (inch)	Thickness (inch)
Small Magnets	1	0.25	0.0625

The components of the new springless vibration energy harvester with 3D printed base can be seen in Table 11.

Table 11: Components of the springless vibration energy harvester with 3D printed base

Component	Version/Type
Harvester base	Harvester base v1.4
Springs	Springs v1
Magnets	Small magnets
Rail	Original metallic rail
Guide	Original metallic guide
3D printed layer	Original 3D printed layer (N=40)
Big steel plate	Original big steel plate
Small steel plate	Original small steel plate

Note that the only parts differing from the original springless vibration energy harvester are the harvester base and the springs used. The magnetic cart representing the seismic mass is the same for both the original harvester and this first iteration (magnets, upper steel plate and lower steel plate).

7.1.3. Cost Analysis of 3D printing the Springless Vibration Energy Harvester

Cost of manufacturing, time, and material and the resulting mass of the product are the main factors subject to possible improvement via 3D printing. Therefore, mass and cost analyses are carried out for comparison between the original springless vibration energy harvester and the first iteration harvester which includes a 3D printed base. Table 12 provides a detailed listing of the parts used in both harvesters, and their masses. The 3D printed base is the only part different between the two harvesters. In spite of this being the first step in the additive manufacturing process, the final harvester mass experienced a reduction in general mass by 16 grams without reducing the seismic mass of the harvester. It is to be mentioned that the data in Table 12 will formulate the baseline for measuring change in the harvester mass within the different iterations.

Table 12: Mass analysis of the harvester

Parts of the Harvester	Original	1st Iteration
Magnetic Cart		
Mass of big steel plate (g)	24	24
Mass of small steel plate (g)	17	17
Mass of copper plates (g)	20	20
Mass of magnets (g)	8	8
Mass of bolts (g)	6 – (x12)	6 – (x12)
Mass of metallic guide (g)	1	1
Mass of original magnetic cart (g)	76	76
Harvester Body		
Mass of harvester base with initial springs (g)	**23 (metallic)**	**7– v1.4 (3D printed)**
Mass of initial magnetic cart (g)	76	76
Mass of metallic rail (g)	2	2
Mass of 3D printed layer with cables attached (g)	3	3
Mass of base bolts (x5) (g)	2	2
Mass of original harvester (g)	**106**	**90**

From a production cost perspective, significant improvement was also realized when comparing 3D printing to traditional manufacturing processes of the base of the harvester. Direct production cost is based on a combination of direct material cost and manufacturing time. As was mentioned in section 7.1.1, additive manufacturing of the vibration energy harvester was selected using the most common materials possible and utilizing a low cost printer. Table 13 shows the direct cost comparison for manufacturing an aluminum harvester base traditionally as opposed to using 3D printing. The cost of producing the base of the harvester using 3D printing was $28.16, compared to traditional aluminum cost of the same part being $111.26, translating the manufacturing time of the parts into money, at a rate of $18 per hour. This is a saving of 74.7% in just one part of the harvester, without consideration to reduction in manufacturing time as well. Appendix 8 includes a detailed listing of the cost items for each of these manufacturing processes.

Table 13: Direct cost of manufacturing the harvester base traditionally and using 3D printing

Manufacturing cost factor	Manufacturing cost ($)	Machining and assembly time (min)
Traditional	111.26 (Aluminum)	369
3D printed (v1.4)	28.16	93

7.1.4. Performance Testing of The Springless Vibration Energy Harvester With 3D Printed Base

The springless vibration energy harvester with 3D printed base was tested using the experimental setup described in section 5. The input sin wave acceleration was kept constant at almost 0.5g, from 5Hz to 25Hz, in both up-sweep and down-sweep entire set of increments. Four measurements were normally taken for each test frequency and the final acceleration experienced by the harvester base, as well as the harvester output were obtained as the average of these four values. To reduce the influence of vibrational noise generated in the accelerometer signal by the harvester and base interactions, the Root Mean Square (RMS) value of all the accelerometer output measurements were calculated and presented. The RMS of the output voltage of the harvester was also calculated and presented as output for the same reason. The main characteristics of this test included the following:

1. The shaker was clamped to the vibration table at two points.
2. The long leg of the L-Section of the connecting base was attached to shaker and the shorter leg hosted the harvester.
3. The accelerometer collecting feedback of the vibration experienced by the harvester was attached to the base of shaker.
4. Frequencies from 5Hz to 25Hz in intervals of 1Hz up-sweep and down-sweep were input to the shaker in a complete incremental set for each direction without any intermediate stops.

5. Ambient noise of 2.5mV RMS in the harvester was observed.
6. Almost constant 0.5gwas maintained during the entire test.
7. The mass of the magnetic cart of the harvester was 76 grams, also known as the seismic mass.
8. The experiment was conducted where the vibrating shaker and the harvester were in a Horizontal configuration.

Figure 16 presents the acceleration RMS values for the harvester with 3D printed base.

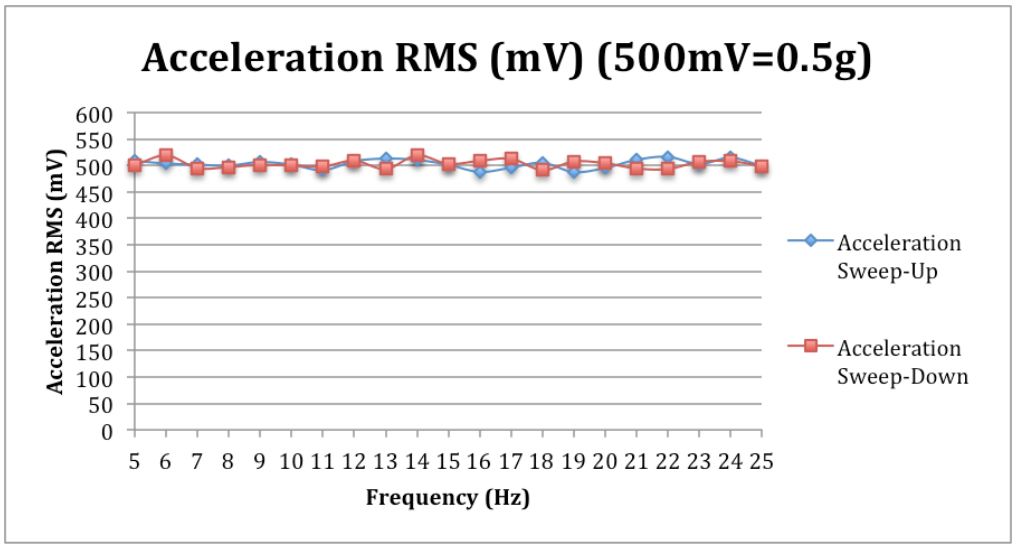

Figure 16: Acceleration RMS plot for the harvester with 3D printed base

The acceleration RMS values for the harvester with 3D printed base can also be seen in Table 14.

Table 14: Acceleration RMS values for the harvester with 3D printed base

Sweeping up		Sweeping down	
Frequency (Hz)	Acceleration RMS (mV)	Frequency (Hz)	Acceleration RMS (mV)
5	508.50	24	508.00
6	503.75	23	507.00
7	501.50	22	493.25
8	499.75	21	494.25
9	506.50	20	504.25
10	501.50	19	507.50
11	491.00	18	491.25
12	508.00	17	512.50
13	513.00	16	508.75
14	510.50	15	503.00
15	501.25	14	519.00
16	487.75	13	493.25
17	495.75	12	509.00
18	505.00	11	498.00
19	487.50	10	500.00
20	495.25	9	501.00
21	510.75	8	497.00
22	516.25	7	495.00
23	502.75	6	519.00
24	514.50	5	500.00
25	498.75	-	-

Figure 17 shows the output RMS voltage obtained for the harvester with 3D printed base. The ambient noise is not considered in the results (2.5mV).

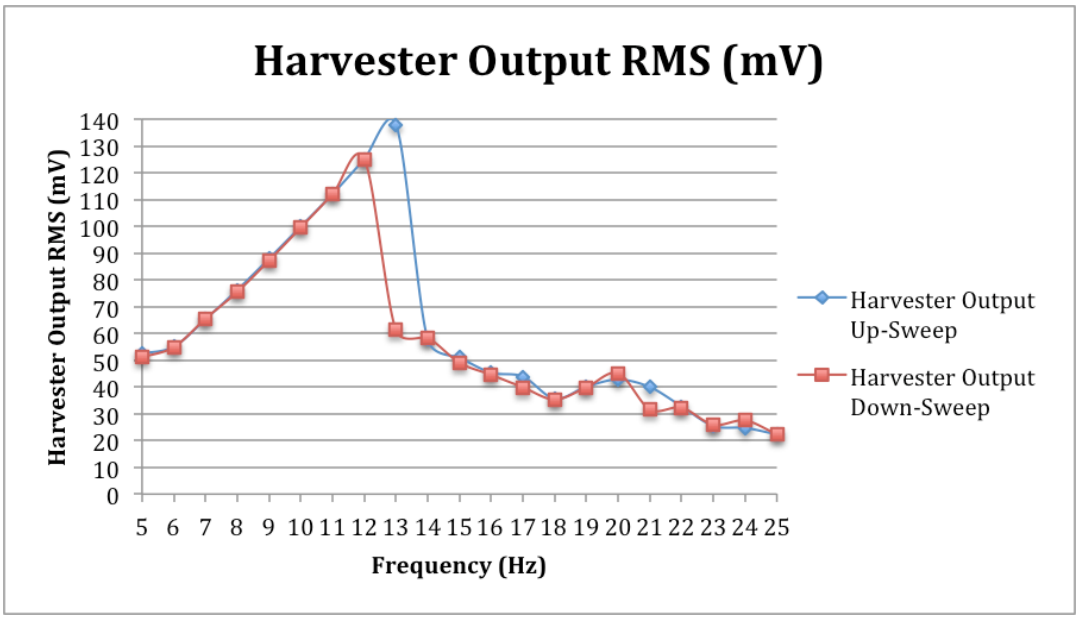

Figure 17: Output RMS voltage for the harvester with 3D printed base

The output RMS voltage of the harvester increases almost linearly with an increase of frequency reaching a maximum value of 138mV at 13Hz. Then the output voltage suddenly drops and slowly decreases until the final frequency value of 25Hz. During the down-sweep the output voltage slowly increased until 12Hz, when the bouncing movement of the magnetic cart increase significantly, and then decreased linearly almost matching the up-sweep curve. Table 15 includes the output RMS voltage values for the harvester with 3D printed base.

Table 15: Output RMS voltage values for the harvester with 3D printed base

Sweeping up		Sweeping down	
Frequency (Hz)	Output RMS (mV)	Frequency (Hz)	Output RMS (mV)
5	52.33	24	27.48
6	55.08	23	25.93
7	65.30	22	32.25
8	76.25	21	31.63
9	87.93	20	45.08
10	99.95	19	39.85
11	112.00	18	35.35
12	125.00	17	39.88
13	138.00	16	44.53
14	57.70	15	49.08
15	51.03	14	58.35
16	45.38	13	61.20
17	43.88	12	125.00
18	35.65	11	112.00
19	40.10	10	99.50
20	42.75	9	87.20
21	39.95	8	75.50
22	32.75	7	65.50
23	25.48	6	54.90
24	24.70	5	51.10
25	22.30	-	-

From the resulting frequency response curves for both the up-sweep and down-sweep inputs, the bandwidth of the harvester was calculated. This bandwidth is defined as the difference between the frequency at peak voltage (V_{peak}=138mV at 13Hz for our case) and the frequency at half power point $\boldsymbol{V_{peak}/\sqrt{2}}$ on the up-sweep branch [33]:

$$\mathbf{Bandwidth = Frequency_{V_{peak}} - Frequency_{V_{peak}/\sqrt{2}} = 13Hz - 9.8Hz = 3.2Hz} \quad (7.2)$$

This bandwidth would be considerably wider than that of a band containing only the resonance frequency corresponding to the peak voltage in a linear vibration energy harvester, which might be in the order of 2Hz.

As an additional comparison, a springless vibration energy harvester with 3D printed base was tested by a partner group at the University of Waterloo to investigate the effect that different experimental setups present in the energy harvesting output. A maximum voltage close to 300mV was obtained by that group for a frequency of 16Hz. If the results presented in Figure 17 are extrapolated to reach a maximum frequency of 16Hz, a maximum voltage of around 175mV could be obtained. The difference in the equipment and experimental setup was significant between both cases. In the setup used by the group in Waterloo sweeping input frequencies is done through a closed continuous loop with increments or decrements of 0.01Hz. However, in the setup used to obtain figurer 17 only a maximum frequency of 13Hz could be reached due to the high frequency increments and decrements of 1Hz applied manually throughout the test. In fact, each time an increment or decrements is applied the test would be stopped to collect the data before moving to the next input. The Waterloo setup allowed for more precise input and output with continuous and consistent change and acceleration controlled closely using a closed loop system. Consequently, this setup improved the performance of the harvester by prolonging the complete bouncing movement of the magnetic cart towards higher frequencies and therefore obtaining higher output voltage values. Also, the setup presented in Figure 3, which was used to obtain results in figure 17, was limited to manual control of the input adding human error as an important aspect to consider. The open loop setup doesn´t allow for an optimal control of the testing parameters and so higher error can be associated to it. On the positive side, the manual

control of the input resembles real testing conditions more accurately and so in real application testing, results might be closer to those in Figure 17.

7.2. Second Iteration: Low Cost Harvester

The second iteration included the design, manufacturing, analysis, and testing of a low cost harvester in which most parts are 3D printed. The only parts which were not 3D printed were the steel plates in the moving cart and the parts which cannot be printed like springs and magnets.

7.2.1. Manufacturing the Low cost Harvester

7.2.1.1. Base of the Low Cost Harvester

Starting with the base produced for the previous harvester, a new base was designed to be 3D printed and to include a 3D printed rail and guide instead of the metallic components used in the previous harvester. A total of 5 versions were produced starting at base v3.0.0 and ending with base v3.1.1, as presented by Table 16 showing each version and the related issues. Learning from the process to manufacture the harvester base v1.4, only the Lulzbot TAZ5 printer was used in its high detail quality mode. Similar manufacturing defects as in the process to 3D print the base v1.4 were obtained and resolved, including layering, hole filling, and buckling. The materials tested were blue and green ABS, HIPS and PET. As shown by Table 16 listing the printing specifications of this part, green ABS was selected to print the base. Detailed information concerning these low cost harvester bases can be found in Appendix 4.

Table 16: Design and manufacturing defects in versions of the low cost harvester bases

Harvester Base Version	Design and Manufacturing Defects
v3.0.0	• Initial test to check dimensions of rail hole
v3.0.1	• Wrong tolerance in the top holes of the harvester's base • Incorrect height of the holes of the base • Minimum spring-magnet contact
v3.0.2	• Wrong tolerance in the top holes of the harvester's base • Incorrect height of the holes of the base • Minimum spring-magnet contact
v3.1.0	• None
v3.1.1	• None

Table 17 presents the principal printing specifications of base v3.1.1.

Table 17: Harvester base v3.1.1 3D printing specifications

Printing Features	Harvester base v3.1.1
3D printer model	Lulzbot TAZ 5
3D printer cost ($)	2200
Printing mass including raft or brim (g)	9
Additional components (raft of brim)	Brim
Final mass (g)	7
Material	Green ABS
Material cost ($/Kg)	19.47
Total cost ($)	0.18
Printing quality	High Detail
Design defects	• None
First component set-up time (min)	8
Printing time (min)	76
Total time (min)	84
Manufacturing defects	• Minor layering gaps • Minor tolerance reduction

The total time presented in Table 17 includes time for printing the part and set-up time of the component. The total cost of the part is calculated as:

$$\textbf{Total cost } (\$) = \frac{\textbf{Total weight (gr)} \times \textbf{Material Cost } (\$/\textbf{kg})}{\textbf{1000}} \quad (7.3)$$

7.2.1.2. Rail of the Low Cost Harvester

One of the most precise-critical parts of the springless vibration energy harvester is the miniature linear guide of the moving cart. This guide is composed of a rail and a box or guide (see Appendix 1). Its function is to support, facilitate, and at the same time limit, the linear movement of the magnetic cart while continuously minimizing the friction. The version of this part used in the fully metallic harvester is purchased from a market supplier where such miniature linear guides are very low friction components that sometimes include their own lubricant storage for better performance. The main problem associated with this component is the limit on supply as there are very few companies that manufacture the specific type of miniature linear guide used in the springless vibration energy harvester. Most of these suppliers are overseas. The problem is compound by the usual issues associated with purchasing parts from overseas limited suppliers. The price of the original miniature linear guide is around $80, with added fees and expenses. These factors significantly increase the appeal of in house 3D printing as a viable solution. The challenge associated with 3D printed miniature linear guides, including a rail and a guide, would be mainly related to the high precision and low friction needed in this part. The iterative design and manufacturing process followed to obtain a 3D printed rail for a low cost vibration energy harvester took multiple trails and versions, particularly while using a low-end, cost-effective printer.

Three initial designs were generated to substitute the metallic and expensive rail of the miniature linear guide of the original springless vibration energy harvester by a 3D printed rail. Selection of the most appropriate design was based upon ease and efficiency of manufacturing combined with the best outcome performance. Appendix 6 includes the three initial designs and detailed information about the 3D printed versions of the rail.

The selected design of the harvester rail includes five holes, where the fasteners that joint the rail to the harvester base are located. Two iterations were needed to achieve the appropriate dimensional and manufacturing characteristics. Capitalizing on previous experiences with base production, no manufacturing defects were observed in this process. Figure 18 presents the dimensions of the mushroom rail v1.0.

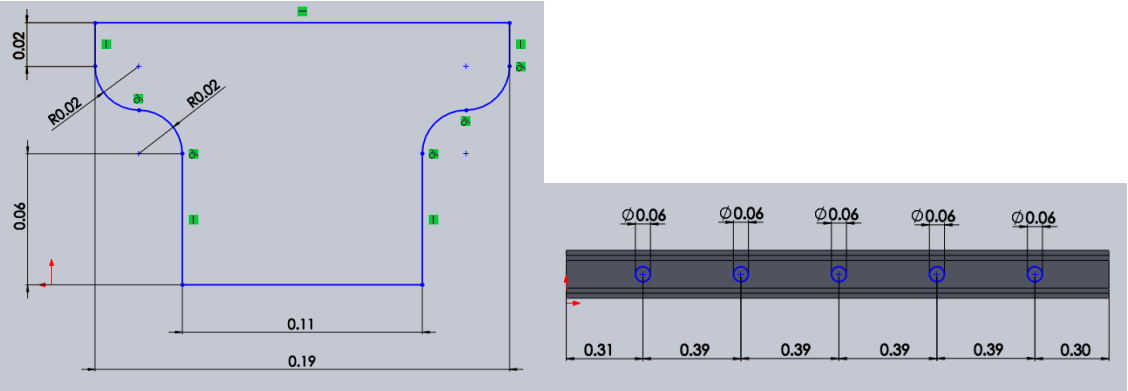

Figure 18: Harvester mushroom rail v1.0 profile sketch and lower side

The holes for the fasteners in the lower side of the 3D printed mushroom rail v1.0 were too deep and so this defect was solved in v1.1. The initial depth of the fastener holes was decreased from 0.10” to 0.09”. Also the diameter of the three middle holes was slightly increased from 0.06” to 0.066” to ease the fastening operation with the harvester base. The 3D printed mushroom rail v1.1 can be seen in Figure 19.

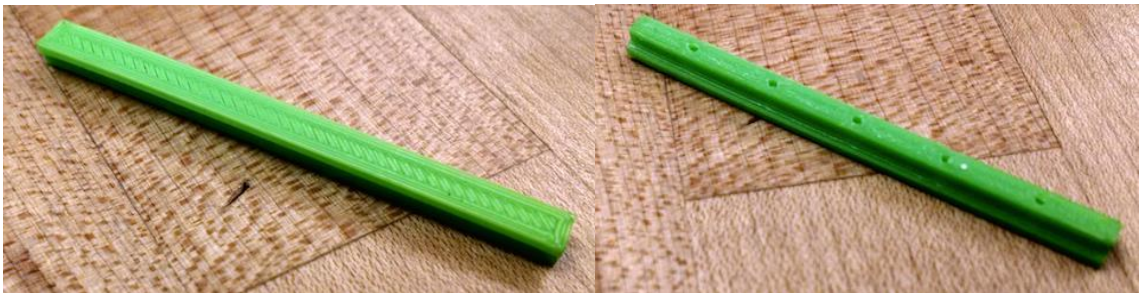
Figure 19: 3D printed mushroom rail v1.1

The manufacturing specifications of the mushroom rail v1.1 can be seen in Table 18.

Table 18: 3D printing specifications of harvester mushroom rail v1.1

Printing Features	Mushroom rail v1.1
3D printer model	Lulzbot TAZ 5
3D printer cost ($)	2200
Printing mass including raft or brim (g)	1
Additional components (raft of brim)	Brim
Final mass (g)	1
Material	Green ABS
Material cost ($/Kg)	19.47
Total cost ($)	0.02
Printing quality	High Detail
Design defects	• None
First component set-up time (min)	8
Printing time (min)	15
Total time (min)	23
Manufacturing defects	• None

7.2.1.3. Guide of the Low Cost Harvester

Following the same design process of the harvester rail, three designs for the harvester guide were created to match each one of the designed harvester rails as a pair. The selected design of the harvester rail resulted in the selection of the pairing guide. The initial guides included a gap where the rail is inserted as well as two additional holes in the upper face of the guide to attach it to the magnetic cart of the harvester. For more information about these initial designs as well as detailed descriptions of all the versions of guides see Appendix 6.

The manufacturing process of the guide for a low cost harvester included 11 iterations and was performed using the Lulzbot TAZ 5 in high detail quality mode. The only materials used were PLA and green ABS. Minor manufacturing defects were observed during this process and were related to the presence of small amounts of material near the upper holes of the guide that limited its performance. Cancelling these holes in the design solved this error.

The selected version of the guide provided the appropriate fit between the rail and the guide, as well as the installation of the additional components of the magnetic cart which include the magnets and the upper and lower steel plates.

The final design of the harvester guide was achieved at v2.1. The dimensions of the harvester guide v2.1 can be seen in Figure 20.

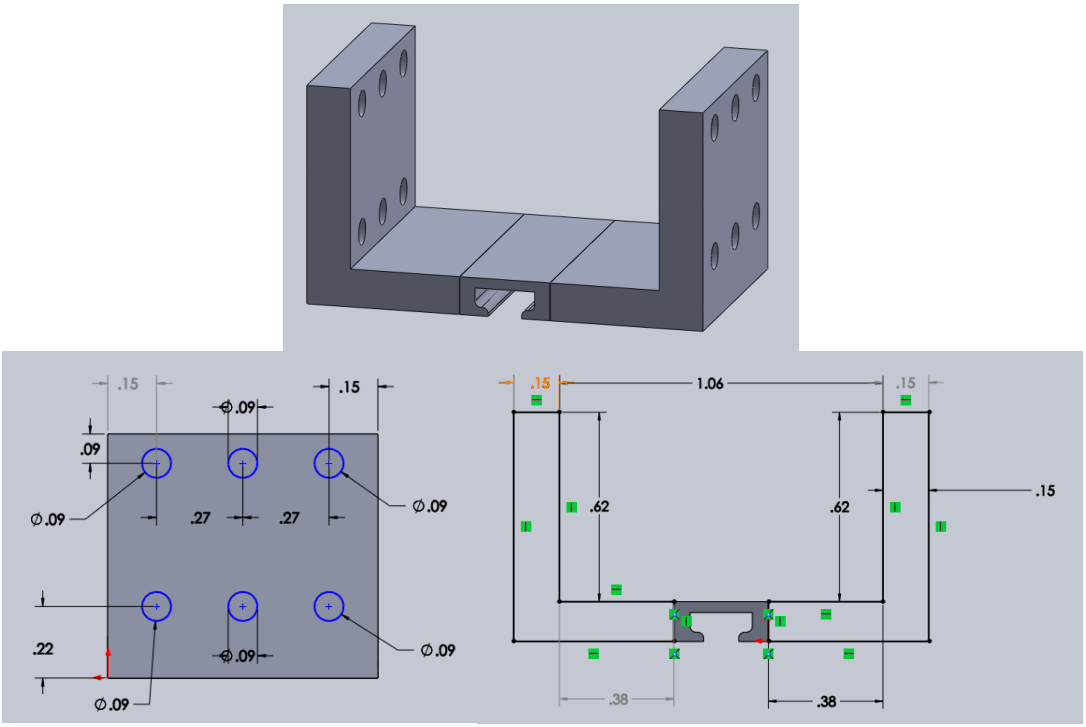

Figure 20: Design and dimensions of harvester guide v2.1

Table 19 presents the different design and manufacturing defects in all the guides for the low cost harvester.

Table 19: Design and manufacturing defects in the guides for low cost harvester

Harvester Guide	Design and Manufacturing Defects
v1.0	• Need to increase the height of the rail gap and reduce its initial width
v1.1	• Need to increase the height of the rail gap
v1.2	• None
v1.3	• Need to increase the height of the rail gap
v1.4	• Need to increase the width of the rail gap
v1.5	• None
v1.6	• None
v2.0.0	• Wrong internal dimensions
v2.0.1	• Wrong internal dimensions
v2.1	• Wrong internal width • Wrong height of first row of holes
v2.2	• Wrong height of first row of holes
v2.3	• None

Figure 21 presents pictures of the final 3D printed guide v2.3.

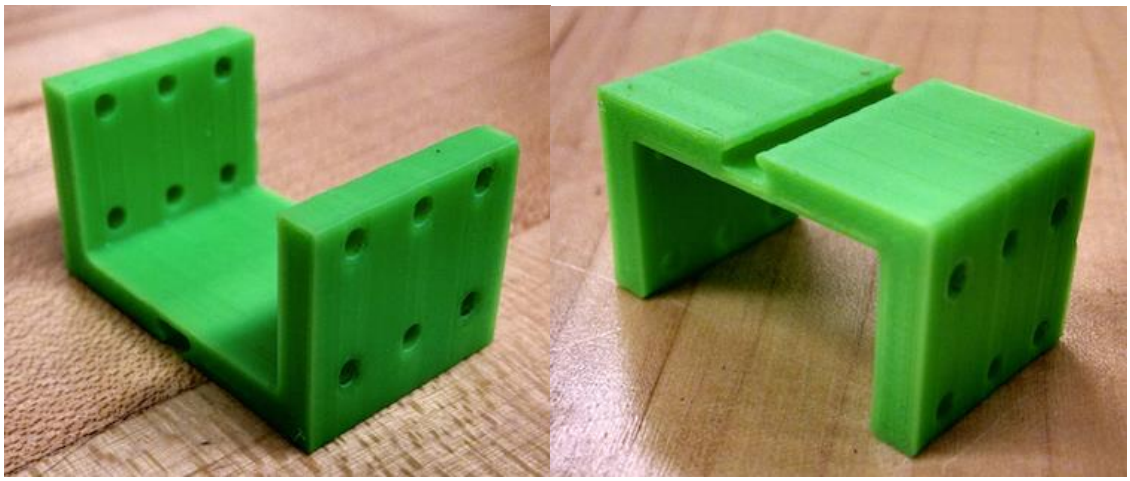

Figure 21: 3D printed harvester guide v2.3

The manufacturing specifications of the harvester guide v2.3 can be seen in Table 20.

Table 20: 3D printing specifications of the harvester guide v2.3

Printing Features	Harvester guide v2.3
3D printer model	Lulzbot TAZ 5
3D printer cost ($)	2200
Printing mass including raft or brim (g)	5
Additional components (raft of brim)	Brim
Final mass (g)	4
Material	Green ABS
Material cost ($/Kg)	19.47
Total cost ($)	0.10
Printing quality	High Detail
Design defects	• None
First component set-up time (min)	8
Printing time (min)	52
Total time (min)	60
Manufacturing defects	• None

7.2.2. Composition and Assembly of the Low Cost Harvester

The 3D printed rail, guide, and base, detailed in the previous sections, were assembled to obtain a low cost harvester. Table 21 presents a listing of all the components that form this low cost harvester.

Table 21: Components of the low cost harvester

Component	Version/Type
Harvester base	Harvester base v3.1.1
Springs	Springs v1
Magnets	Small magnets
Rail	Mushroom rail v1.1
Guide	Guide v2.3
3D printed layer	Original 3D printed layer (N=40)
Big steel plate	Original big steel plate
Small steel plate	Original small steel plate

For this low cost harvester, the only parts that matched the original metallic springless vibration energy harvester are the magnets, 3D printed top cover layer, and both big and small steel plates. This low cost harvester can be seen in Figure 22.

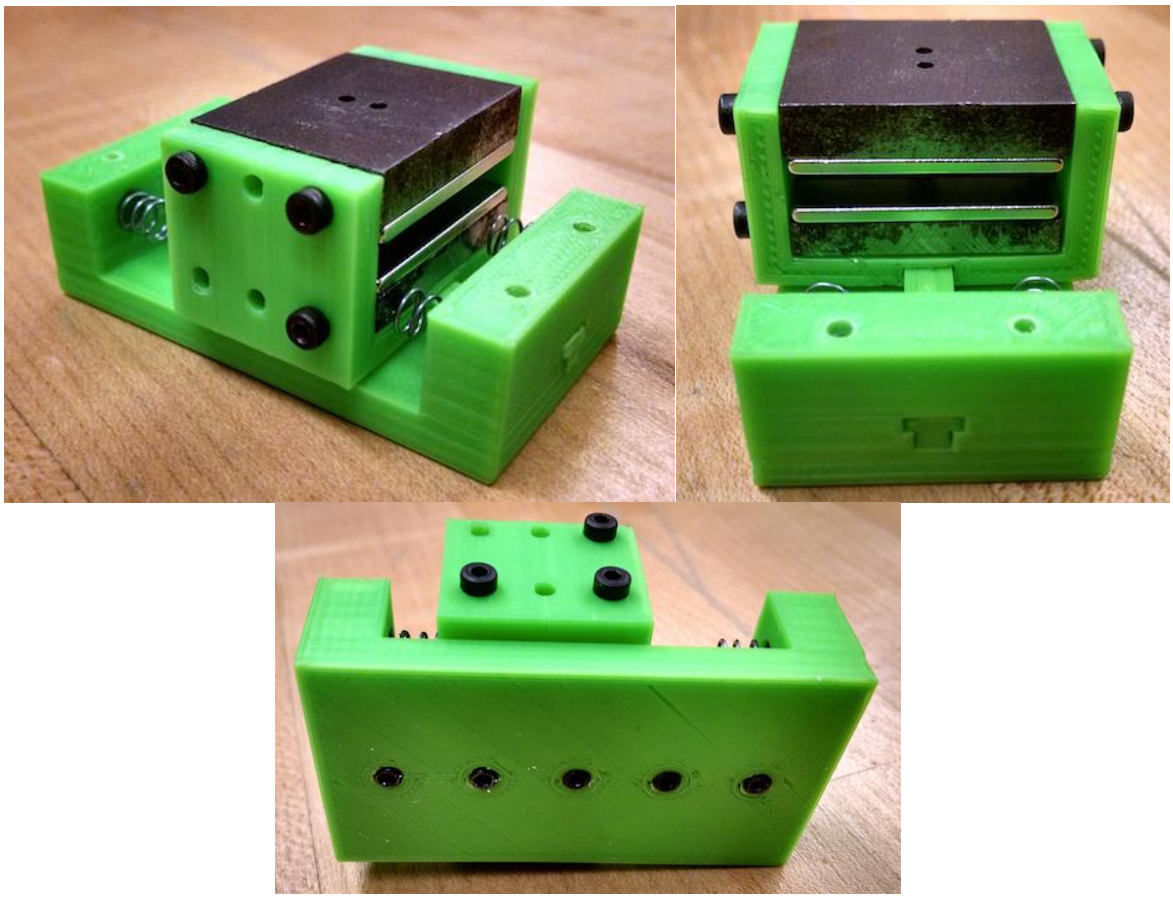

Figure 22: Low cost harvester

7.2.3. Cost Analysis of the Low Cost Harvester

A cost analysis of the new low-cost harvester, similar to the one reported in section 7.1.4, was carried out. A comparative analysis is provided in Table 22.

Table 22: Comparative mass analysis of the harvester

Parts of the Harvester	Original	1st Iteration	2nd Iteration
Magnetic Cart			
Mass of big steel plate (g)	24	24	24
Mass of small steel plate (g)	17	17	17
Mass of copper plates (g)	20	20	20
Mass of magnets (g)	8	8	8
Mass of bolts (g)	6 – (x12)	6 – (x12)	3 - (x6)
Mass of metallic guide (g)	1	1	4 - v2.3 (3D printed)
Mass of original magnetic cart (g)	76	76	76
Harvester Body			
Mass of harvester base with initial springs (g)	23 (metallic)	7- v1.4 (3D printed)	7 – v3.1.1 (3D printed)
Mass of initial magnetic cart (g)	76	76	76
Mass of rail (g)	2 (metallic)	2 (metallic)	1 (3D printed)
Mass of 3D printed layer with cables attached (g)	3	3	3
Mass of base bolts (x5) (g)	2	2	2
Mass of original harvester (g)	**106**	**90**	**89**

The copper plates of the original springless vibration energy harvester were added on top of this new magnetic cart in order to obtain the same mass as the previous magnetic carts, this is, 76 grams. This similar mass is needed to compare test results. A mass reduction of 1 gram is obtained in the low cost harvester when compared to the springless vibration energy harvester with 3D printed base.

Table 23 shows the direct cost comparison for manufacturing the rail and guide of the harvester base using 3D printing against purchasing these parts at $80 direct cost. Although shipping time and cost hast not been considered in the purchasing price of a traditional rail and guide, translating the manufacturing time of the 3D printed parts into money, at a rate of $18 per hour, the cost of the 3D printed part becomes $25.02. The reduction in direct

manufacturing cost by moving to 3D printing from purchasing is 68.7%. Appendix 8 includes a detailed listing of the cost items for each of these manufacturing processes.

Table 23: Direct cost of manufacturing the rail and guide for the harvester using 3D printing compared to purchasing

Manufacturing cost factor	Manufacturing cost ($)	Manufacturing and assembly time (min)
Traditional	80.00 (Purchased)	0
3D printed rail v1.1 & guide v2.3	25.02	83

7.2.4. Performance Testing of The Low Cost Harvester

The low cost harvester was assembled and tested using the experimental setup presented in section 5. The test parameters were the same as those used to test the previous harvester (springless energy harvester with 3D printed base). These parameters included an input acceleration constant at 0.5g with input frequency swept from 5Hz to 17Hz up-sweep and down-sweep separately. Four measurements were considered for each test frequency and the final acceleration and harvester output values were obtained as the average of these four values. To improve the frictional properties of the ABS 3D printed parts (mushroom rail v1.1 and guide v2.3) lithium grease was used. This type of lubricant is selected because its non-affinity with ABS. The main characteristics of this test included the following:

1. The shaker was clamped to the vibration table at two points.
2. The long leg of the L-Section of the connecting base was attached to shaker and the shorter leg hosted the harvester.
3. The accelerometer collecting feedback of the vibration experienced by the harvester was attached to the base of shaker.

4. Frequencies from 5Hz to 17Hz in intervals of 1Hz up-sweep and down-sweep were input to the shaker in a complete incremental set for each direction without any intermediate stops.
5. Ambient noise of 4.02mV RMS in the harvester was observed.
6. Almost constant 0.5g was maintained during the entire test.
7. The mass of the magnetic cart of the harvester was 76 grams, also known as the seismic mass.
8. The experiment was conducted where the vibrating shaker and the harvester were in a Horizontal configuration.

Figure 23 presents the RMS value of the input acceleration to the low cost harvester as seen by the feedback accelerometer.

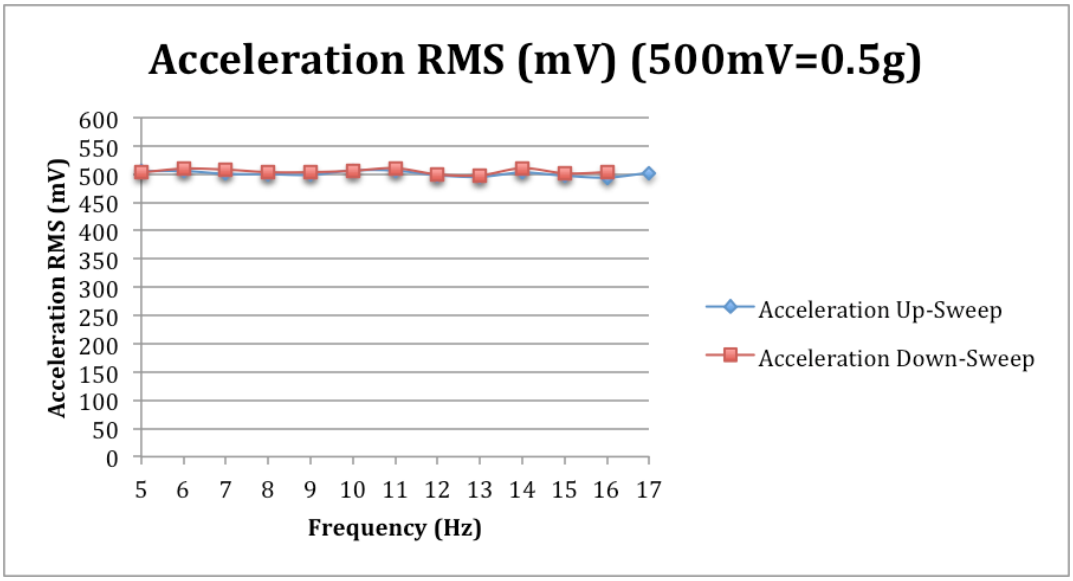

Figure 23: Acceleration RMS plot for the low cost harvester

The acceleration RMS values for the low cost harvester can also be seen in Table 24.

Table 24: Acceleration RMS values for the low cost harvester

Frequency (Hz)	Acceleration RMS (mV)	Frequency (Hz)	Acceleration RMS (mV)
5	504.75	16	503.00
6	505.50	15	501.50
7	500.50	14	510.50
8	500.00	13	498.00
9	498.75	12	499.50
10	506.50	11	510.50
11	506.25	10	506.00
12	498.00	9	503.50
13	495.25	8	503.50
14	502.75	7	508.00
16	497.25	6	509.75
17	494.00	5	503.00
15	502.50	-	-

Figure 24 shows the output RMS voltage obtained for the low cost harvester. The ambient noise is not considered in the results although its value was mentioned at the beginning of this test (4.02mV).

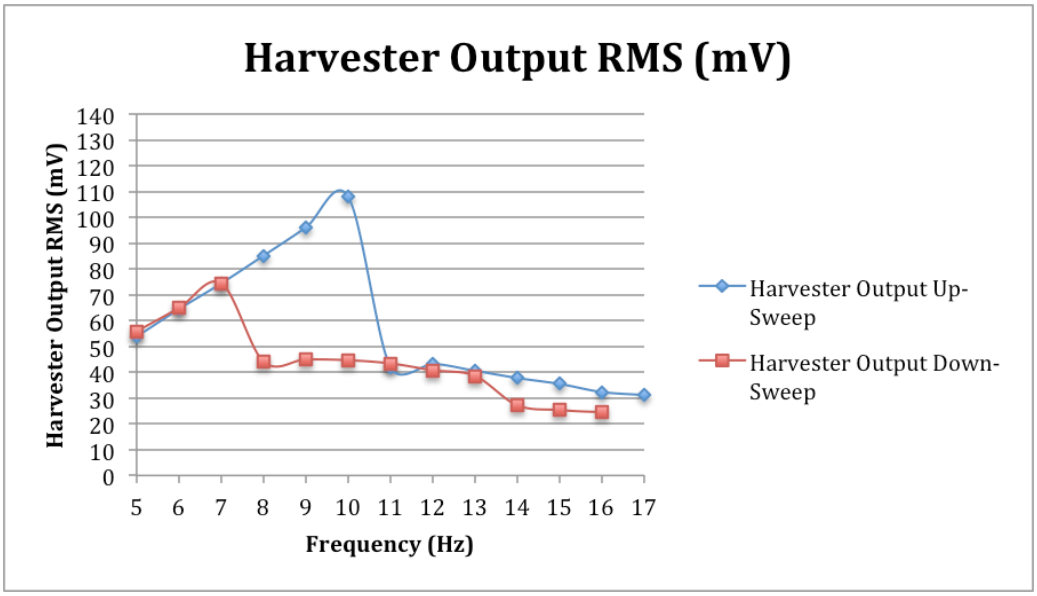

Figure 24: Output RMS voltage plot for the low cost harvester

The output RMS voltage of the harvester increases almost linearly with an increase of frequency reaching a maximum value of 108mV at 10Hz. Then the output voltage suddenly drops and slowly decreases until the final frequency value of 17Hz. During the down-sweep the output voltage slowly increased until 7Hz, when the bouncing movement of the magnetic cart began again, and then decreased linearly following the up-sweep curve. The difference in the frequency value at which the maximum output voltage is obtained between the up-sweep and down-sweep curves (due to the hysteresis phenomenon) can be expressed by the hysteresis interval. The hysteresis interval of the low cost harvester reaches a value of 3Hz. This high value is related to the increase of friction due to the inclusion of a 3D printed miniature linear guide as well as the high value of seismic mass, which is 76 grams in this case. Table 25 includes the output RMS voltage obtained for the low cost harvester.

Table 25: Output RMS voltage values for the low cost harvester

Frequency (Hz)	Output RMS (mV)	Frequency (Hz)	Output RMS (mV)
5	53.70	16	24.38
6	64.43	15	25.35
7	74.40	14	27.18
8	85.13	13	38.55
9	96.05	12	40.78
10	108.00	11	43.40
11	42.03	10	44.65
12	43.23	9	44.95
13	40.55	8	44.18
14	37.75	7	74.48
15	35.45	6	64.88
16	32.33	5	55.80
15	31.15	-	-

Having built the complete frequency response curve with both the up-sweep and down-sweep curves, the bandwidth of the harvester was calculated. This bandwidth is defined as

the difference between the frequency at peak voltage (V_{peak}=108mV at 10Hz for our case) and the frequency at half power point $\boldsymbol{V_{peak}/\sqrt{2}}$ on the up-sweep branch:

$$\boldsymbol{Bandwidth = Frequency_{V_{peak}} - Frequency_{\frac{V_{peak}}{\sqrt{2}}} = 10Hz - 7.18Hz = 2.82Hz}$$

(7.4)

This bandwidth is wider than the bandwidth of any equivalent linear vibration energy harvester, which might be in the order of 2Hz, but narrower than the bandwidth of the springless vibration energy harvester with 3D printed base, which is 3.2Hz.

The maximum RMS output voltage in the low cost harvester was 108mV for a frequency of 10Hz, which is lower than the value obtained in the baseline at 138mV for 13Hz. This decrease of peak voltage can be explained by the higher friction experienced when using 3D printing material to produce the linear guide where the physical motion of the seismic mass takes place. This is the reason an extra lubricant was needed to ensure the closeness of the newly produced harvester functionality to the metallic harvester. Although this maximum output value is lower, the voltage values from 5Hz to 10Hz are slightly higher in the low cost harvester for the same seismic mass.

7.3. Third Iteration: Fully 3D Printed Harvester

The goal of the third iteration was to design, manufacture, and test a fully 3D printed harvester. This harvester is technically based on the same idea of the original springless vibration energy harvester but with a new design suitable for manufacturing using 3D printing and with experience gained from the previous two iterations. Several versions with

variation of components like magnet size were manufactured and tested. Following are the details of the iteration.

7.3.1. Manufacturing the Fully 3D Printed Harvester

The fully 3D printed harvester was based on the previous low cost harvester. The only metallic parts left in the low cost harvester were: bolts, springs, magnets and steel plates. Among those four types of components, bolts, springs and magnets cannot be reproduced for this harvester via the 3D printing processes. However, it is possible to replace the steel plates by 3D printed plates.

7.3.1.1. Replacement of the Steel Plates with 3D Printed Plates

Two different steel plates, denominated as big and small steel plates due to their dimensions, were needed for this harvester. The small steel plate is located on the lower part of the magnetic cart, whereas the big steel plate is located on its upper part. These components were initially designed to accommodate the use of small magnets glued to them, similar to those used in the previous iterations of the springless vibration energy harvester. However, another version was designed and manufactured to accommodate the use of big magnets as a variation from the original harvester.

A total of 5 versions of steel plates were manufactured using the Lulzbot TAZ5 printer in high detail quality mode. It was originally decided to obtain those plates using ABS, and so the 3D printed steel plates v1.0 and v1.1.0 were manufactured. Figure 25 shows the design drawings of the small steel plate v1.0. Appendix 7 includes detailed information about all versions of the 3D printed steel plates.

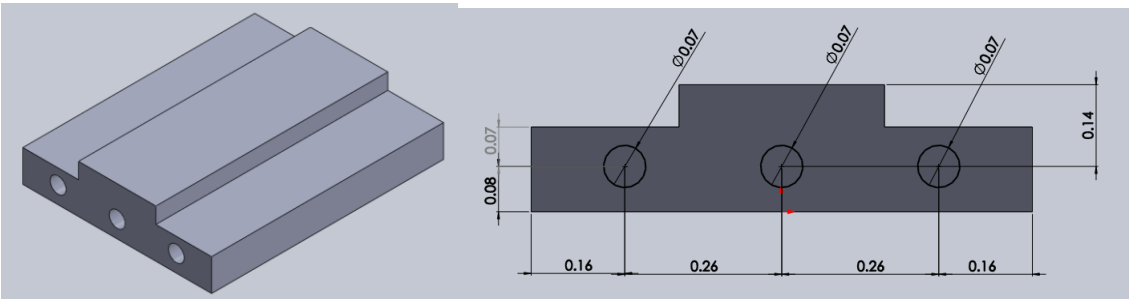

Figure 25: Design drawings of small steel plate v1.0

Figure 26 shows the design drawings of the big steel plate v1.0.

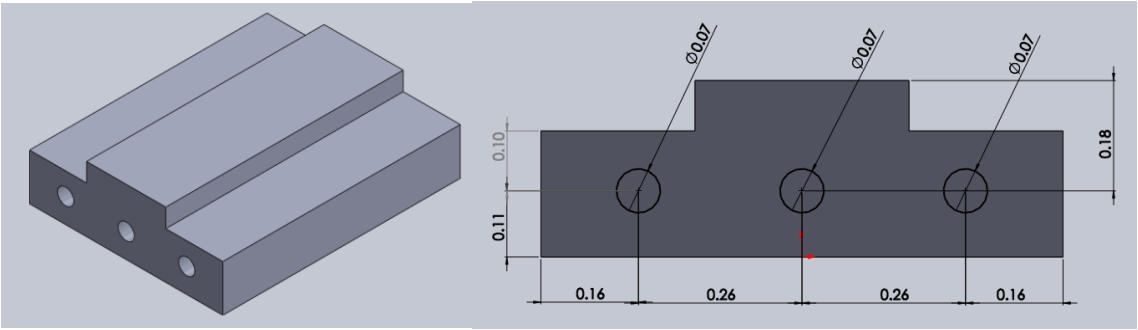

Figure 26: Design drawings of big steel plate v1.0

Table 26 presents the design and manufacturing defects in all the 3D printed steel plates using ABS.

Table 26: Design and manufacturing defects in the 3D printed steel plates using ABS

Steel Plate	Design and Manufacturing Defects
Small v1.0	• Wrong distance between holes • Small hole diameter
Big v1.0	• Wrong distance between holes • Small hole diameter • Wrong distance between holes and upper part of component
Small v1.1.0	• None
Big v1.1.0	• None

ABS is not a ferromagnetic material and would cause the magnetic field generated in between the magnets and coil to escape the harvester. To solve this problem a new

ferromagnetic 3D printed material known as Magnetic Iron PLA was used to build the plates. This material presented ferromagnetic properties and was also magnetic, which became important in the process of attaching the magnets to it. It presented similar properties to PLA although it had iron powder embedded in it. Table 27 includes the properties of this magnetic iron PLA material.

Table 27: Magnetic Iron PLA 3D printing material properties

	Magnetic Iron Polylactic Acid
Material Abbreviation	Magnetic Iron PLA
Material Heating Temperature (C)	230
Material Bed Temperature (C)	60
Filament Spool Price ($)	34.99
Filament Spool Mass (Kg)	0.5

Using magnetic iron PLA allowed the 3D printed plates to behave and influence the harvester structure and functionality similar to the way steel plates would do. However, this material was really difficult to integrate in the available 3D printer (Lulzbot TAZ 5). Several attempts were carried out using different printing temperatures and speeds to produce acceptable plates, but a consistent set of parameters could not be achieved. Based on literature information from users of the same material, manufacturing defects are common while using magnetic iron PLA due to heat creep. Heat creep is caused by a higher than appropriate temperature in the 3D printer right before the extruder, which causes an expansion of the material, and an inconsistent filament (material) flow, which appears in long time prints. To solve this problem a more effective cooling method is needed to dissipate the printer heat more efficiently. A bigger fan to be installed in the 3D printer would be a possible solution. This problem was in fact what caused so many deficiencies in the magnetic iron PLA prints since this material presents similar material properties to PLA.

In spite of the heat creep problem, some decent parts were obtained using magnetic iron PLA. The manufacturing specifications of one set of acceptable 3D printed plates (v1.1.0) can be seen in Table 28. Notice that due to the adhesive properties of the new material, the use of brim was neglected.

Table 28: 3D printing specifications of steel plates replacement v1.1.1

Printing Features	Small steel plate v1.1.1	Big steel plate v1.1.1
3D printer model	Lulzbot TAZ 5	Lulzbot TAZ 5
3D printer cost ($)	2200	2200
Printing mass including raft or brim (g)	5	6
Additional components (raft of brim)	-	-
Final mass (g)	5	6
Material	Magnetic iron PLA	Magnetic iron PLA
Material cost ($/Kg)	69.98	69.98
Total cost ($)	0.35	0.42
Printing quality	High Detail	High Detail
Design defects	• None	• None
First component set-up time (min)	8	8
Printing time (min)	25	35
Total time (min)	33	43
Manufacturing defects	• Heat creep	• Heat creep

To allow a variation on the original design by including a bigger set of magnets in the 3D printed plates, and therefore in the magnetic cart, the dimensions of the 3D printed plates v1.1.1 were modified. The dimensions of these new magnets can be seen in Table 29.

Table 29: Dimensions of big magnets

	Length (inch)	Width (inch)	Thickness (inch)
Small Magnets	1	0.25	0.0625
Big Magnets	1	0.375	0.0625

Similar heat creep defects occurred in some of these prints although two sets of proper 3D printed plates were obtained. These two sets are referred as v1.2.0 and v1.2.1. Design drawings of these new components can be seen in Figure 27.

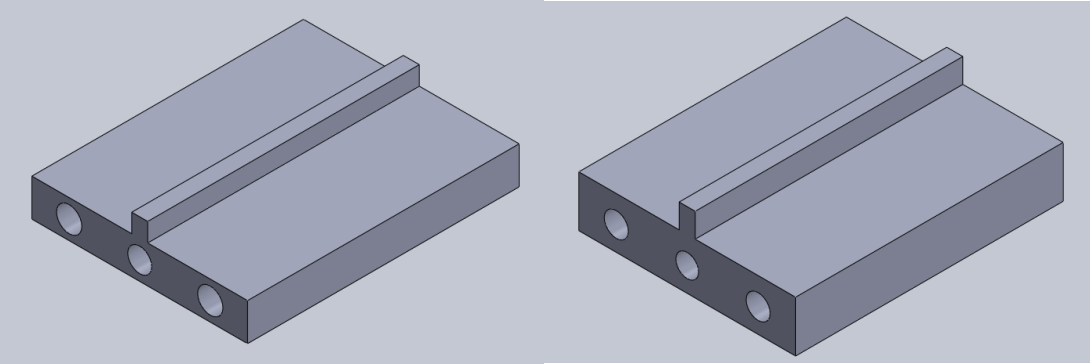

Figure 27: Design drawings of 3D printed small (left) and big (right) plates v1.2

The manufacturing specifications of 3D printed plates v1.2.0 can be seen in Table 30.

Table 30: 3D printing specifications of 3D printed plates v1.2.0

Printing Features	Small steel plate v1.2.0	Big steel plate v1.2.0
3D printer model	Lulzbot TAZ 5	Lulzbot TAZ 5
3D printer cost ($)	2200	2200
Printing mass including raft or brim (g)	3	4
Additional components (raft of brim)	-	-
Final mass (g)	3	4
Material	Magnetic iron PLA	Magnetic iron PLA
Material cost ($/Kg)	69.98	69.98
Total cost ($)	0.21	0.28
Printing quality	High Detail	High Detail
Design defects	• None	• None
First component set-up time (min)	8	8
Printing time (min)	21	29
Total time (min)	29	37
Manufacturing defects	• Heat creep	• Heat creep

The manufacturing specifications of 3D printed plates v1.2.1 can be seen in Table 31.

Table 31: 3D printing specifications of 3D printed plates v1.2.1

Printing Features	Small steel plate v1.2.1	Big steel plate v1.2.1
3D printer model	Lulzbot TAZ 5	Lulzbot TAZ 5
3D printer cost ($)	2200	2200
Printing mass including raft or brim (g)	4	6
Additional components (raft of brim)	-	-
Final mass (g)	4	6
Material	Magnetic iron PLA	Magnetic iron PLA
Material cost ($/Kg)	69.98	69.98
Total cost ($)	0.28	0.42
Printing quality	High Detail	High Detail
Design defects	• None	• None
First component set-up time (min)	8	8
Printing time (min)	21	29
Total time (min)	29	37
Manufacturing defects	• Heat creep	• Heat creep

7.3.2. Composition and Assembly of the Fully 3D Printed Harvester

To test the new fully 3D printed harvester, all components were assembled where two new 3D printed plates, one for small magnets and one for big magnets, were used as well as guide v2.3, and their respective magnets. This generated magnetic cart was then installed in the harvester base v3.1.1 (with springs v1 attached to it). During the assembly process, magnetic attraction was noticed between the springs v1 and the 3D printed plates. This attraction caused the cart to stick longer to the magnets in its departure motion before separating from the springs. The magnetic iron PLA material of the 3D printed plates was magnetized by the presence of the magnets attached to them and therefore attracting the springs to them. This new effect was limiting and worsening the movement of the magnetic cart.

To cancel this magnetic interaction, non-magnetic springs were installed replacing the original steel springs. Stainless steel springs were used, as a non-ferromagnetic material. The dimensions of the new springs, denominated as springs v2, can be seen in Table 32.

Table 32: Dimensions of stainless steel springs v2

	Outside Diameter (inch)	Wire Diameter (inch)	Total Length (inch)	Rate (lbs/inch)	Material
Springs v1	0.18	0.018	0.25	13.5	Music wire
Springs v2	0.125	0.016	0.25	16.22	Stainless steel

However, a slight magnetic attraction could still be felt between the springs and the magnetic iron PLA components. Therefore, a redesign of the harvester base was considered where the holes for the springs to be installed in the harvester base were lowered below the level of the plates. This would result in the contact between the springs and the cart occurring at the guide v2.3 (ABS component) and not at the 3D printed small plate.

The modifications of the base design were also required to accommodate the new stainless steel springs within harvester base v3.1.1. These modifications were applied in the harvester base v3.2.0 including a smaller diameter for the spring holes (0.135") as well as lowering these holes to 0.32" from the top to avoid magnetic attraction. In a following version, v3.2.1, a minor modification was added by increasing its total height from 0.57" to 0.585". This variation was considered to avoid possible contact between the original 3D printed layer (as well as the 3D printed layer v1.1) and the magnetic cart.

Figure 28 shows the design drawing of the modified harvester base v3.2.0.

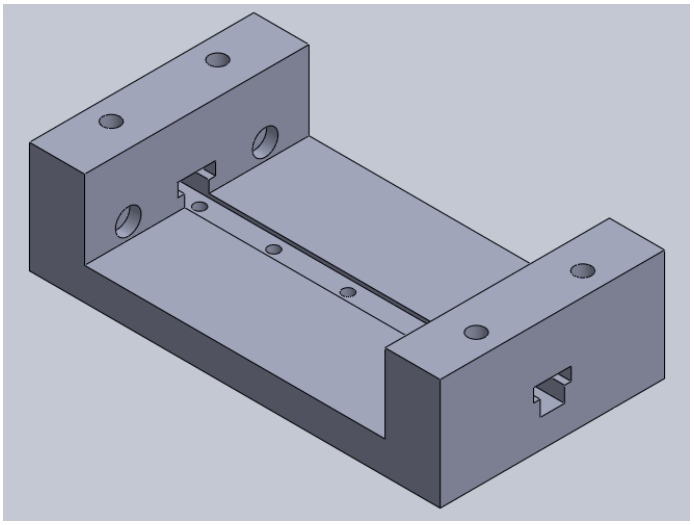

Figure 28: Design drawing of harvester base v3.2.0

The 3D printing specifications of the base v3.2.0 can be seen in Table 33.

Table 33: Harvester base v3.2.0 3D printing specifications

Printing Features	Harvester base v3.2.0
3D printer model	Lulzbot TAZ 5
3D printer cost ($)	2200
Printing mass including raft or brim (g)	9
Additional components (raft of brim)	Brim
Final mass (g)	7
Material	Green ABS
Material cost ($/Kg)	19.47
Total cost ($)	0.18
Printing quality	High Detail
Design defects	• None
First component set-up time (min)	8
Printing time (min)	76
Total time (min)	84
Manufacturing defects	• None

The 3D printing specifications of the base v3.2.1 can be seen in Table 34.

Table 34: Harvester base v3.2.1 3D printing specifications

Printing Features	Harvester base v3.2.1
3D printer model	Lulzbot TAZ 5
3D printer cost ($)	2200
Printing mass including raft or brim (g)	9
Additional components (raft of brim)	Brim
Final mass (g)	7
Material	Green ABS
Material cost ($/Kg)	19.47
Total cost ($)	0.18
Printing quality	High Detail
Design defects	• None
First component set-up time (min)	8
Printing time (min)	76
Total time (min)	84
Manufacturing defects	• None

The modification of the design of the harvester base v3.2.1 resulted in a design modification trickling back to the harvester guide v2.3. In a new modified version, guide v2.4, the total height of the harvester guide was increased from 0.75" to 0.78".

The manufacturing specifications of the harvester guide v2.4 can be seen in Table 35.

Table 35: 3D printing specifications of harvester guide v2.4

Printing Features	Harvester guide v2.3
3D printer model	Lulzbot TAZ 5
3D printer cost ($)	2200
Printing mass including raft or brim (g)	5
Additional components (raft of brim)	Brim
Final mass (g)	4
Material	Green ABS
Material cost ($/Kg)	19.47
Total cost ($)	0.10
Printing quality	High Detail
Design defects	• None
First component set-up time (min)	8
Printing time (min)	52
Total time (min)	60
Manufacturing defects	• None

7.3.3. Composition and Assembly of the Fully 3D Printed Harvester

The 3D printed plates v1.1.1 and the small magnets were mounted on guide v2.3 to assemble the magnetic cart of the fully 3D printed harvester with small magnets. This magnetic cart is referred to as v1.1.1. The magnets were partially attracted by the magnetic iron PLA plates causing added cohesion to the glue. The polarity arrangement of the magnets installed in the magnetic cart v1.1.1 can be seen in Figure 29.

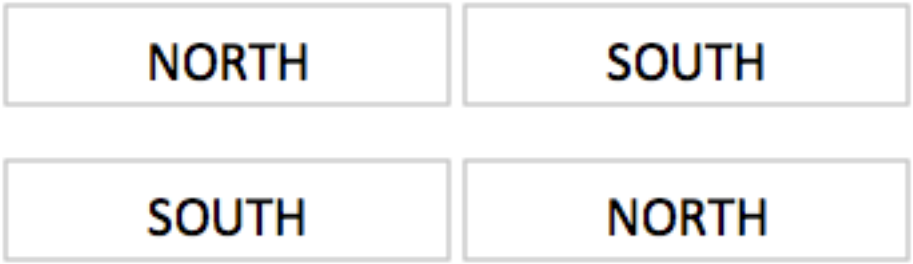

Figure 29: Polarity of magnets in magnetic cart v1.1.1

This magnetic cart was assembled to the mushroom rail v1.1 and the harvester base v3.2.0 to form the fully 3D printed harvester with small magnets v1.1.1. The assembly of the small magnets to the 3D printed plate v1.1.1 can be seen in Figure 30.

Figure 30: Assembly of magnets in big 3D printed plate v1.1.1

The components that form this fully 3D printed harvester with small magnets v1.1.1 are presented in Table 36.

Table 36: Components of the fully 3D printed harvester with small magnets v1.1.1

Component	Version/Type
Harvester base	Harvester base v3.2.0
Springs	Springs v2
Magnets	Small magnets
Rail	Mushroom rail v1.1
Guide	Guide v2.3
3D printed layer	Original 3D printed layer (N=40)
Big steel plate	3D printed big steel plate v1.1.1
Small steel plate	3D printed small steel plate v1.1.1

In a similar fashion, the big magnets and the 3D printed steel plates (v1.2.0 or v1.2.1) were assembled to the guide v2.4 to form the magnetic cart of the fully 3D printed harvester with big magnets (v1.2.0 or v1.2.1 respectively). The orientation of the magnets was also similar to that considered for the small magnets. The use of different types of magnets would allow testing with different magnetic fluxes to compare how this parameter affects the amount of voltage harvested. As an example, the assembly of the big magnets to the 3D printed big plate v1.2.0 can be seen in Figure 31.

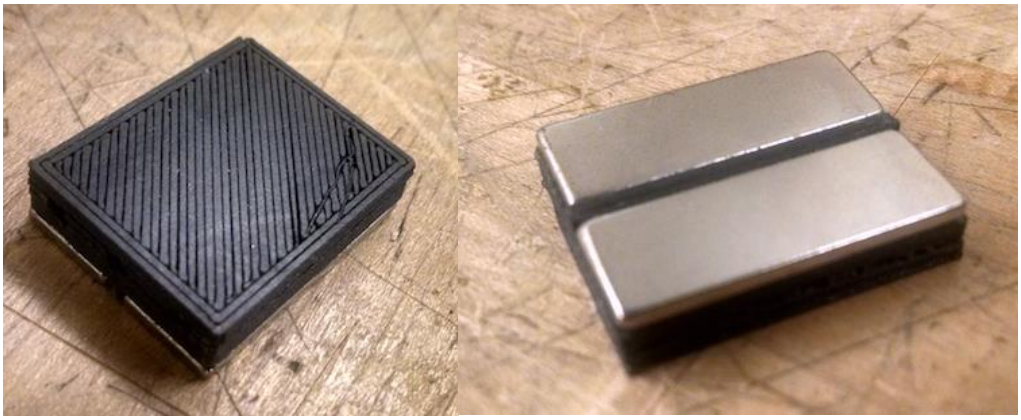

Figure 31: Assembly of magnets in small 3D printed plate v1.2.0

Also, the assembly of the fully 3D printed magnetic cart v1.2.0 with big magnets can be seen in Figure 32.

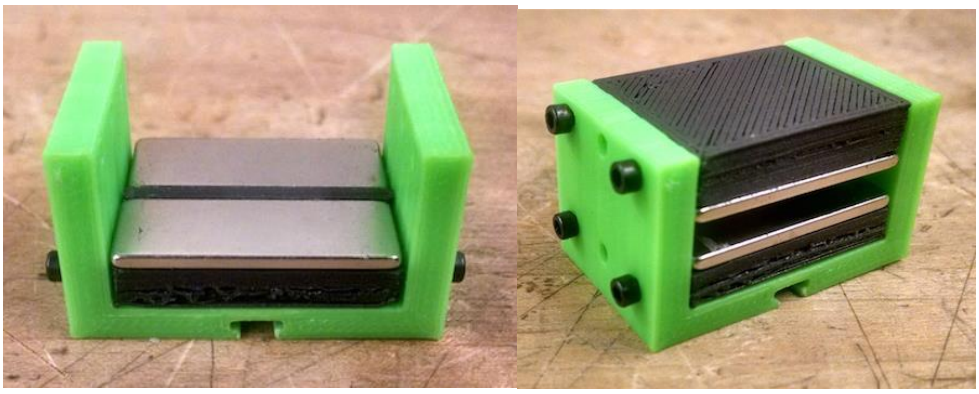

Figure 32: Assembly of fully 3D printed magnetic cart with big magnets v1.2.0

This magnetic cart (v1.2.0 or v1.2.1) was assembled to the mushroom rail v1.1 and the harvester base v3.2.1 to form the fully 3D printed harvester with big magnets (v1.2.0 or v1.2.1 respectively). The components that form this fully 3D printed harvester with big magnets are presented in Table 37.

Table 37: Components of the fully 3D printed harvester with big magnets v1.2.0/v1.2.1

Component	Version/Type
Harvester base	Harvester base v3.2.1
Springs	Springs v2
Magnets	Big magnets
Rail	Mushroom rail v1.1
Guide	Guide v2.4
3D printed layer	Original 3D printed layer (N=40)
Big steel plate	3D printed big steel plate v1.2.0 / v1.2.1
Small steel plate	3D printed small steel plate v1.2.0 / v1.2.1

7.3.4. Cost analysis of the Fully 3D Printed Harvester

Cost analysis was carried out for all versions of the fully 3D printed harvester. Table 38 presents a comparative listing of related details.

Table 38: Comparative mass analysis of all the 3D fully printed harvester versions (Iteration 3 only)

Parts of the Harvester	Small magnet v1.1.1	Big magnet v1.2.0	Big magnet v1.2.1
Magnetic Cart			
Mass of big printed plate (g)	6	4	6
Mass of small printed plate (g)	5	3	4
Mass of copper plates (g)	0	0	0
Mass of magnets (g)	8	12	12
Mass of bolts (x6) (g)	1	1	1
Mass of metallic guide (g)	4	4	4
Mass of original magnetic cart (g)	24	24	27
Harvester Body			
Mass of harvester base with springs (g)	8	8	8
Mass of magnetic cart (g)	24	24	27
Mass of printed rail (g)	1	1	1
Mass of 3D printed layer w/ cables attached (g)	3	3	3
Mass of original harvester (g)	**36**	**36**	**39**

The table above shows a considerable seismic mass reduction for the three versions of fully 3D printed harvesters with respect to the low cost harvester magnetic cart and the magnetic cart of the springless vibration energy harvester with 3D printed base. This reduction in mass is expected to proportionally decrease the harvester output voltage for the same input vibration compared to the harvesters in previous iterations.

The increase in magnet size in v1.2.0 affects the amount of 3D printed material allowed in the 3D printed steel plates v1.2.0 for the same fixed volume as in v1.1.1. This reduction in the amount of 3D printed material in the plates v1.2.0 generates a mass reduction of the 3D printed plates that combined with a 33.33% mass increase in the magnets ends up with a seismic mass identical to that of v1.1.1. The increase in magnet mass combined with an improvement in the 3D printing parameters, allows for a global seismic mass increase from

24 grams in v1.1.1 and v1.2.0 to 27 grams in v1.2.1. These new 3D printing parameters increase the 3D printing density by decreasing the 3D printing filament thickness.

Table 39 shows the direct cost comparison for manufacturing steel plates of the harvester cart, with a small magnet, traditionally, as opposed to using 3D printing. Translating manufacturing time into monetary value at the same hourly rate of $18/hour, the cost of traditional manufacturing becomes $181 while the cost of 3D printing for the same parts becomes $23.57. The saving of this change is 87% in this particular part of the harvester. Appendix 8 includes a detailed listing of the cost items for each of these manufacturing processes.

Table 39: Direct cost of manufacturing of steel plates for the harvester traditionally and using 3D printing with replacement material

Manufacturing cost factor	Material cost ($)	Machining and assembly time (min)
Traditional	181 (1215 Carbon Steel)	369
3D printed (v1.1.1)	23.57 (Magnetic iron PLA)	76

Table 40 includes the details of the cost and time of the fully 3D printed harvester.

Table 40: Cost and time analysis of the fully 3D printed harvester

Fully 3D printed harvester				
	Small magnets v1.1.1		Big magnets v1.2.0	
	Time (min)	Cost ($)	Time (min)	Cost ($)
Harvester base v3.2.0	84	0.18	84	0.18
Springs v2 (x4)	-	3.34	-	3.34
Harvester base bolts (x5)	-	0.32	-	0.32
Mushroom rail v1.1	23	0.02	23	0.02
Guide v2.3	60	0.10	60	0.10
Guide bolts (x12)	-	1.06	-	1.06
3D printed layer v1.1	21	0.09	21	0.09
3D printed layer bolts (x4)	-	0.26	-	0.26
Big steel plate v1.1.1	25	0.42	29	0.28
Small steel plate v1.1.1	35	0.35	21	0.21
Small magnets (x4)	-	3.16	-	4.32
Total	248	9.29	238	10.17

7.3.5. Performance Testing of the Fully 3D Printed Harvesters

Performance of the different versions of the fully 3D printed harvester was tested at the following conditions and characteristics:

1. The shaker was clamped to the vibration table at two points.
2. The long leg of the L-Section of the connecting base was attached to shaker and the shorter leg hosted the harvester.
3. The accelerometer collecting feedback of the vibration experienced by the harvester was attached to the base of shaker.
4. Frequencies from 5Hz to 15Hz in intervals of 1Hz up-sweep and down-sweep were input to the shaker in a complete incremental set for each direction without any intermediate stops.
5. Ambient noise of 4.02mV RMS in the harvester was observed.
6. Almost constant 0.5g was maintained during the entire test.

7. The experiment was conducted where the vibrating shaker and the harvester were in a Horizontal configuration.
8. The mass of the magnetic cart was different for each version.

7.3.5.1. Test of the fully 3D printed harvester with small magnets v1.1.1

In this test the mass if the magnetic cart, or the seismic mass was 24 grams. Four measurements were considered for each test frequency and the final acceleration and harvester output values were obtained as the average of these four values. Figure 33 presents the acceleration RMS values for the fully 3D printed harvester with small magnets v1.1.1.

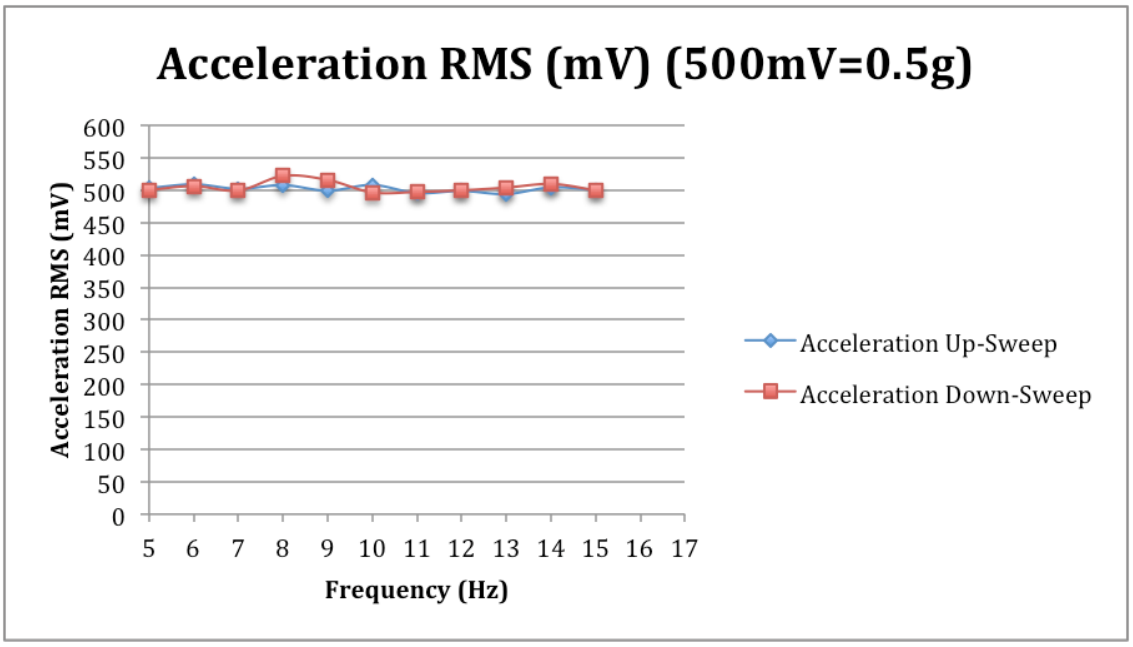

Figure 33: Acceleration RMS plot for the fully 3D printed harvester with small magnets v1.1.1

The acceleration RMS values for the fully 3D printed harvester with small magnets v1.1.1 can also be seen in Table 41.

Table 41: Acceleration RMS values for the fully 3D printed harvester with small magnets v1.1.1

Frequency (Hz)	Acceleration RMS (mV)	Frequency (Hz)	Acceleration RMS (mV)
5	502.75	14	509.50
6	509.00	13	504.00
7	502.00	12	499.75
8	507.75	11	497.25
9	499.25	10	496.50
10	508.00	9	515.75
11	495.50	8	522.00
12	498.75	7	499.50
13	494.00	6	506.25
14	504.25	5	500.25
15	500.50	-	-

Figure 34 shows the output RMS voltage obtained for the fully 3D printed harvester with small magnets v1.1.1. The ambient noise is not considered in the results although its value was mentioned at the beginning of this test (4.02mV).

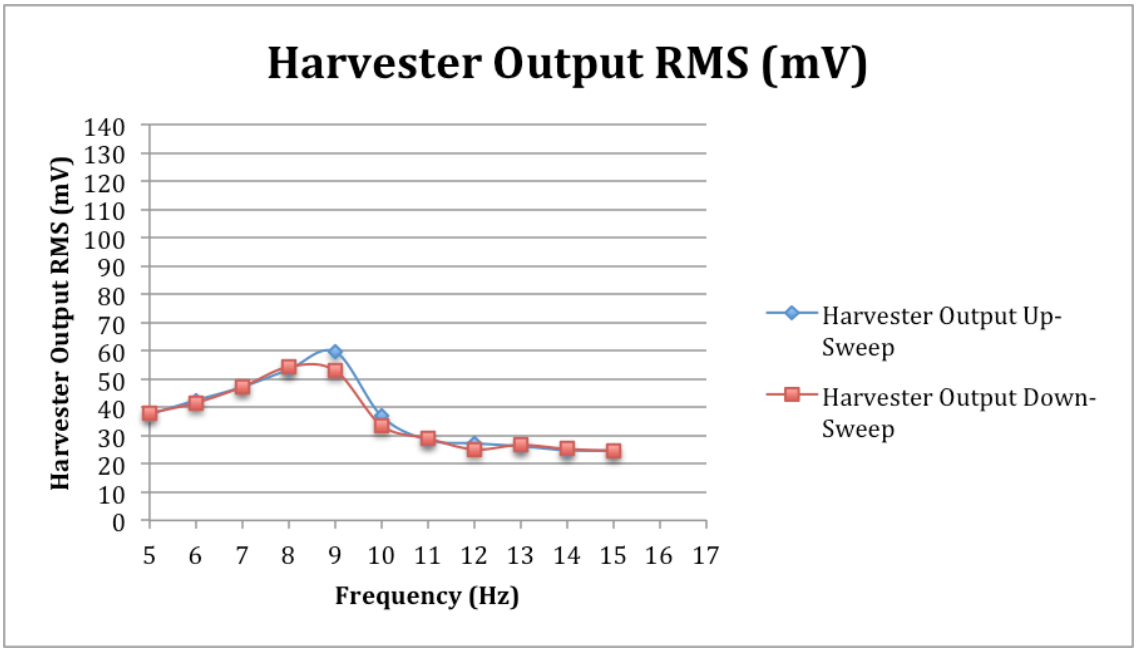

Figure 34: Output RMS voltage plot for the fully 3D printed harvester with small magnets v1.1.1

The output RMS voltage of the harvester increases almost linearly with an increase of frequency reaching a maximum value of 59.58mV at 9Hz. Then the output voltage suddenly

drops and slowly decreases until the final frequency value of 15Hz. During the down-sweep the output voltage slowly increased until 9Hz, when the bouncing movement of the magnetic cart began again, and then decreased linearly following the up-sweep curve. A great reduction in the harvester hysteresis interval can be appreciated when comparing with Figure 24 (hysteresis interval of 3Hz). This reduction is due to the decrease of seismic mass from 76 grams to 24 grams, when considering identical components in the miniature linear guide. The lower seismic mass reduces the friction in between the guide and the rail of the miniature linear guide and then the bouncing movement of the magnetic cart in the down-sweep cycle can begin for a higher frequency. Table 42 includes the output RMS voltage obtained for the fully 3D printed harvester with small magnets v1.1.1.

Table 42: Output RMS voltage values for the fully 3D printed harvester with small magnets v1.1.1

Frequency (Hz)	Output RMS (mV)	Frequency (Hz)	Output RMS (mV)
5	37.58	14	25.25
6	42.48	13	26.68
7	47.20	12	25.08
8	53.35	11	28.98
9	59.58	10	33.55
10	36.93	9	52.93
11	28.43	8	54.28
12	27.25	7	47.20
13	26.23	6	41.58
14	24.78	5	37.95
15	24.63	-	-

Having built the complete frequency response curve with both the up-sweep and down-sweep curves, the bandwidth of the harvester was calculated. This bandwidth is defined as the difference between the frequency at peak voltage (V_{peak}=59.58mV at 9Hz for our case) and the frequency at half power point $\boldsymbol{V_{peak}/\sqrt{2}}$ on the up-sweep branch:

$$\boldsymbol{Bandwidth = Frequency_{V_{peak}} - Frequency_{\frac{V_{peak}}{\sqrt{2}}} = 9Hz - 5.93Hz = 3.07Hz}$$

(7.5)

This bandwidth is also considerably wider that the bandwidth of linear vibration energy harvester, which might be around 2Hz.

7.3.5.2. Test of Fully 3D printed harvester with small magnets v1.1.1 and increased mass

Mass of the small magnet harvester v1.1.1 was increased to monitor the effect on the output voltage and the harvester's global displacement behavior. The original steel plates of the springless vibration energy harvester were glued to the top of the magnetic cart. These additional components increased the mass of the magnetic cart from 24 grams to 63 grams. The same testing characteristics and ambient noise as in the initial fully 3D printed harvester with small magnets v1.1.1 were used (except the magnetic cart mass).

Figure 35 shows the position of the steel plates on top of the magnetic cart of the harvester and the setup during the test.

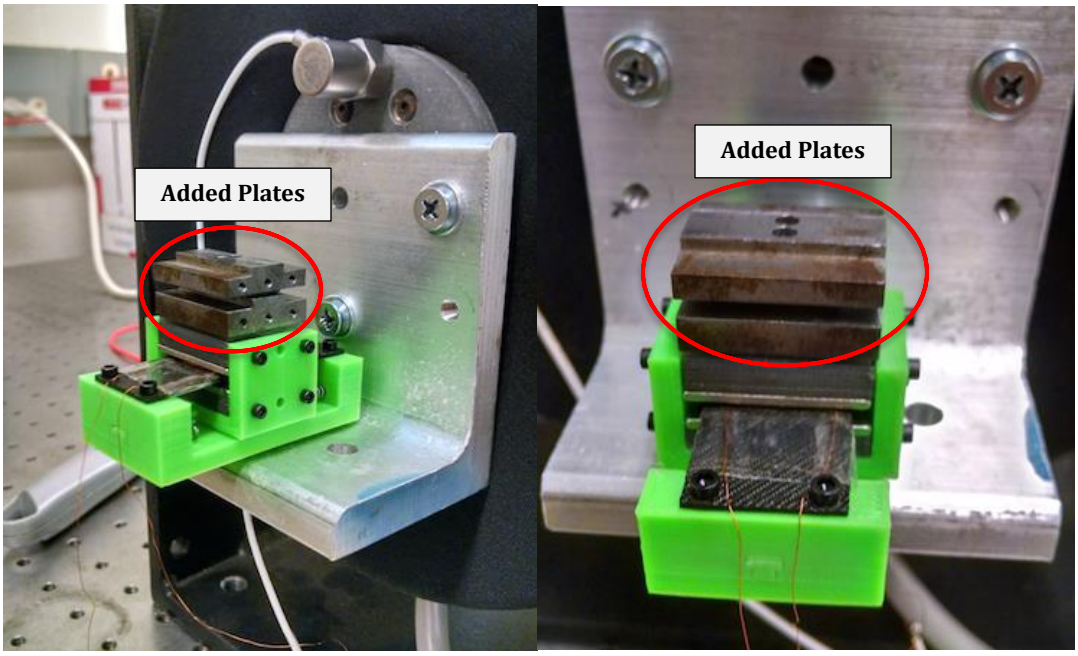

Figure 35: Test setup of fully 3D printed harvester with small magnets v1.1.1 and increased mass

Figure 36 presents the acceleration RMS values for the fully 3D printed harvester with small magnets v1.1.1 and increased mass.

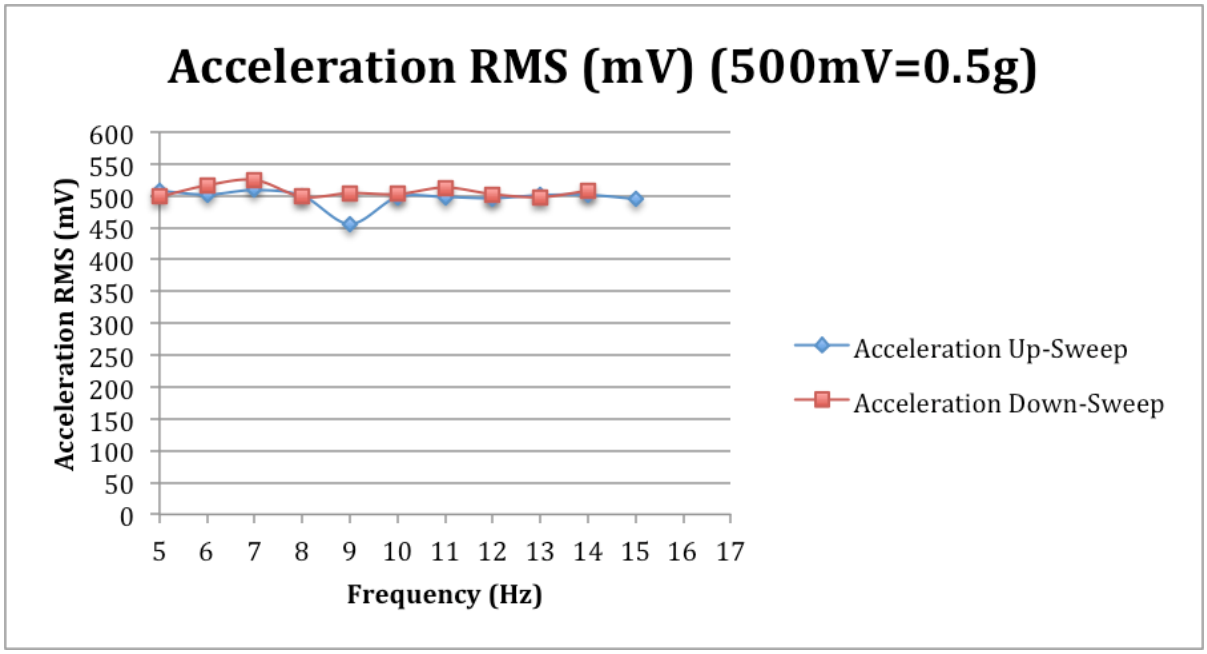

Figure 36: Acceleration RMS plot for the fully 3D printed harvester with small magnets v1.1.1 and increased mass

The acceleration RMS values for the fully 3D printed harvester with small magnets v1.1.1 and increased mass can also be seen in Table 43.

Table 43: Acceleration RMS values for the fully 3D printed harvester with small magnets v1.1.1 and increased mass

Frequency (Hz)	Acceleration RMS (mV)	Frequency (Hz)	Acceleration RMS (mV)
5	507.75	14	508.25
6	502.00	13	498.00
7	509.00	12	502.50
8	500.00	11	513.00
9	456.00	10	502.75
10	498.00	9	504.25
11	498.25	8	498.50
12	496.25	7	524.75
13	501.00	6	516.50
14	501.50	5	498.50
15	495.00	-	-

Figure 37 shows the output RMS voltage obtained for the fully 3D printed harvester with small magnets v1.1.1 and increased mass. The ambient noise is not considered in the results although its value was mentioned at the beginning of this test (4.02mV).

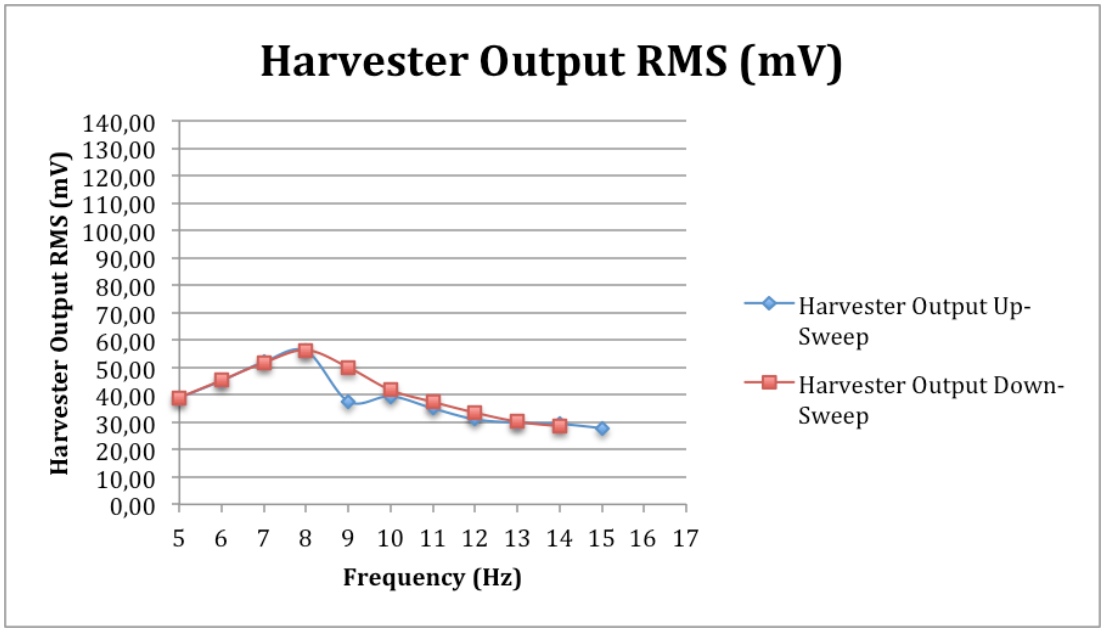

Figure 37: Output RMS voltage plot for the fully 3D printed harvester with small magnets v1.1.1 and increased mass

The output RMS voltage of the harvester increases almost linearly with an increase of frequency reaching a maximum value of 55.9mV at 8Hz. Then the output voltage suddenly drops and slowly decreases until the final frequency value of 15Hz. During the down-sweep the output voltage slowly increased until 8Hz, when the bouncing movement of the magnetic cart began again, and then decreased linearly following the up-sweep curve. Note that a small increase in output RMS maximum voltage is obtained in this harvester up to 8Hz when compared to the fully 3D printed harvester with small magnets v1.1.1 due to the increase in mass (55.9mV for 63 grams at 8HZ versus 53.35mV for 24 grams at 8Hz). The increase of output maximum voltage at this frequency is relatively small compared to the increase of mass. This is due to the instability that the additional mass creates in the system by displacing the center of mass to a more un-centered position. The movement of the seismic mass becomes unstable and unpredictable and so the bandwidth decreases. When comparing the output voltage at 9 Hz the addition of mass seems to be counterproductive. Table 44 includes the output RMS voltage obtained for the fully 3D printed harvester with small magnets v1.1.1 and increased mass.

Table 44: Output RMS voltage for the fully 3D printed harvester with small magnets v1.1.1 and increased mass

Frequency (Hz)	Output RMS (mV)	Frequency (Hz)	Output RMS (mV)
5	39.00	14	28.40
6	45.13	13	30.18
7	51.98	12	33.45
8	55.90	11	37.38
9	37.58	10	41.73
10	39.43	9	49.98
11	35.03	8	56.28
12	31.03	7	51.68
13	29.83	6	45.30
14	29.35	5	39.00
15	27.83	-	-

Having built the complete frequency response curve with both the up-sweep and down-sweep curves, the bandwidth of the harvester was calculated. This bandwidth is defined as the difference between the frequency at peak voltage (V_{peak}=55.90mV at 8Hz for our case) and the frequency at half power point $\boldsymbol{V_{peak}/\sqrt{2}}$ on the up-sweep branch:

$$\boldsymbol{Bandwidth = Frequency_{V_{peak}} - Frequency_{\frac{V_{peak}}{\sqrt{2}}} = 8Hz - 5.09Hz = 2.91Hz}$$

(7.6)

This bandwidth is also considerably wider that the bandwidth of linear vibration energy harvester, which might be in the order of 2Hz.

7.3.5.3. Test of Fully3D printed harvester with big magnets v1.2.0

The same test conditions and ambient noise as in the initial fully 3D printed harvester with small magnets v1.1.1 were used. The mass of the magnetic cart was 24 grams. Figure 38 presents the acceleration RMS values for the fully 3D printed harvester with big magnets v1.2.0.

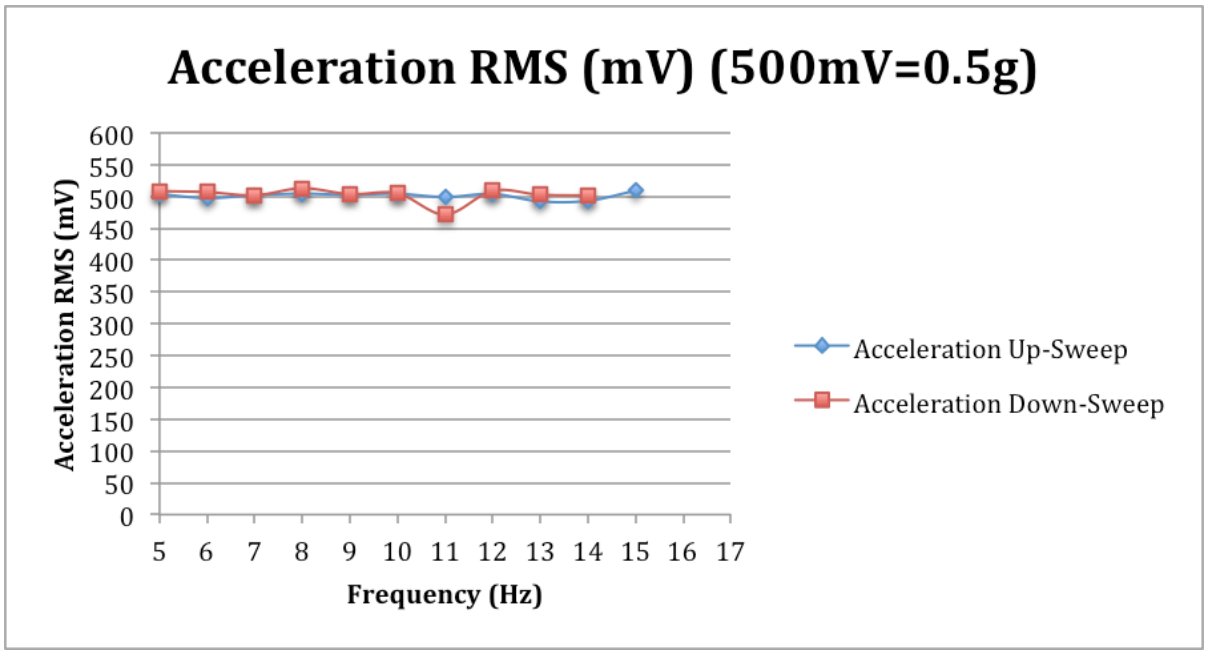

Figure 38: Acceleration RMS plot for the fully 3D printed harvester with big magnets v1.2.0

The acceleration RMS values for the fully 3D printed harvester with big magnets v1.2.0 can also be seen in Table 45.

Table 45: Acceleration RMS values for the fully 3D printed harvester with big magnets v1.2.0

Frequency (Hz)	Acceleration RMS (mV)	Frequency (Hz)	Acceleration RMS (mV)
5	504.00	14	502.00
6	497.50	13	502.75
7	502.25	12	509.00
8	504.50	11	471.75
9	502.75	10	505.00
10	504.25	9	503.75
11	499.25	8	513.00
12	504.00	7	502.00
13	492.25	6	507.00
14	493.25	5	508.50
15	509.25	-	-

Figure 39 shows the output RMS voltage obtained for the fully 3D printed harvester with big magnets v1.2.0. The ambient noise is not considered in the results although its value was mentioned at the beginning of this test (4.02mV).

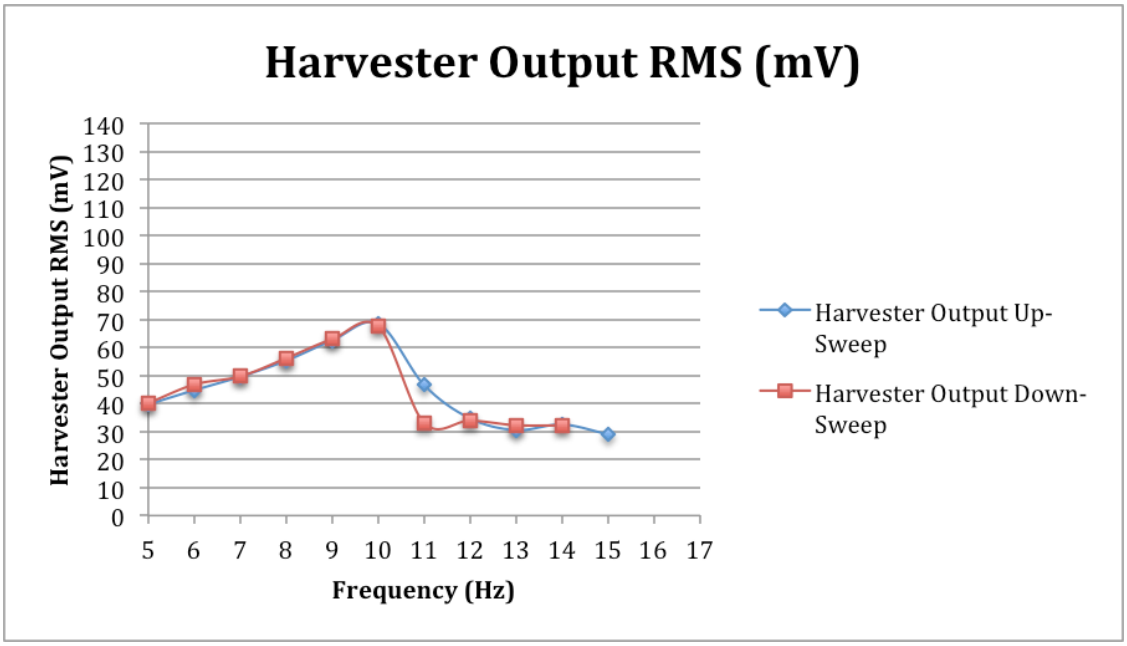

Figure 39: Output RMS voltage plot for the fully 3D printed harvester with big magnets v1.2.0

The output RMS voltage of the harvester increases almost linearly with an increase of frequency reaching a maximum value of 68.5mV at 10Hz. Then the output voltage suddenly drops and slowly decreases until the final frequency value of 15Hz. During the down-sweep the output voltage slowly increased until 10Hz, when the bouncing movement of the magnetic cart began again, and then decreased linearly following the up-sweep curve. Note that a small increase in output maximum voltage is obtained in the fully 3D printed harvester with big magnets v1.2.0 when compared to the fully 3D printed harvester with small magnets v1.1.1 due to the variation in magnets size and mass (68.5mV for the fully 3D printed harvester with big magnets v1.2.0 versus 59.58mV for the fully 3D printed harvester with small magnets v1.1.1). This variation of 13% in the maximum output voltage is obtained

through an increase in magnetic mass of 33.33%. It can be then deduced that this method of improving the performance of the harvester via increasing the magnetic mass is not very effective. In addition it needs to be considered the fact that since the amount of ferromagnetic material in the 3D printed steel plates is reduced in this version of iteration 3, more magnetic flux is escaping the magnetic cage, rendering the harvester less effective. A similar hysteresis interval is obtained for both v1.1.1 and v1.2.0. Table 46 includes the output RMS voltage obtained for the fully 3D printed harvester with big magnets v1.2.0.

Table 46: Output RMS voltage values for the fully 3D printed harvester with big magnets v1.2.0

Frequency (Hz)	Output RMS (mV)	Frequency (Hz)	Output RMS (mV)
5	39.73	14	32.28
6	44.75	13	32.25
7	49.58	12	33.90
8	55.30	11	33.08
9	62.53	10	67.50
10	68.50	9	63.00
11	46.58	8	56.18
12	34.65	7	49.70
13	30.50	6	46.78
14	32.50	5	40.13
15	29.00	-	-

Having built the complete frequency response curve with both the up-sweep and down-sweep curves, the bandwidth of the harvester was calculated. This bandwidth is defined as the difference between the frequency at peak voltage (V_{peak}=68.5mV at 10Hz for our case) and the frequency at half power point $\boldsymbol{V_{peak}/\sqrt{2}}$ on the up-sweep branch:

$$\boldsymbol{Bandwidth = Frequency_{V_{peak}} - Frequency_{\frac{V_{peak}}{\sqrt{2}}} = 10Hz - 6.76Hz = 3.24Hz} \quad (7.7)$$

This bandwidth is also considerably wider that the bandwidth of linear vibration energy harvester, which might be in the order of 2Hz.

7.3.5.4. Test of Fully 3D printed harvester with big magnets v1.2.1

Version 1.2.1 of the fully 3D harvester with big magnets had an increased seismic mass from 24 g, which was the mass of version 1.2.0, to 27g. The mass variation was due to the quality of the magnetic PLA 3D printed plates. The quality of these parts increased and so did the mass. The same testing characteristics as in the fully 3D printed harvester with small magnets v1.1.1 were used (except the magnetic cart mass).

Figure 40 presents the acceleration RMS values for the fully 3D printed harvester with big magnets v1.2.1.

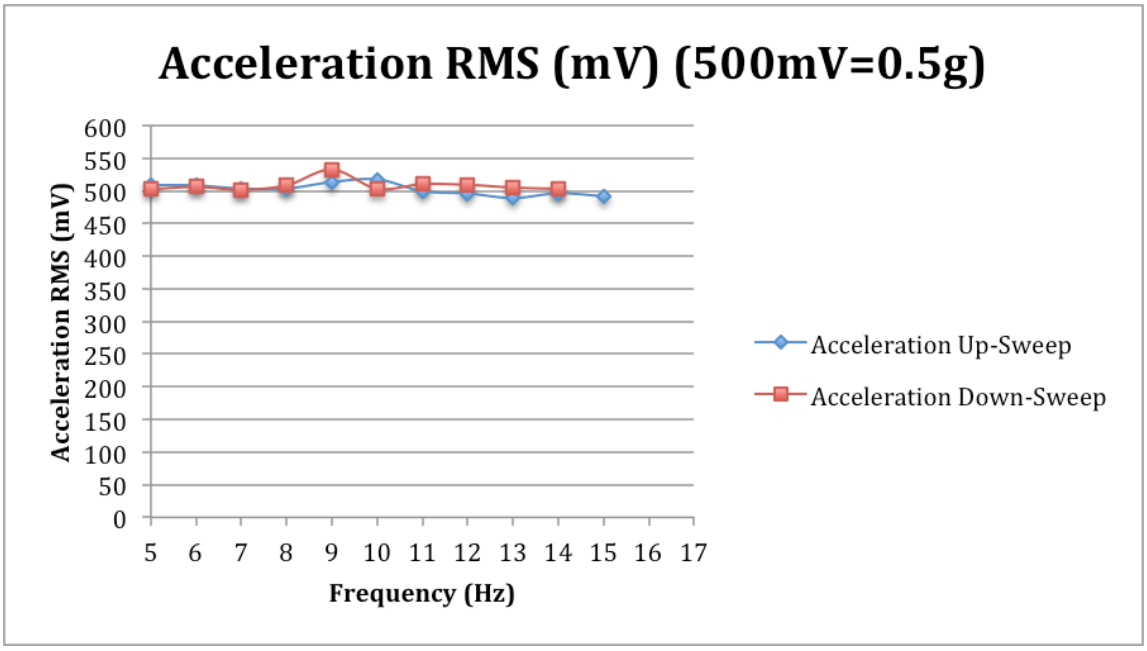

Figure 40: Acceleration RMS plot for the fully 3D printed harvester with big magnetsv1.2.1

The acceleration RMS values for the fully 3D printed harvester with big magnets v1.2.1 can also be seen in Table 47.

Table 47: Acceleration RMS values for the fully 3D printed harvester with big magnets v1.2.1

Frequency (Hz)	Acceleration RMS (mV)	Frequency (Hz)	Acceleration RMS (mV)
5	509.00	14	503.00
6	508.25	13	505.00
7	503.50	12	509.25
8	503.50	11	510.25
9	513.50	10	503.25
10	517.50	9	532.50
11	499.50	8	508.50
12	496.00	7	501.75
13	489.00	6	506.00
14	496.25	5	502.50
15	491.75	-	-

Figure 41 shows the output RMS voltage obtained for the fully 3D printed harvester with big magnets v1.2.1. The ambient noise is not considered in the results although its value was mentioned at the beginning of this test (4.02mV).

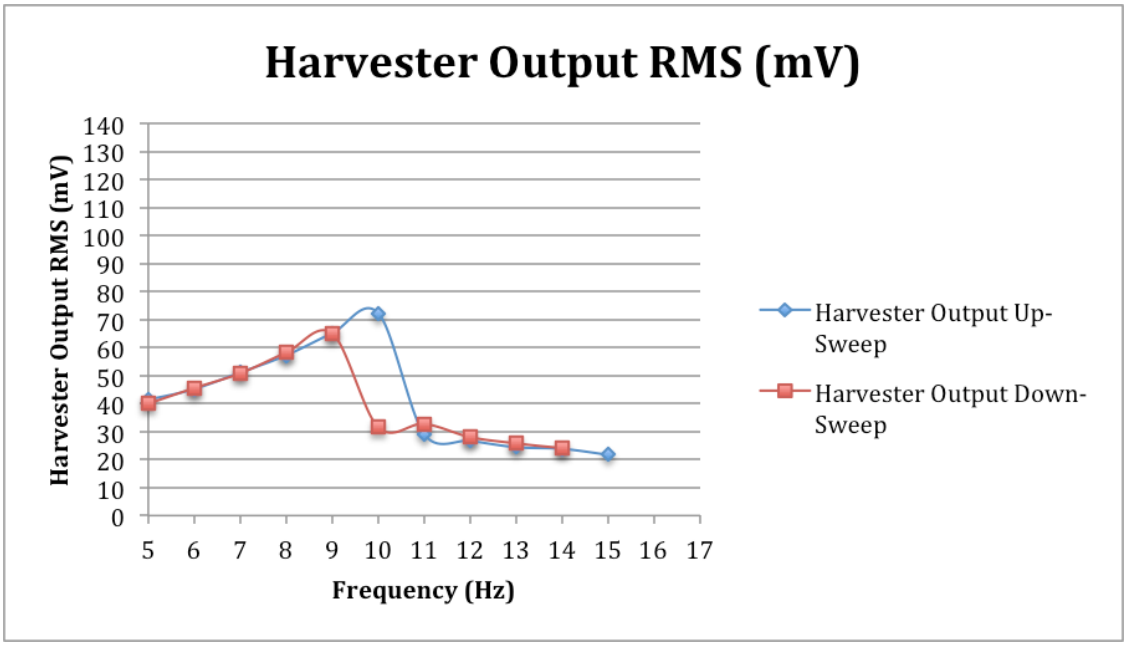

Figure 41: Output RMS voltage plot for the fully 3D printed harvester with big magnetsv1.2.1

The output RMS voltage of the harvester increases almost linearly with an increase of frequency reaching a maximum value of 72.23mV at 10Hz. Then the output voltage suddenly

drops and slowly decreases until the final frequency value of 15Hz. During the down-sweep the output voltage slowly increased until 9Hz, when the bouncing movement of the magnetic cart began again, and then decreased linearly following the up-sweep curve. Note that a small increase in output maximum voltage is obtained in v1.2.1 when compared to the v1.2.0 due to the small increase in mass (72.23mV for 27 grams versus 68.5mV for 24 grams). In this case the hysteresis interval increases to 1Hz when compared to both v1.1.1 and v1.2.0. This increment can be related to the slight increase in seismic mass from 24 grams to 27 grams. Table 48 includes the output RMS voltage obtained for the fully 3D printed harvester with big magnets v1.2.1.

Table 48: Output RMS voltage values for the fully 3D printed harvester with big magnetsv1.2.1

Frequency (Hz)	Output RMS (mV)	Frequency (Hz)	Output RMS (mV)
5	41.23	14	23.95
6	45.18	13	25.78
7	51.08	12	28.00
8	57.20	11	32.73
9	65.10	10	31.58
10	72.23	9	64.95
11	29.10	8	58.20
12	26.70	7	50.78
13	24.40	6	45.53
14	23.83	5	39.95
15	21.70	-	-

Having built the complete frequency response curve with both the up-sweep and down-sweep curves, the bandwidth of the harvester was calculated. This bandwidth is defined as the difference between the frequency at peak voltage (V_{peak}=72.23mV at 10Hz for our case) and the frequency at half power point $\boldsymbol{V_{peak}/\sqrt{2}}$ on the up-sweep branch:

$$\boldsymbol{Bandwidth = Frequency_{V_{peak}} - Frequency_{\frac{V_{peak}}{\sqrt{2}}} = 10Hz - 7Hz = 3Hz} \quad (7.8)$$

This bandwidth is also considerably wider that the bandwidth of linear vibration energy harvester, which might be in the order of 2Hz.

7.4. Comparison of Harvesters

The different iterations of harvesters were compared in terms of components and test results. To reiterate, the following list includes the harvesters which were considered:

i. Springless vibration energy harvester with 3D printed base (baseline)---magnetic cart mass of 76 grams
ii. Low cost harvester---magnetic cart mass of 76 grams
iii. Fully 3D printed harvester with small magnets v1.1.1---magnetic cart mass of 24 grams
iv. Fully 3D printed harvester with big magnets v1.2.0---magnetic cart mass of 24 grams

Figure 42 shows the output RMS voltage for the selected harvesters during the up-sweep part of the test while performing in the range of 5-15Hz.

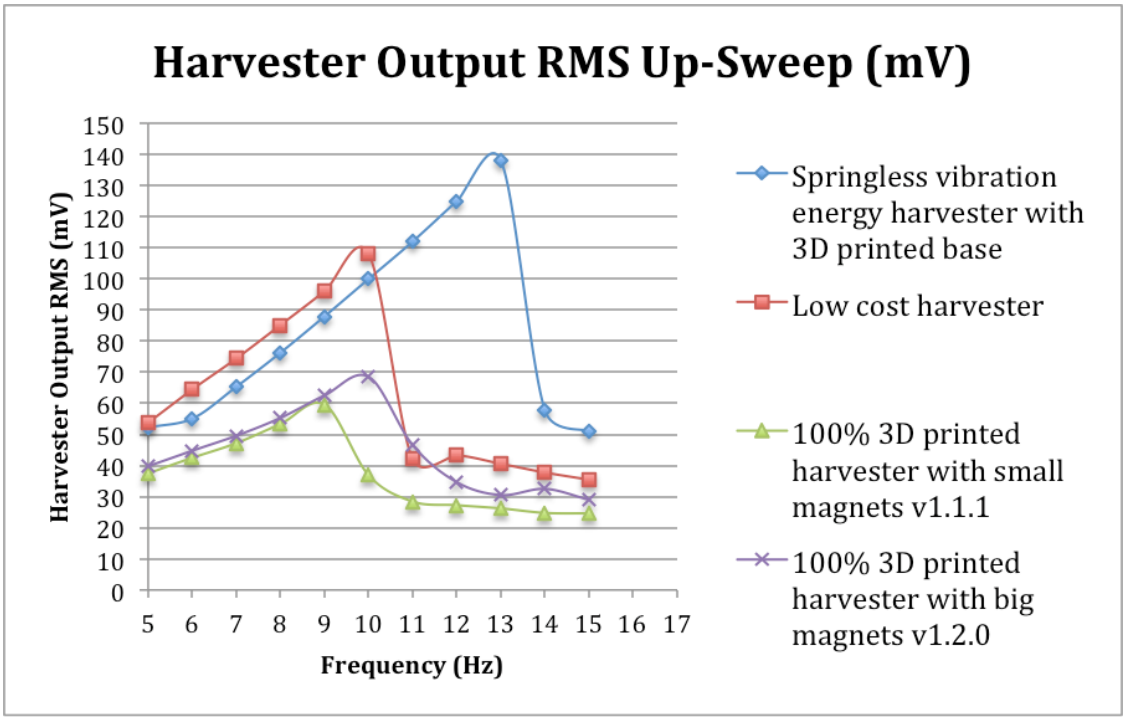

Figure 42: Output RMS voltage for selected harvester during up-sweep

The results show that the output voltage decreases for every single modification of the vibration energy harvester. This reduction is related to the increase of friction caused by the quality of the 3D printed material and the quality of manufacturing, or printing, the material. Since the method of 3D printing was chosen to be the least costly, these factors are expected and could be significantly reduced by improving the material and manufacturing quality of the 3D printing. In addition, the decrease of seismic mass will naturally reduce the amount of power produced by an electromagnetic harvester, which is a concept supported by the theoretical models presented in chapter 4. However, the reduction in power generation was not proportional to the seismic mass reduction but rather less than expected. Further investigation of the results reveals that the modification of the original miniature linear guide, for a 3D printed rail and guide, decreased the maximum output RMS voltage around a 20% (from 138mV to 108mV). This is an expected outcome related to the decrease of the

frequency level of this voltage peak (13Hz compared to 10Hz) due to the increase of friction imposed by the 3D printed materials. Meanwhile, it is to be noted that even with this increase of friction, in the range from 5-10Hz, the harvested voltage in the low cost harvester is higher than that in the springless vibration energy harvester with 3D printed base. When the seismic mass is reduced from the low cost harvester to the fully 3D printed harvesters, the reduction in output voltage is evident.

The difference in output voltage between the fully 3D printed harvester with small magnets and the one with big magnets is caused by the magnet size which influences proportionally the magnetic flux generated. A higher maximum voltage value is obtained using bigger magnets for a frequency of 10Hz when compared to 9Hz for smaller magnets and this result is supported by the theoretical models explained in chapter 4.

Figure 43 presents results from the down-sweep performance of the same harvesters.

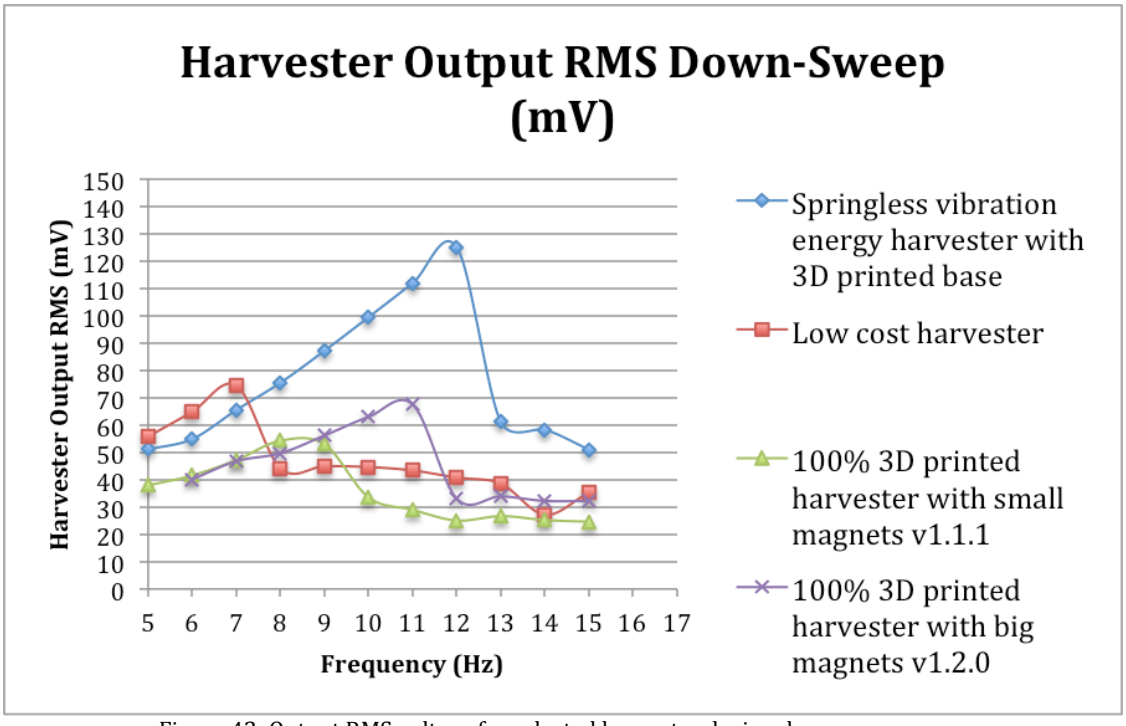

Figure 43: Output RMS voltage for selected harvester during down-sweep

In this case the low cost harvester presents the worst power generation results due to the high levels of hysteresis present in its performance. The other harvesters present less than 1Hz wide hysteresis to almost none at all.

Investigating the global dimensions and properties of the harvesters, Table 49 and Table 50 present a detailed comparison for the selected harvesters. In this case all the harvesters produced in this work are analyzed, including the springless vibration energy harvester.

Table 49: Detailed harvester properties 1/2

Harvester property	Springless vibration energy harvester	Springless vibration energy harvester with 3D printed base	Low cost harvester	
Number of wire turns	40	40	40	**Wire Data**
Wire gauge, AWG	34	34	34	
Wire nominal diameter (inch)	0.0063	0.0063	0.0063	
Wire nominal diameter with film (inch)	0.0069	0.0069	0.0069	
Resistance (Ohms)	3.2	3.2	3.2	
Inductance (microH)	102.5	102.5	102.5	
Wire material	Copper	Copper	Copper	
Number of springs	4	4	4	**Springs Data**
Spring wire diameter (inch)	0.016	0.018	0.018	
Spring outside diameter (inch)	0.18	0.18	0.18	
Spring compressed length (inch)	0.060	0.100	0.100	
Spring uncompressed length (inch)	0.150	0.250	0.250	
Spring rate (lbs/inch)	-	13.50	13.50	
Spring material	Steel music wire	Steel music wire	Steel music wire	
Number of magnets	4.00	4.00	4.00	**Magnets Data**
Magnet length (inch)	1.00	1.00	1.00	
Magnet width (inch)	0.250	0.250	0.250	
Magnet thickness (inch)	0.0625	0.0625	0.0625	
Magnet material	NdFeB	NdFeB	NdFeB	
Magnetic cart mass (g)	76.00	76.00	76.00	**Magnetic Cart Data**
Magnetic cart length (inch)	1.340	1.340	1.340	
Magnetic cart width (inch)	0.831	0.831	0.831	
Magnetic cart height (inch)	0.615	0.615	0.615	
Harvester mass (g)	106.00	90.00	89.00	**Harvester Data**
Harvester length (inch)	2.170	2.180	2.180	
Harvester width (inch)	1.180	1.180	1.180	
Harvester height (inch)	0.560	0.590	0.590	
Length of track (inch)	1.570	1.570	1.570	

Table 50: Detailed harvester properties 2/2

Harvester property	Low cost harvester	Fully 3D printed with small magnets v1.1.1	Fully 3D printed with big magnets v1.2.0	Fully 3D printed with big magnets v1.2.1	
Number of wire turns	40	40	40	40	**Wire Data**
Wire gauge, AWG	34	34	34	34	
Wire nominal diameter (inch)	0.0063	0.0063	0.0063	0.0063	
Wire nominal diameter with film (inch)	0.0069	0.0069	0.0069	0.0069	
Resistance (Ohms)	3.2	3.2	3.2	3.2	
Inductance (microH)	102.5	102.5	102.5	102.5	
Wire material	Copper	Copper	Copper	Copper	
Number of springs	4	4	4	4	**Springs Data**
Spring wire diameter (inch)	0.018	0.016	0.016	0.016	
Spring outside diameter (inch)	0.18	0.125	0.125	0.125	
Spring compressed length (inch)	0.100	0.110	0.110	0.110	
Spring uncompressed length (inch)	0.250	0.250	0.250	0.250	
Spring rate (lbs/inch)	13.50	16.22	16.22	16.22	
Spring material	Steel music wire	302 stainless steel	302 stainless steel	302 stainless steel	
Number of magnets	4.00	4.00	4.00	4.00	**Magnets Data**
Magnet length (inch)	1.00	1.00	1.00	1.00	
Magnet width (inch)	0.250	0.250	0.375	0.375	
Magnet thickness (inch)	0.0625	0.0625	0.0625	0.0625	
Magnet material	NdFeB	NdFeB	NdFeB	NdFeB	
Magnetic cart mass (g)	76.00	24.00	24.00	27.00	**Magnetic Cart Data**
Magnetic cart length (inch)	1.340	1.350	1.350	1.350	
Magnetic cart width (inch)	0.831	0.830	0.830	0.830	
Magnetic cart height (inch)	0.615	0.760	0.780	0.780	
Harvester mass (g)	89.00	36.00	36.00	39.00	**Harvester Data**
Harvester length (inch)	2.180	2.180	2.180	2.180	
Harvester width (inch)	1.180	1.180	1.180	1.180	
Harvester height (inch)	0.560	0.590	0.590	0.590	
Length of track (inch)	1.570	1.570	1.570	1.570	

The wire type used to form the coil moving within the magnetic flux, its dimensions, and number of loops used, were identical for all the harvesters. The rest of the components evolved in parallel with the manufacturing evolution towards a fully 3D printed harvester. The evolution of the springs was related to the evolution in the harvester design and the problems with spring-magnet attraction. The variation in magnet size allowed studying the influence of the magnet dimensions on the output voltage. The global dimensions of the

magnetic cart, as well as the harvesters, were kept almost constant to reduce the effect of this factor on the results and allow for easier comparison between harvesters.

7.5. Additional Benefits of 3D Printing

The main benefits of 3D printing have been presented, developed, and discussed throughout this thesis work. The flexibility in production machines and location combined with the ability to rapidly change and produce parts with much less time and cost of material, tooling, and training, establishes 3D printing technology as a top-edge liable production method that can be applied to energy harvesting

8. Conclusions

The main problematic concerning vibration energy harvesting is related to the interval of frequencies where a reasonable amount of voltage can be harvested. To increase this interval of frequencies, or bandwidth, nonlinear techniques are reproduced in this thesis work. In addition, new cost effective manufacturing processes need to be developed if energy harvesting is to become a global technology.

With the previous issues in mind, the springless, nonlinear based, vibration energy harvester was evolved through three iterations, finally obtaining a fully 3D printed harvester through a significantly cost effective manufacturing process. The performance of the harvester experienced a degree of degradation observed through a reduction of the level of power output but with less proportionality to the gains in mass and cost of the harvester. Bandwidth of the frequencies where energy harvesting could be effective continued to be wider than linear harvesters, with minor variations due to changes in the structure of the harvester. Variations through these three iterations were influenced relatively less by changes in the seismic mass as opposed to more significantly by frictional properties of the material and quality of manufacturing of the harvester.

Table 51 shows a summary of the results obtained for each of the harvesters produced in this work in terms of 5 elements: maximum output voltage, bandwidth, cost, seismic mass, and harvester mass.

Table 51: Comparison of main elements in the different harvester iterations relative to the first version in the table

Harvester Iteration	Max. Output Voltage (mV)	Change %	Bandwidth (Hz)	Change %	Cost ($)	Change %	Seismic Mass (g)	Change %	Harvester Mass (g)	Change %
Springless vibration energy harvester with 3D printed base	138	N/A	3.2	N/A	>300	N/A	76	N/A	90	N/A
Low cost harvester	108	-22	2.82	-12	>200	-33	76	0	89	-1
Fully 3D printed with small magnets v1.1.1	59.58	-57	3.07	-4	9.29	-97	24	-68	36	-60
Fully 3D printed with big magnets v1.2.0	68.5	-50	3.24	+1	10.17	-97	24	-68	36	-60
Fully 3D printed with big magnets v1.2.1	72.23	-48	3	-6	10.17	-97	27	-64	39	-57

The first iteration, considered as the baseline, achieved a maximum output voltage of 138mV using a 76g metallic seismic mass. Iteration number 2 experienced a decrease in output voltage of 22% compared to iteration number 1 with a cost reduction of 18.84% (see Appendix 8), consisting of modifying the miniature linear guide. The reduction in output voltage was proportional to the increase in friction due to the use of cost-effective 3D printing materials and a low-end 3D printer. The higher seismic mass of iteration number 2 combined with the presence of high friction 3D printed materials in the miniature linear guide resulted in an increase in the hysteresis interval of this harvester, which presented a value of 3Hz.

The three harvesters obtained in iteration number 3 presented an output voltage loss between 48% and 57% compared to iteration number 1, with a seismic mass reduction of 64-68% and a significant global cost reduction of hundreds of dollars. This output voltage reduction was related to the decrease of seismic mass as well as to the introduction of the same low quality 3D printing materials in the miniature linear guide as in iteration number 2.

The use of high friction 3D printed materials in the miniature linear guide combined with lower seismic mass, 24 grams in v1.1.1 and v1.2.0 and 27 grams in v1.2.1, allowed for a better performance in the hysteresis interval of these harvesters, reaching values of 0Hz and 1Hz respectively. The variation of the hysteresis interval of a harvester being in direct relation to the seismic mass, when using 3D printing materials in the miniature linear guide, suggests the need for calculating the optimal seismic mass that would allow achieving the best combination of frictional performance and output voltage. The variations in output voltage between the three harvesters in iteration number 3 were also related to the size of magnets used and to the small variation in seismic mass. The higher output voltage was obtained when bigger magnets and bigger seismic mass are used. Although higher output energy is more desirable for a harvester, using a lower seismic mass in a vibration energy harvester would be as desirable. The lower seismic mass used in the harvesters in iteration number 3 can widen the range of applications of energy harvesters, becoming useful in daily human applications, and even in space applications. Also the cost reduction imbedded in 3D printing technologies can widen the use of energy harvesting suggesting personal house applications as well as educational applications.

In terms of bandwidth, every harvester presents a considerable improvement compared to linear harvesters, presenting the best results in iteration number 1 and iteration number 3 using plates v1.2.0.

These results prove that even with a decreasing output voltage throughout the iterations, the parallel decrease of cost and seismic mass generate a global increased performance. This means that the fully 3D printed set of harvesters globally outperforms both the low cost harvester and the springless vibration energy harvester with 3D printed base.

The problems associated with the use of a low-end 3D printer include the limited use of high quality 3D printing materials, which would reduce the material friction, the decrease in component density, quality, and repeatability, and an increase in manufacturing errors. These problems could be solved using a higher-end 3D printed with higher quality 3D printing materials.

More research using high quality 3D printing materials, more evolved 3D printers and better lubricants are then necessary, and would allow for an improvement of the presented thesis results. Also a better understanding of the frictional properties of the harvesters combined with a better knowledge of frictional parameters of different 3D printed materials would allow for a global performance improvement.

9. Future Improvements

Energy harvesting is a field that is in continuous expansion and development and so multiple improvements and developments can be added to this thesis project. Some of these ideas are presented here.

1) Theoretical and practical frictional analysis of the nonlinear motion of the harvesters using different metallic and 3D printed materials. Calculation of the optimal seismic mass for the best combination of frictional properties and output voltage.
2) Study using different lubricants to see which one allows the highest friction reduction in the 3D printed components
    - PTFE filled oil
    - PTFE filled grease
    - Graphite powder
    - Silicon lubricant
3) Combine the harvesters with electric circuitry allowing energy storage and utilization in real application. The fully 3D printed harvester can be installed in a bridge, shoe, or backpack, and the voltage harvester can be measured and analyzed. Capitalizing on the flexibility and rapid production ability provided by 3D printing, harvester redesign to accommodate applications can now be achieved in much less time and test would take comparatively less time to be conducted.
4) Harvester design and composition modification with flexibility and rapid prototyping provided by 3D printing. Test multiple springs with different rates and analyze the impact of them in the voltage harvested.

5) Develop and build a super capacitor that can store the energy generated by the fully 3D printed energy harvester.
6) Build a rectifying circuit that allows visualizing when the fully 3D printed harvester is functioning or not. This can be easily implemented using an LED light.
7) Create a control loop for the experimental setup that allows maintaining a constant 0.5g in the tests. This would allow for better output results and shorten the testing time length.
8) Explore the benefits of higher end 3D printers in the quality and performance of the manufactured parts and implement new materials in the manufacturing process. The Lulzbot TAZ6 should be used as a departing point.
9) Theoretical comparison of the output voltage and bandwidth of the thesis nonlinear harvesters and linear harvesters with the same global parameters.
10) Conduct more tests on these same harvesters using different experimental setups and levels of advanced equipment to understand the effect of input sequencing and sweeping arrangement on the output of these devices.

Appendix 1: Components of the Springless Vibration Energy Harvester

The components that form the springless vibration energy harvester are now listed and evaluated:

1) Base of the harvester: formed by two Lexan rectangular plates attached to an aluminum rectangular plate. The junction is secured via four small metallic pins, two in each plastic component. Each of the Lexan members has two holes drilled on their upper side and a square slot through them. The metallic base includes five holes with an initial larger diameter to fit the head of the bolts. The main dimensions of the base of the harvester are detailed in Table 52.

Table 52: Dimensions of the base of the harvester

	Thickness (inch)	**Length (inch)**	**Width (inch)**	**Dimensions of slot (inch)**	**Diameter of holes (inch)**
Aluminum plate	0.16	2.17	1.18	-	0.11/0.05
Plastic plate	0.29	1.18	0.41	0.10	0.08

Figure 44 shows the base of the harvester including the springs attached to it.

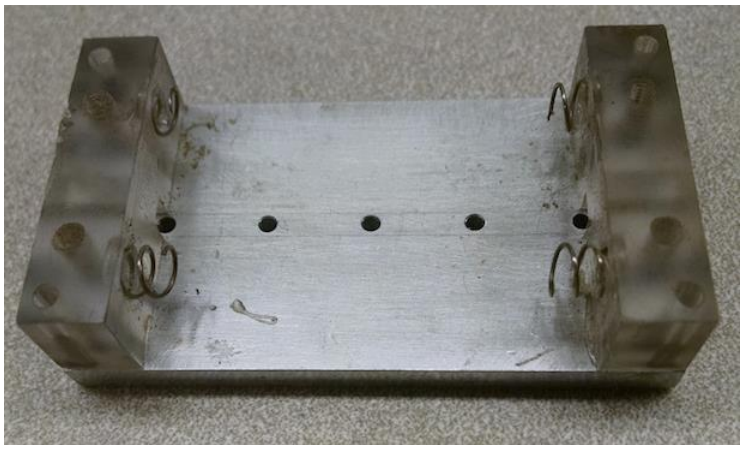

Figure 44: Base of the harvester with springs attached

2) Springs: four zinc-plated steel music wire springs attached to the Lexan lateral plates of the harvester base. The connection is done using superglue. The springs

are obtained by cutting in half 0.3" springs. The dimensions of the installed springs can be seen in Table 53.

Table 53: Spring dimensions

	Outside Diameter (inch)	Wire Diameter (inch)	Uncompressed Length (inch)
Springs	0.18	0.016	0.15

3) Magnetic cart: the magnetic cart is the most important component of the harvester and its function is to generate a variable electromagnetic field throughout its movement. The magnetic cart presents the shape of a rectangular prism with two lateral brass plates and two steel upper and lower plates connected by six bolts each. There are four magnets located in the interior of the assembly, connected to the steel plates and leaving a middle air gap all the way through. This connection is done via magnetic attraction. Two NdFeB magnets with different polarities can be found attached to each steel plate. The magnetic cart can be seen in Figure 45.

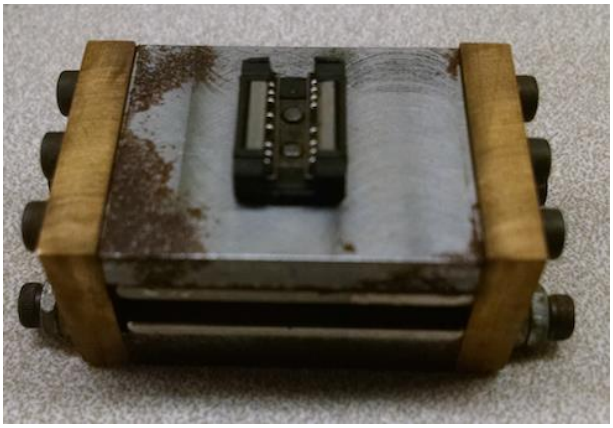

Figure 45: Magnetic cart

The dimensions of the magnetic cart and magnets are included in Table 54.

Table 54: Dimensions of the magnetic cart and magnets

	Thickness (inch)	Length (inch)	Width (inch)
Magnets	0.0625	1.00	0.25
Brass Plate	0.16	0.831	0.615
Steel plate	0.29	1.02	0.831

4) Miniature linear guide (MR3M): this part of the harvester facilitates the linear movement while reducing the friction. Two pieces are included in the miniature linear guide, a guide and a rail. The first goes attached to the magnetic cart by two bolts. The second can be inserted in the harvester by the square slots of the Lexan plates of the harvester base and bolted to the aluminum plate of the harvester base in five points. The box includes miniaturized spheres in both sides of it, where the rail slides, to minimize friction and therefore save energy. Figure 46 shows the components of the miniature linear guide.

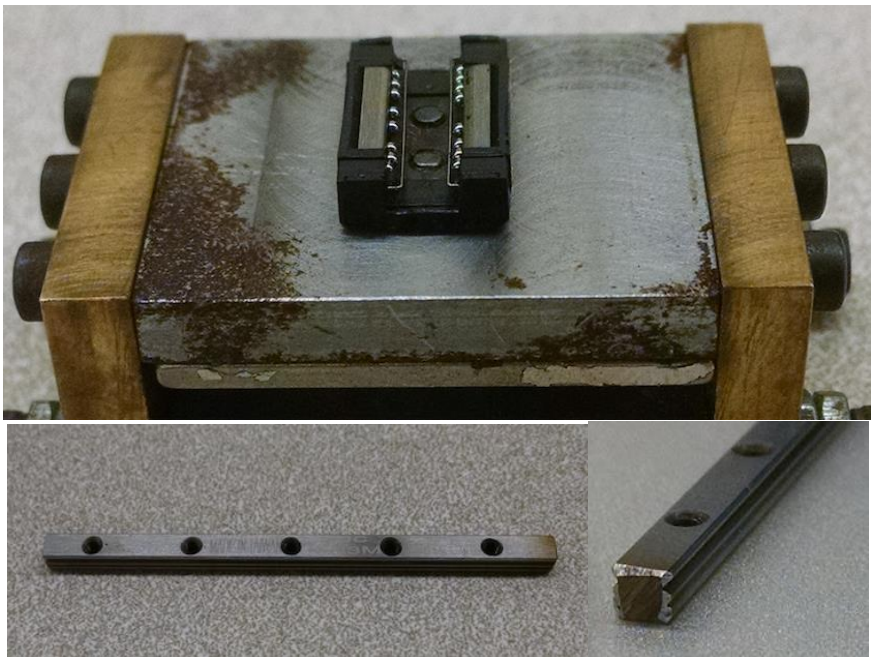

Figure 46: Miniature linear guide

5) 3D printed layer with coil: this 3D printed part includes a predefined number of loops of copper coil (40) and is fixed on top of the Lexan plates of the harvester base with four bolts. The 3D printed layer is positioned inside the air gap of the magnetic cart. The linear movement of the magnetic cart modifies the surface of the magnets on top of the coils and so the electromagnetic field is generated. An image of this layer with the coil around it can be seen in Figure 47.

Figure 47: 3D printed layer and coil

The dimensions of this component can be seen in Table 55.

Table 55: Dimensions of the 3D printed layer

	Thickness (inch)	**Length (inch)**	**Width (inch)**	**Diameter of holes (inch)**
3D Printed Layer	0.04	2.11	0.18	0.08

6) Bolts: a total of five bolts join the rail of the miniature linear guide to the base of the harvester. Four extra bolts connect the 3D printed layer to the Lexan plates of the harvester base. Regarding the magnetic cart two bolts attach the box of the linear guide to it and ten more bolts join the rest of components.

Appendix 2: Rational for Selection of the Setup Structure

The purpose of this section is to present the rational for selection regarding the construction of a structure whose function is to connect the harvester to the shaker, and to which the harvester is attached to. The need for this construction is considered due to the lack of a proper and efficient structure since the existing assembly couldn't fulfill the expectations of the experiment. Also there exists a great amount of vibrational noise in the initial setup, in particular the noise generated in the accelerometer by the bouncing movement of the harvester. In order to minimize or cancel this noise, a more consistent structure is desired.

The requirements of this structure are:

- Allow both horizontal and vertical vibration modes of the shaker
- Easy and cheap to manufacture
- Easy to attach to the shaker and to the harvester

The shaker used in the set-up includes a metallic circular base with five threaded holes (four forming a square shape and a middle one) where additional structural members can be attached. The dimensions of this base can be seen in Table 56.

Table 56: Dimensions of the shaker base

	Diameter (inch)	**Thickness (inch)**	**Holes Diameter (inch)**
Shaker Base	2.72	0.20	0.18

Figure 48 shows the base of the shaker.

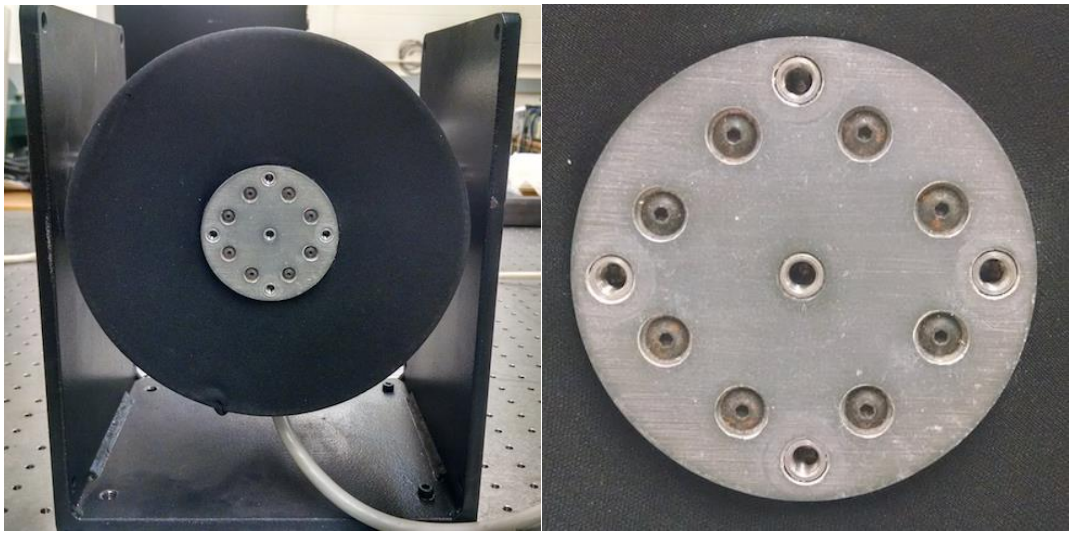

Figure 48: Base of the shaker

The initial structure attached to the shaker consisted of:

i. Cylindrical stoppers (x4): components in contact with the base of the shaker. Their function is to separate the assembly from the shaker.

ii. Washers (x24): six washers per cylindrical stopper to increase the distance in between the shaker and the assembly.

iii. First square aluminum plate (x1): this part was bolted to the cylindrical stoppers and washers (four 0.20” diameter holes) and to the second aluminum plate (two 0.31” diameter holes). It also presented a threaded 0.16” diameter hole to attach an accelerometer. Its global dimensions were 5.76”x5.76”x0.24”.

iv. Second rectangular aluminum plate (x1): attached to the first aluminum plate by two 0.27”diameter holes and to four aluminum pieces on top of it. Its global dimensions were 8.28”x8.52”.

v. Small rectangular aluminum pieces (x4): parts positioned in the top of the assembly with unknown functionality. Dimensions of 2.01”x1.5”x0.36”.

Figure 49 presents some design drawings of the original assembly before any modifications were included.

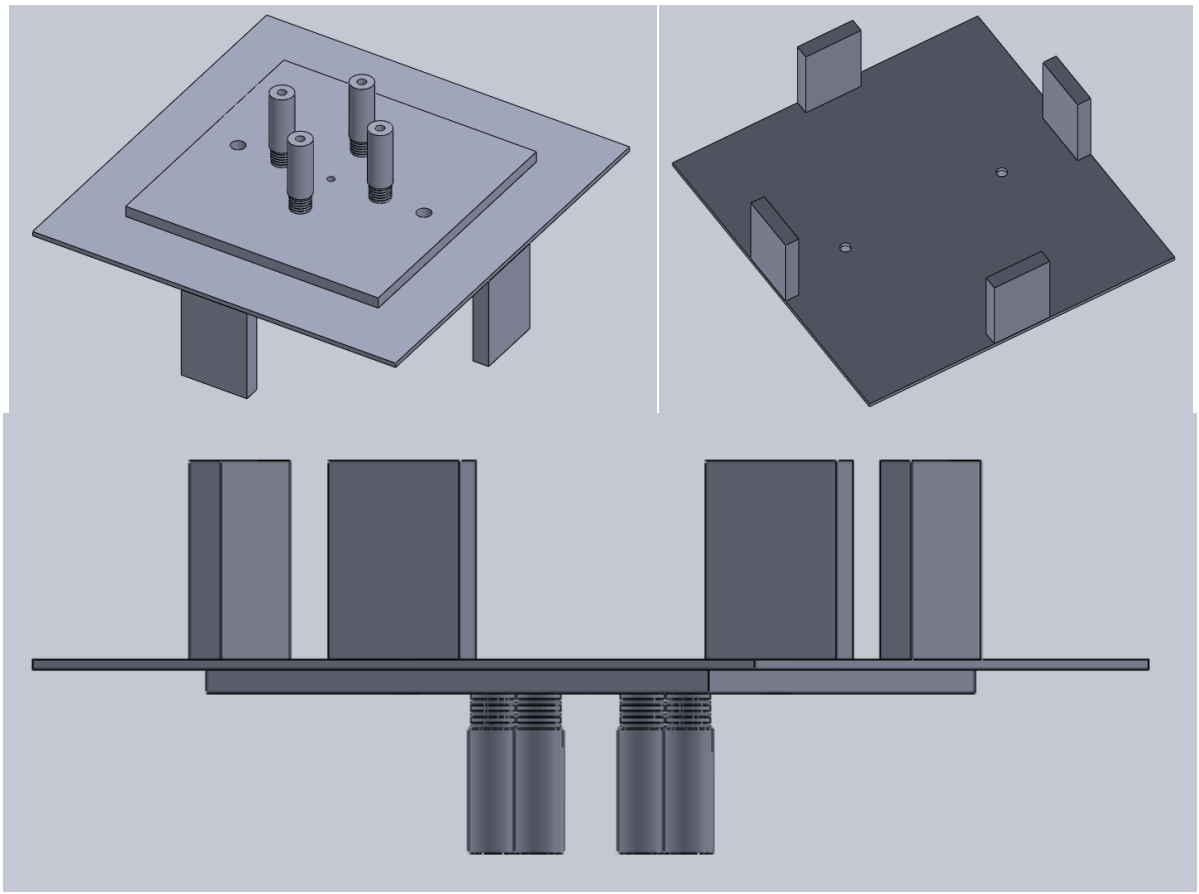

Figure 49: Components of the initial structure

The accelerometer is also designed in Solidworks and it can be seen in Figure 50.

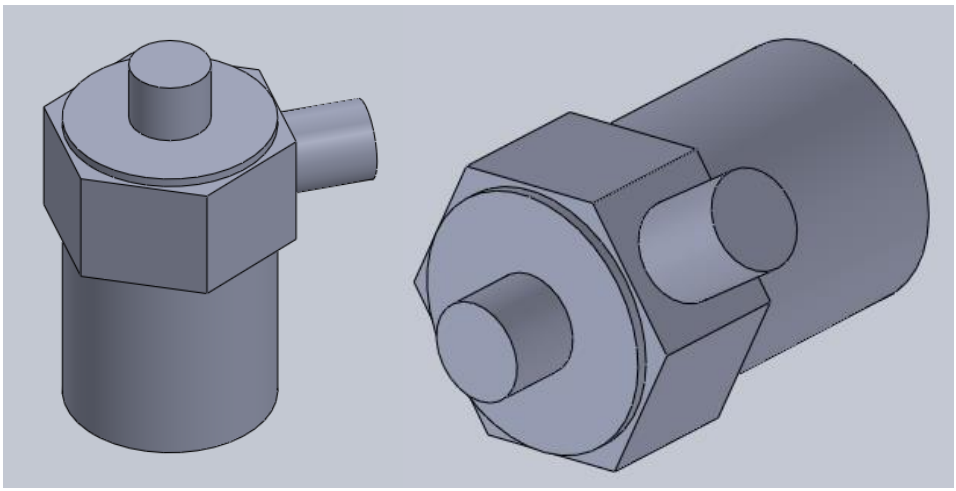

Figure 50: Model of accelerometer

Figure 51 shows the initial assembly, which includes the previous structure, the shaker and the accelerometer.

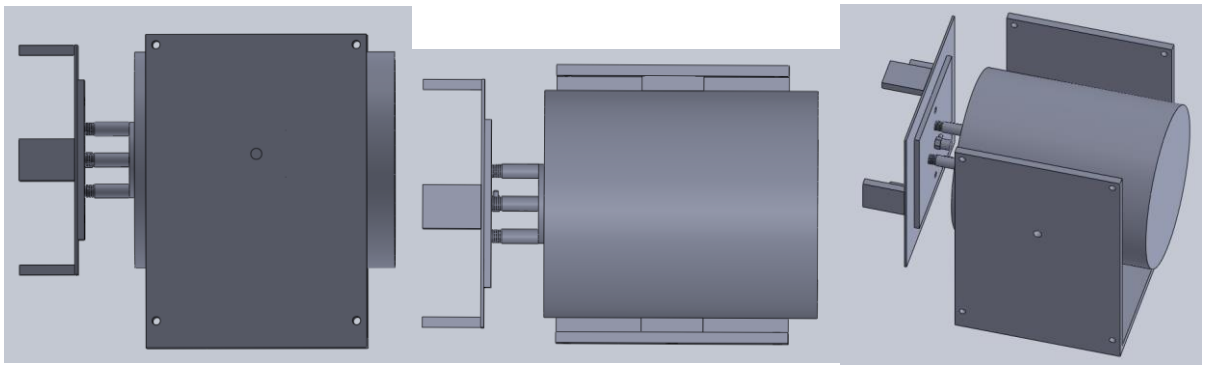

Figure 51: Lateral (left), upper (center) and isometric view (right) of initial assembly

The considerations for the selection of the new platform are here established.

Model Number 1

Description

The first model consisted of an aluminum U-Section structure with rails machined in it to clamp the VEH in both Y and Z-axis of movement. The movement in the X-axis was impeded using bolts (one in the upper part of the U-Section and another one in its lower

part). These bolts were fastened in the rails and clamped perfectly the harvester. Two images of this component designed in Solidworks can be seen in Figure 52.

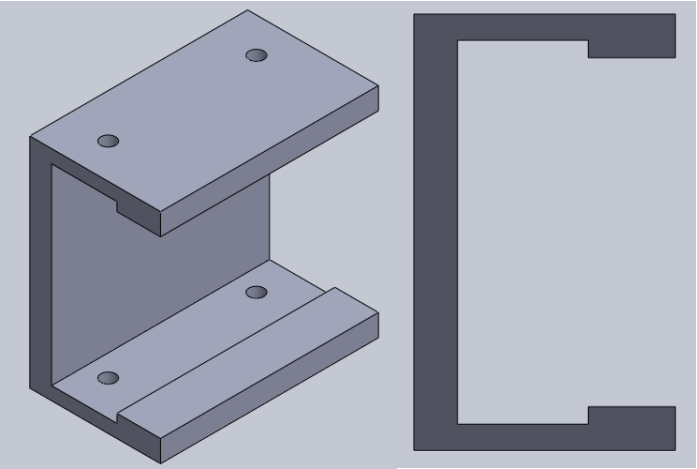

Figure 52: Model number 1 U-Section

The cylindrical stoppers, washers and first square aluminum plate existent from the initial structure were used to clamp this model to the shaker. Figure 53 shows the assembly of model 1.

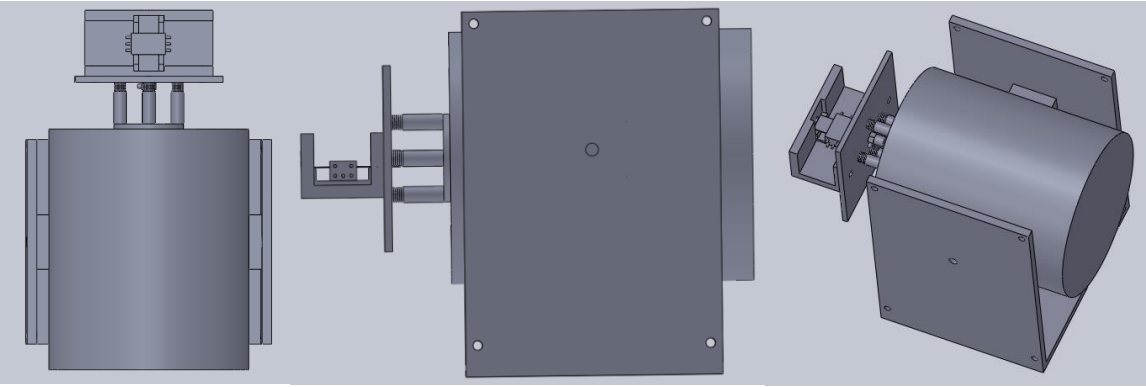

Figure 53: Model number 1 assembly

Problematic

A U-Section with the appropriate dimensions that could fit the pre-established dimensions of the harvester didn't exist in the market, or at least it was impossible to find it for a reasonable cost.

Model Number 2

Description

Instead of using a U-Section (see the problematic of Model 1), an L-Section was selected. An L-Section piece of aluminum 6061 was obtained (scratch parts from the machine shop) with 3" and 2"long legs and 1/4" thick. This component was reduced to the appropriate length dimension (5.76") and two holes were milled in it with a separation between holes of 5.24". This last dimension was fixed by the dimensions of the holes present in the first square plate of the initial assembly. The harvester was attached to the aluminum L-Section using double-sided adhesive tape. The adhesive tape was the most resistant that the user could find in the market, resisting up to 100lb per 60". The selection of adhesive tape as fastening method was based on its simplicity and as a way to replicate the structure used in the University of Waterloo. Figure 54 shows the L-Section used in this model.

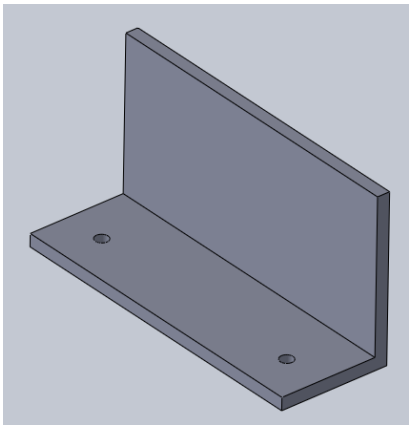

Figure 54: Model number 2 L-Section

The cylindrical stoppers, washers and first square aluminum plate existent from the initial structure were also used to clamp this model to the shaker. Figure 55 shows the assembly of model number 2.

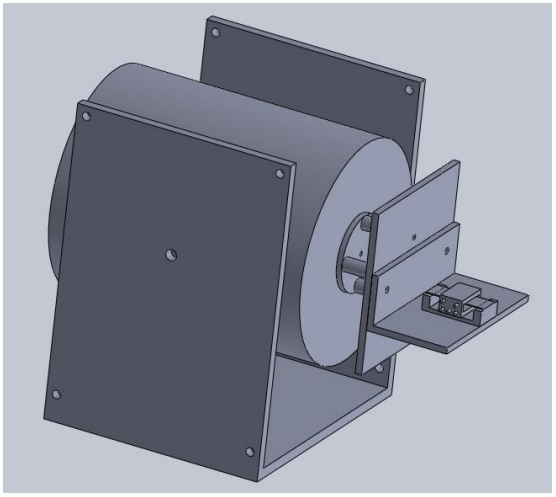

Figure 55: Model number 2 assembly

Problematic

It was considered that this structure was to simplistic and some improvements could be added to it.

Model Number 3

Description

In this third iteration, it was decided to modify and improve the L-Section design. A foot of L-Section multipurpose aluminum 6061 with 3” and 2”long legs and 3/8” thick was purchased. The higher thickness was selected as a method to add rigidity to the structure and absorb vibrations. The design was similar to the initial U-Section including two rails in both inner walls of the L-Section. These rails constrained two directions of movement, being the third constrained using bolts. Figure 56 presents this new model.

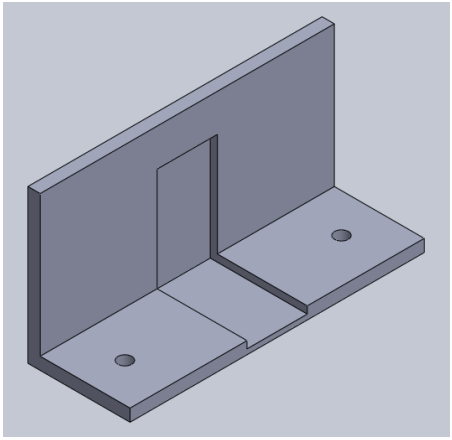

Figure 56: Model number 3 L-Section

Problematic

The construction of this component wasn’t feasible with the tools present in the machine shop (lack of appropriate end mills). This model was then discarded because obtaining new specific end mills would add higher cost to the project.

Finally, the simple L-Section with two-sided adhesive tape (model number 1) was selected as the support structure for the harvester due to both lack of appropriate material and machine shop equipment. This structure might not have been the most structurally evolved but allowed simplicity to the design and adaptability to newer designs of the harvester.

The first tests using the L-Section structure revealed that a huge amount of vibrations were being transmitted from the harvester to the accelerometer. In order to minimize these vibrations, some new modifications and tests were implemented:

a) A rubber layer was added to the L-Section in between this component and the first square aluminum plate (double side adhesive tape was used again for convenience).
b) The harvester was distanced from the base of its L-Section platform.
c) The harvester was moved along different horizontals in its L-Section platform.

None of these solutions showed a positive outcome considering the reduction of the harvester's impact on the accelerometer signal and so new and more elaborated theories were conceived. The main idea was to create a new independent platform for the harvester. This should allow having the harvester and the accelerometer in separated platforms. Then the noise induced by the harvester in the accelerometer, when the harvester's cart bounced against the springs, should be minimized or cancelled. By doing this it might be possible to maintain the lecture of the accelerometer at 0.5g.

Solution Number 1

Description

The accelerometer was moved in first instance from the first square aluminum plate, where it initially resided, to the base of the shaker. There already existed a hole in this shaker's base where the accelerometer could be installed without drilling any additional hole or making any major modification.

Problematic

It was thought that the harvester vibrations should not have affected the accelerometer at this new position but the hypothesis was incorrect. The bouncing movement of the harvester's cart still affected the accelerometer measurements.

Solution Number 2

Description

Before the construction of a new separated platform for the accelerometer another solution was proposed. As previously mentioned, the accelerometer was originally installed in a hole in the first square aluminum plate, to which the harvester's L-Section platform was attached. It was considered that creating a new hole far away from the center of plate base might reduce the amount of vibrations generated in the accelerometer by the harvester's bouncing. In order to avoid making a new hole in this base, the harvester was moved outside of the central line of the harvester's L-Section. Distancing the harvester from the centerline of its platform should have a similar outcome as distancing the accelerometer from the centerline of the first square aluminum plate.

Problematic

The result of this variation was still negative, meaning that the harvester's vibrations were still transferred to the accelerometer.

Solution Number 3

Description

The construction of a new separated platform for the accelerometer was finally considered. It was believed less probable now, after the outcome of solutions 1 and 2, that solution 3 would have a positive result. The vibrations of the harvester might be transferred to the shaker and from the shaker to the separated accelerometer's platform.

Anyway two different platforms were built using scrap material from one of the previously used harvester's L-Section platforms. The first design would attach the short leg of the L-Section to the shaker's base and the second design would attach the longer leg of the L-Section to the shaker's base. In both designs the accelerometer would be initially connected to the shaker's base. If too many vibrations from the harvester's platform to the accelerometer were still present, an additional platform would be constructed for the accelerometer and the new L-Section harvester's platforms would be distanced from the shaker via metallic separators.

Both L-Section platforms were connected to the base of the shaker, as well as accelerometer. This means that all the components of the initial structure were here avoided (aluminum plates, stoppers and washers). Figure 57 shows the L-Sections implemented during this solution.

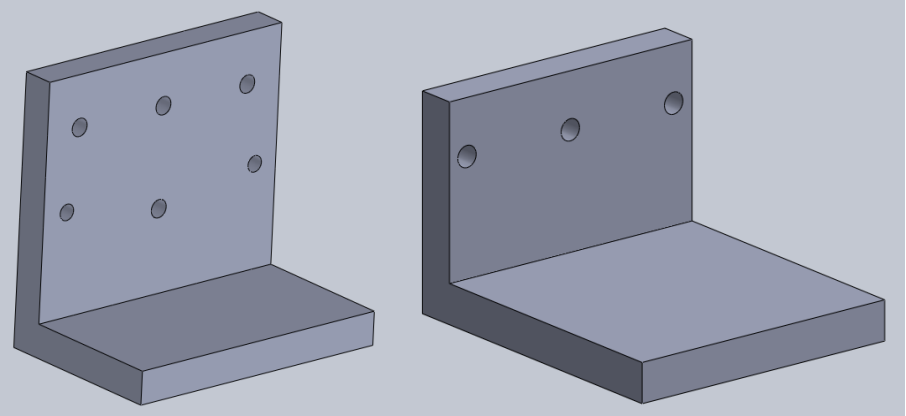

Figure 57: Long leg L-Section (left) and short leg L-Section (right) for solution number 3

Notice that the long leg L-Section presents a total of six holes drilled in it while the short leg L-Section only includes three. The long leg L-Section is attached to the base of the shaker in three or four holes (depending if the middle upper holes is used) and the short leg L-Section in only two or three (depending if the middle upper holes is used). The two additional holes in the long leg platform are threaded holes to possibly attach the accelerometer to the L-Section instead of the shaker's base. Figure 58 shows this possibility.

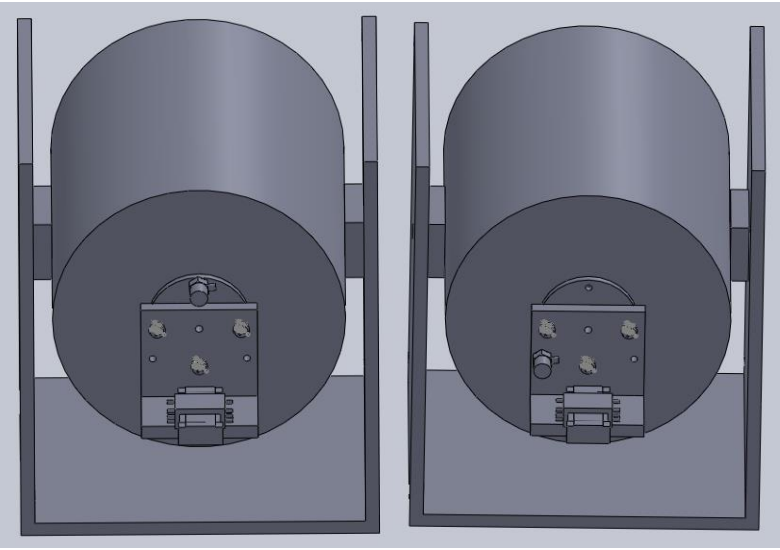

Figure 58: Long leg L-Section configuration with accelerometer in the base of the harvester and L-Section

Problematic

Similar interference in between the harvester and the accelerometer was obtained. This corroborated the tendency that the harvester's bounces against the springs were going to affect the accelerometer measurement no matter what solution was chosen (considering the use of the same accelerometer and shaker).

It is interesting to mention that the structural configuration used in Waterloo did not differ from this previously analyzed configuration. In Figure 59 it can be seen how their L-Section platform, to which the harvester is attached, was directly connected to the shaker and the accelerometer was plugged to the L-Section platform.

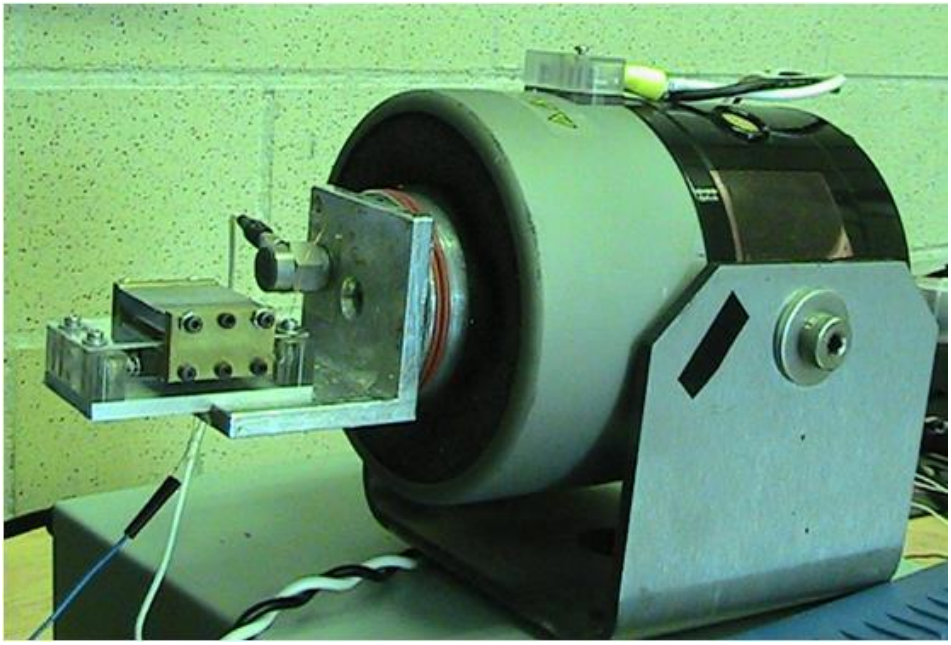

Figure 59: Structural disposition in Waterloo

Then if the platform and the harvester were similar to ours, it could be thought that our problem resided either in the accelerometer or in the shaker. It might have been possible that the shaker was transmitting vibrations to the accelerometer or that the quality of the accelerometer was lower than theirs and the vibrations were easier to transfer.

Solution Number 4

Description

By adding an external mass to the shaker's base the effect of the harvester's vibrations on the accelerometer could decrease. A heavy steel or lead plate could be installed in between the shaker's base and the harvester's L-shape platform. The accelerometer would also be connected to this heavy plate at the opposite side of the harvester's platform.

Problematic

This solution was not implemented because due to the results of the previous solutions it was believed that it would give the same outcome as before.

Solution Number 5

Description

Testing another shaker might be a good way of checking the proper working of the currently used shaker. In the lab there was a second shaker available that allowed the connection of the accelerometer and possibly of an L-Section platform. After a new configuration was obtained with this shaker, if the effect of the harvester's vibrations on the accelerometer still persisted, it could be concluded that the problem was not due to the shaker. If on the other hand the effect on the accelerometer was reduced or canceled, it could be deduced that the shaker that was initially used, presented some internal problem and new solutions should be proposed.

The 2 new L-Section platforms built in solution number 3 were tested on the new shaker. A middle hole needed to be drilled in order to link the middle rod of the shaker with the platform. The accelerometer was connected along this middle rod to save the drilling of a

threaded hole in the aluminum plate. Figure 60 shows a model of the long leg L-Section installed in the new shaker.

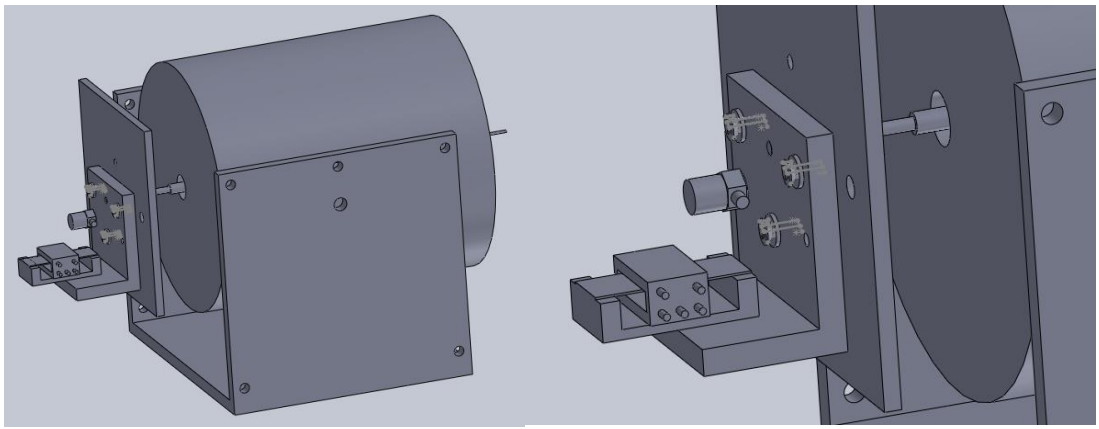

Figure 60: Model of long leg L-Section installed in new shaker

Figure 61 shows an image of the short leg L-Section installed in the new shaker with the accelerometer attached in the middle hole of the platform.

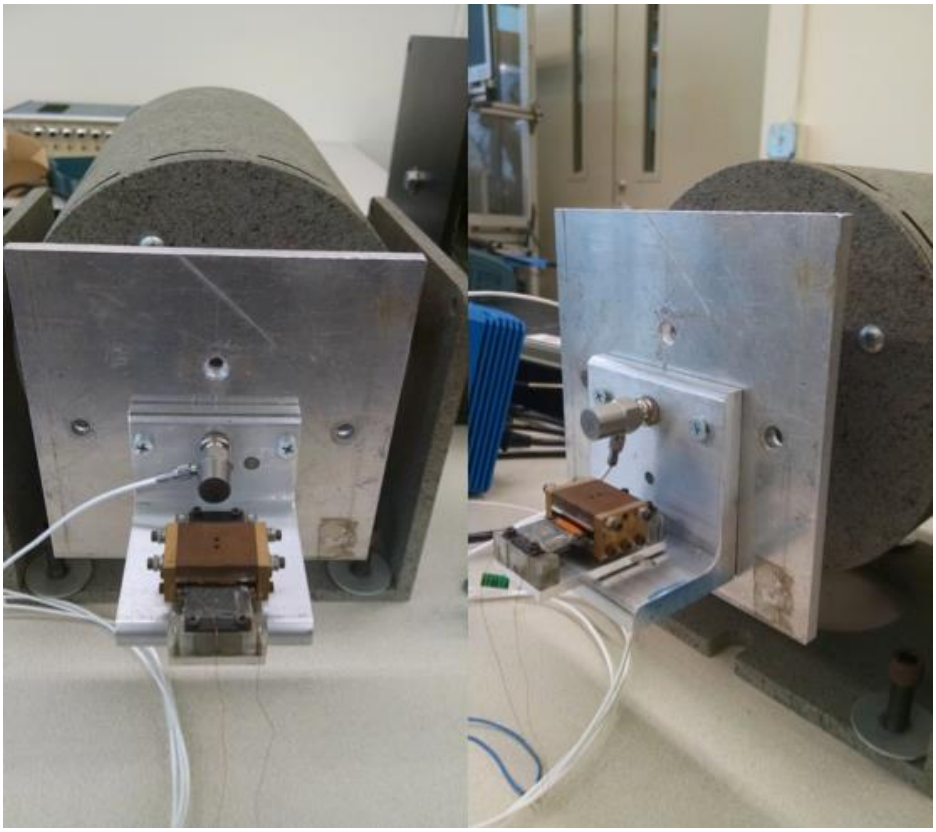

Figure 61: Short leg L-Section installed in new harvester

Problematic

The result of both configurations was negative. This meant that the vibrations of the harvester still affected the outcome of the accelerometer. It is also interesting to mention that since a single rod now sustained all the structure instead of a base in the shaker, these new two configurations presented some bending movement, which in fact would have affected the final energy results.

It can be concluded that the initial selection of the shaker looked accurate even if the results were not what could be expected by now.

Since the results in the lab weren't satisfactory, the set-up was moved to a vibrations lab. In this lab there was a table whose only purpose was to run vibrations tests. The table presented an upper metal layer and an internal marble block for higher rigidity. The metal surface of the table had multiple threaded holes to attach shakers and other instruments. The problematic with attaching the shaker to the table was that the threaded holes in the table were not the same as the threaded holes in the shaker's structure.

An initial test was run on the table with no attachments between the shaker and the table and no difference was seen in the results when compared to the previous results obtained in a normal table. Expert consultation explained that only when attached, the results would be visible. For that some steps were taken into consideration:

- The shaker should be the only instrument on top of the table to minimize both secondary vibrations and noise generated from other instruments or objects. Other instruments and objects should me moved to adjacent tables
- A small gap should be left in between the vibrations table and the adjacent tables so no interference exists.

- The shaker should be attached to the table in as many points as possible. For that, 2 of the 4 holes in the shaker's platform were initially connected to the table, using bolts that fit the table´s threaded holes. If there were some improvement after this modification, a metallic base could be built to fit the four shaker's holes and four table's holes.

All these aspects were considered and the shaker was attached to the vibrations table using two bolts whose diameter was coincident with the holes in the table. Figure 62 shows the attachments of the shaker to the vibrations table.

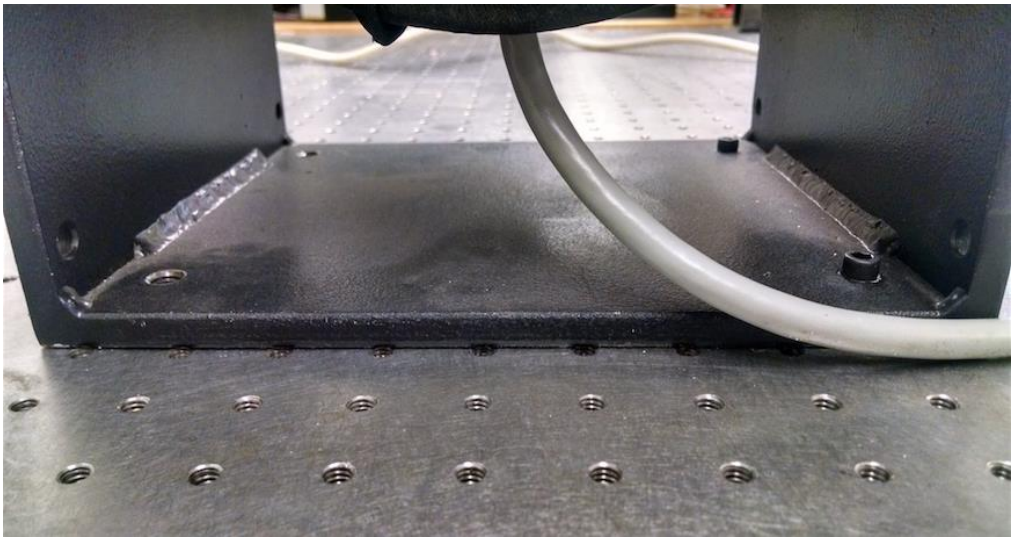

Figure 62: Connection of the shaker to the vibrations table

A quick test was run and it was noticed that even with the new connections to the table, the accelerometer signal still presented high frequency noise. It could be concluded that the surface where the test is being run was not in fact a critical aspect.

After all the structural and other various modification the problematic of the noise in the accelerometer signal was still recurrent and none of the proposed solutions appeared to solve the problematic. As a final option it was decided to measure the acceleration using the RMS (root mean square) of the signal instead of its peak-to-peak values. This small variation

allowed running tests and obtaining results while avoiding the noise present at the output of the accelerometer. The long leg L-Section manufactured in Solution 3 was used during all the tests run in this thesis work.

Appendix 3: Additional Tests of Harvesters

The following tests all have in common that their results were not completely correct. They are added in this appendix as additional information and to show some of the mistakes and problems that were encountered and solved while testing the different harvester versions. Some of the tests run were incomplete while others showed incongruent results. Also in some of them the procedure considered to obtain results wasn't appropriate. All these complications are now detailed before the test results are shown:

I. Broken Springs in the Springless Vibration Energy Harvester

When the springless vibration energy harvester was dismantled to take measurements for a possible 3D printed replication, the presence of two small pieces of metal inside the magnetic cart was noticed. This fact was not given a lot of importance to since it was believed that they were internal components of the magnetic cart. A couple of days later, the decision to see what they were, and to remove them, was taken. It came to the attention of the author that those two pieces of metal were in fact pieces of spring. It was then checked that those two components had been removed from two of the springs of the base and absorbed by the magnets so it had been impossible to notice them until the dismantling operation. Figure 63 shows an image of the base of the harvester where the missing parts of spring can be noticed.

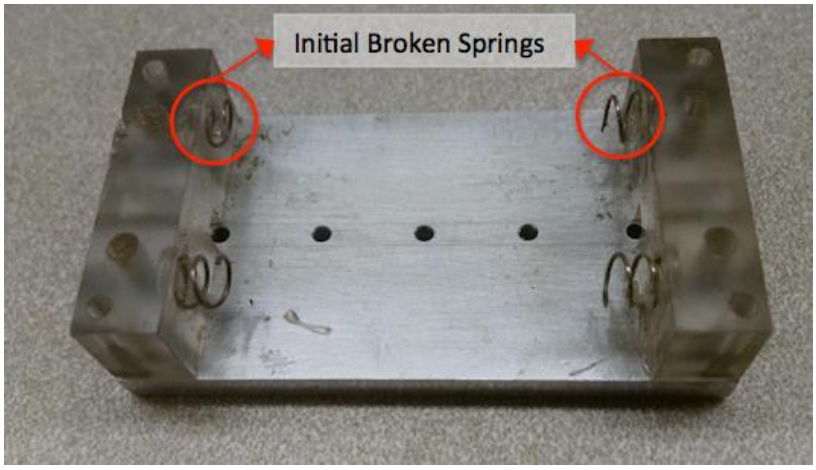

Figure 63: Initial broken springs in the springless vibration energy harvester

While running a test, the harvester suddenly stopped moving. After further examination, it was noticed that a third piece of spring (belonging to a third spring, different from the previously two broken springs) impeded the movement, since it was attached to the 3D printed layer, inside the magnetic cart. Figure 64 shows the third broken spring and the base of the harvester after this incident.

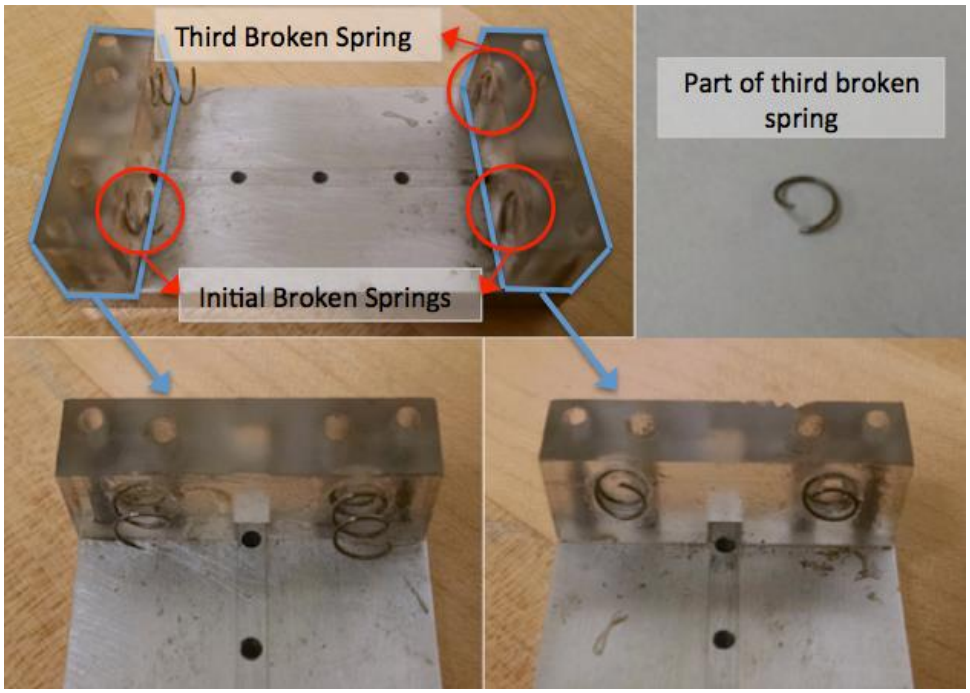

Figure 64: Third broken spring in the springless vibration energy harvester

II. Broken Measuring Probe

A probe is used in the experimental setup to obtain the output RMS voltage of the harvesters. This probe connects the harvester and the oscilloscope. The initial probe didn't measure correct voltage values since its ground connection was broken. Once this probe was replaced, proper voltage values were obtained.

III. Constant Acceleration Throughout the Test

A constant acceleration of 0.5g was used during the tests to replicate the acceleration level of real applications [33]. This acceleration value is not compatible with a continuous bouncing movement of the magnetic cart against the springs throughout the interval of frequencies of the test. This phenomenon is normal since the typical frequency response curve of the springless vibration energy harvester shows a linear voltage increase followed by a voltage drop. This drop occurs when the movement of the magnetic cart becomes eclectic, and the bouncing movement stops.

Some of the tests don't consider a constant acceleration along the interval of frequencies and so the frequency response curve is not correct. Instead, they show an acceleration peak to maintain the bouncing movement of the magnetic cart against the springs in the harvester.

A. Tests in the Springless Vibration Energy Harvester

- **Test Number 1**

Test number 1 was run in the vibrations lab using the springless vibration energy harvester on February 9th 2016. The test presented the following characteristics:

- Shaker clamped to vibrations table in two points

- Long leg L-Section attached to shaker's base
- Accelerometer attached to base of the shaker
- Frequencies from 5Hz to 12Hz in intervals of 1Hz up-sweep and down-sweep
- Ambient noise of 2.26mV RMS
- Almost constant 0.5g
- Horizontal configuration
- Mass of magnetic cart 76 grams

The problems encountered during this test included:

- Two of the springs were broken
- The voltage measuring probe was also broken
- The acceleration wasn't kept constant

Figure 65 shows the acceleration RMS level during the test for the different frequencies. Remember that using a scale value in the charge amplifier of 1V/g, an output value of 500mV is equivalent to an acceleration of 0.5g.

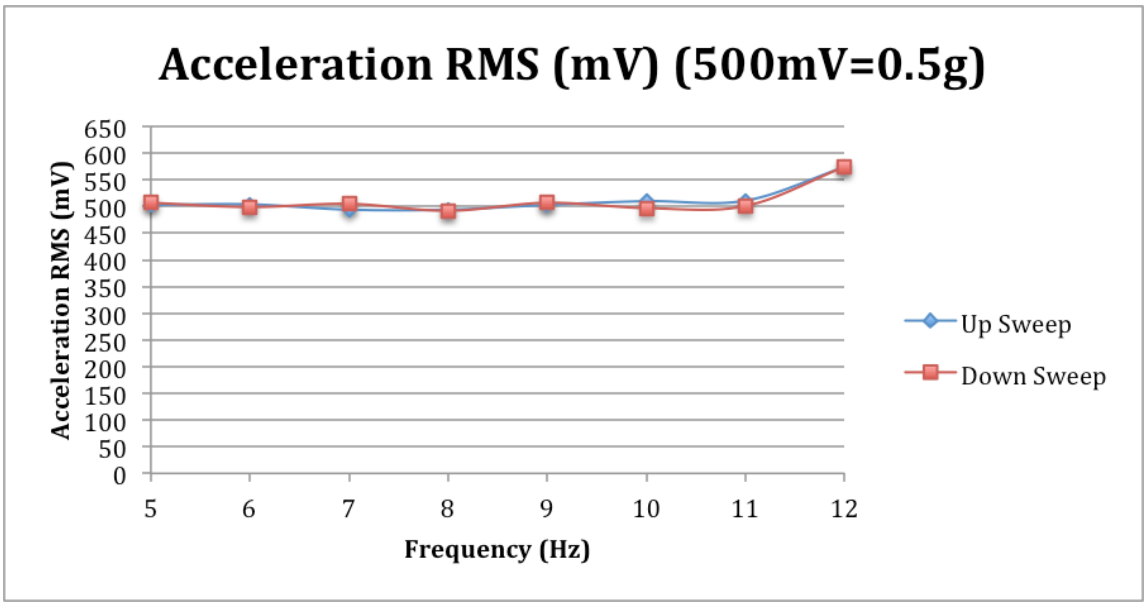

Figure 65: Acceleration RMS plot of test number 1

The acceleration RMS values can be seen in Table 57 for the interval of frequencies used.

Table 57: Acceleration RMS values of test number 1

Frequency (Hz)	Acceleration RMS (mV)
5	503
6	504
7	494
8	494
9	503
10	510
11	511
12	574
11	501
10	497
9	507
8	492
7	505
6	499
5	507

It can be noticed that for 12 Hz the acceleration level was increased to almost 600mV (0.6g).

The harvester output RMS voltage can be seen in Figure 66.

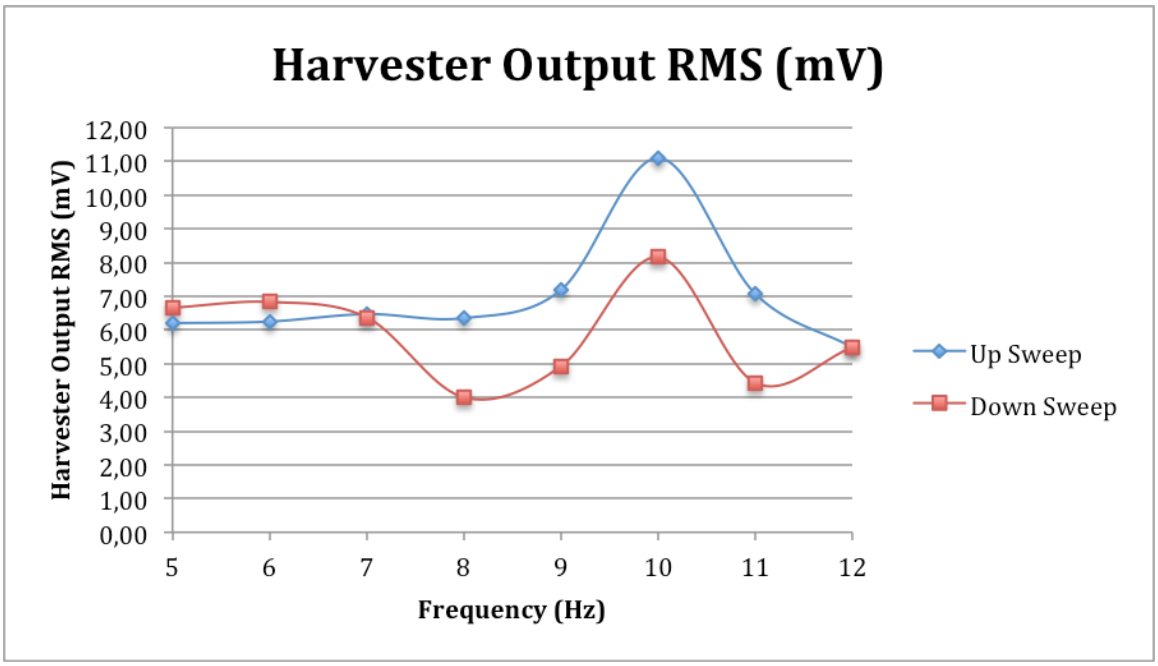

Figure 66: Harvester output RMS voltage plot of test number 1

The values of the harvester output RMS voltage can be seen in Table 58.

Table 58: Harvester output RMS voltage values of test number 1

Frequency (Hz)	Harvester Output RMS (mV)
5	6.20
6	6.25
7	6.47
8	6.35
9	7.19
10	11.10
11	7.07
12	5.48
11	4.43
10	8.16
9	4.93
8	4.00
7	6.37
6	6.83
5	6.66

The results obtained during test number 1 were similar to typical results from linear harvesters since there was a single peak of voltage around 10Hz. This peak could be considered as the resonance frequency of the harvester. The shape of the curve might have been induced by the problematic with the broken springs. The low voltage level obtained during the test pointed out to a problem in the setup, in particular with the voltage probe.

- **Test Number 2**

A second test was run on February 10th 2016 trying to replicate the results of test number 1 on the springless vibration energy harvester. The same testing conditions were replicated. Noise levels of 2.18mV and 2.07mV RMS were obtained in two different measurements, corroborating that an ambient noise level of around 2mV could be obtained, replicating the noise values obtained in Waterloo [50]. The problems encountered during this test included:

- Two of the springs were initially broken
- The voltage measuring probe was also broken

The test was run up to 7Hz noticing that the output values were similar between them for all the frequencies, with values lower than in the test effectuated the previous day. While running at 7Hz, a third spring broke. The test was pursued but after this incident the voltage values were almost constant and around 4mV, without a peak around 10Hz. This constant value of 4mV corresponded almost with the noise value and it could be assumed that the harvester in these conditions was barely generating energy.

These pieces of broken springs served to generate a hypothesis (not completely correct) concerning all the experimental trouble that had been noticed from the beginning of the experiment:

1. Since two of the springs were initially broken, more vibrations were transferred to the structure and to the accelerometer. This could clarify why the accelerometer signal presented much more noise compared to Waterloo's results. In fact all the structural modifications and the fact of changing the test room had little effect on the external vibrations perceived in the accelerometer.
2. When the frequencies of the test were increased to 12Hz or more, a level of 0.5g constant couldn't be maintained or the harvester's cart wouldn't bounce against the springs. Since the broken springs and the structure were absorbing a part of the energy, less energy was passed through bounces and the only way of making the harvester bounce against the springs was to increase the gain through the amplifier (the increase of the gain also increased the level of the signal of the accelerometer).
3. The level of energy obtained in the harvester was lower than expected. This could also be explained because the springs were not transferring energy during the bounces. The harvester itself during the bouncing movement was absorbing a big part of the energy generated.

The resonance peak obtained in the results of test number 1 could be also explained due to the absence of functioning springs. The springless vibration energy harvester is a non-linear harvester and therefore a more gradual harvester output RMS voltage increase or a wider peak in the harvester output RMS voltage was expected. Since the springs were broken, the nonlinearities had disappeared and the harvester transformed into a linear generator.

The solution considered to solve the problem with the broken springs consisted of manufacturing a 3D printed base, attaching new springs to it. This is how the springless vibration energy harvester with 3D printed base was conceived.

It is interesting to mention that the springs used in the initial base had been cut in half prior to installation, and then glued to the base leaving the flat part of the springs (this is the part that hadn't been modified) in contact with the magnetic cart. This cutting process might have been a reason for failure, decreasing the contact area with the magnetic cart and increasing the load in the springs during the bouncing movement. Another reason, and probably the most critical, might be the fatigue loads to which these springs are subjected during the repetitive cycling. To minimize the rate of failure of the springs this cutting operation should be avoided in the future.

It was mentioned before that the hypothesis of the broken springs being the problem to not obtaining good test results wasn't completely correct. In fact the reason to obtaining low test voltage values was caused by a deficient measuring probe. Once the probe was replaced, values in the order of 100mV were obtained in the springless vibration energy harvester with 3D printed base.

B. Tests of Springless Vibration Energy Harvester With 3D Printed Base

Tests number 3 and 4 were run in the springless vibration energy harvester with 3D printed base v1.2.4 in the vibrations lab. Remember that the harvester assembled using this base presented spring-magnet contact and this might reduce the voltage harvested due to the attraction of those components, complicating and limiting the linear displacement of the magnetic cart.

Tests number 5 and 6 were run in the vibrations lab using the harvester base v1.4. This harvester base solved the spring-magnet contact of base v1.2.4 and therefore more harvested voltage was initially expected from these tests.

- **Test Number 3**

The main characteristics of this test are:

- Shaker clamped to vibrations table in two points
- Long leg L-Section attached to shaker's base
- Accelerometer attached to base of the shaker
- Frequencies from 5Hz to 14Hz in intervals of 1Hz up sweep and down sweep
- Ambient noise of 1.48mV RMS in the harvester
- Almost constant 0.5g
- Horizontal configuration
- Mass of magnetic cart 76 grams

The problems encountered during this test included:

- The voltage measuring probe was broken
- The acceleration wasn't kept constant
- Spring-magnet interaction

Figure 67 presents the acceleration RMS values for the interval of frequencies of the test.

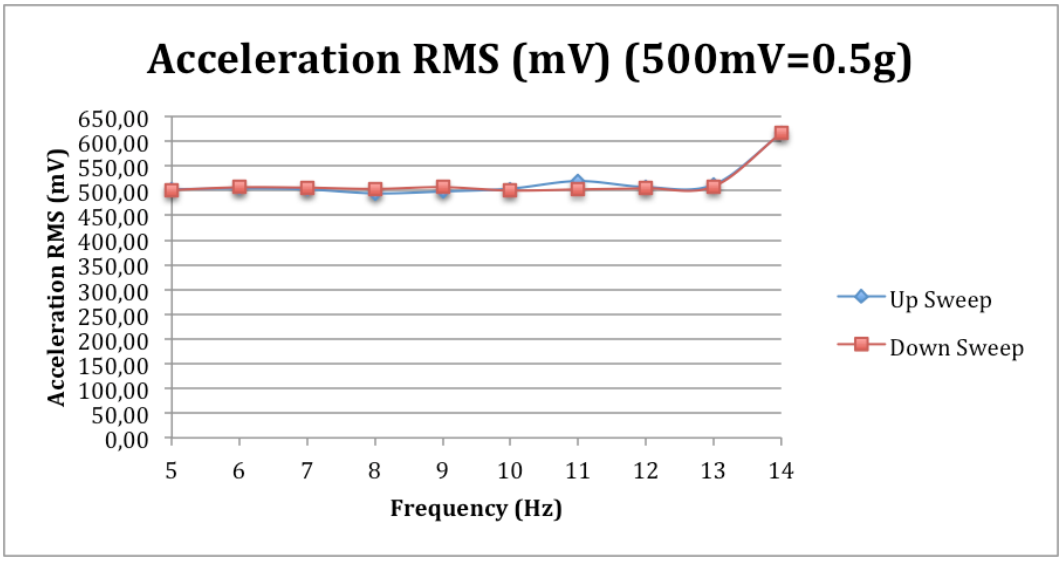

Figure 67: Acceleration RMS plot of test number 3

Note that the acceleration RMS values were kept almost constant around 500mV except for the last frequency value, where the acceleration increased to 615.75mV (0.616g).

The acceleration RMS values of test 3 can be seen in Table 59.

Table 59: Acceleration RMS values of test number 3

Frequency (Hz)	Acceleration RMS (mV)
5	502.25
6	504.50
7	502.50
8	494.50
9	498.25
10	504.00
11	519.25
12	507.25
13	512.00
14	615.75
13	508.50
12	504.75
11	502.50
10	500.25
9	507.00
8	503.50
7	506.00
6	506.75
5	501.25

Figure 68 shows the harvester output RMS voltage obtained in test number 3.

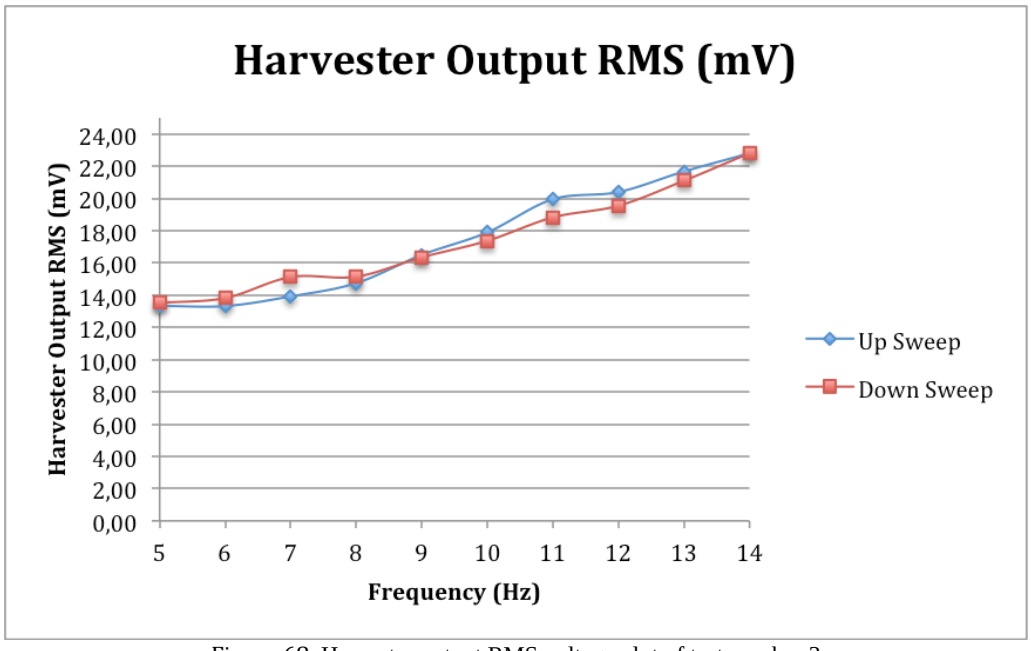

Figure 68: Harvester output RMS voltage plot of test number 3

The output RMS voltage of the harvester increases almost linearly with an increase of frequency. Table 60 includes the output RMS voltage values of test number 3.

Table 60: Output RMS voltage values of test number 3

Frequency (Hz)	Harvester Output RMS (mV)
5	13.35
6	13.33
7	13.93
8	14.75
9	16.50
10	17.90
11	19.95
12	20.40
13	21.68
14	22.80
13	21.10
12	19.55
11	18.83
10	17.38
9	16.35
8	15.15
7	15.13
6	13.83
5	13.53

- **Test Number 4**

The test characteristics were identical to those of test number 3 except for the ambient level noise of the harvester, which was now 1.31mV. The problems encountered during this test included:

- The voltage measuring probe was broken
- The acceleration wasn't kept constant
- Spring-magnet interaction

The acceleration value was kept constant at a value of around 500mV except for 14Hz (acceleration value of 610mV). A plot of these results can be seen in Figure 69.

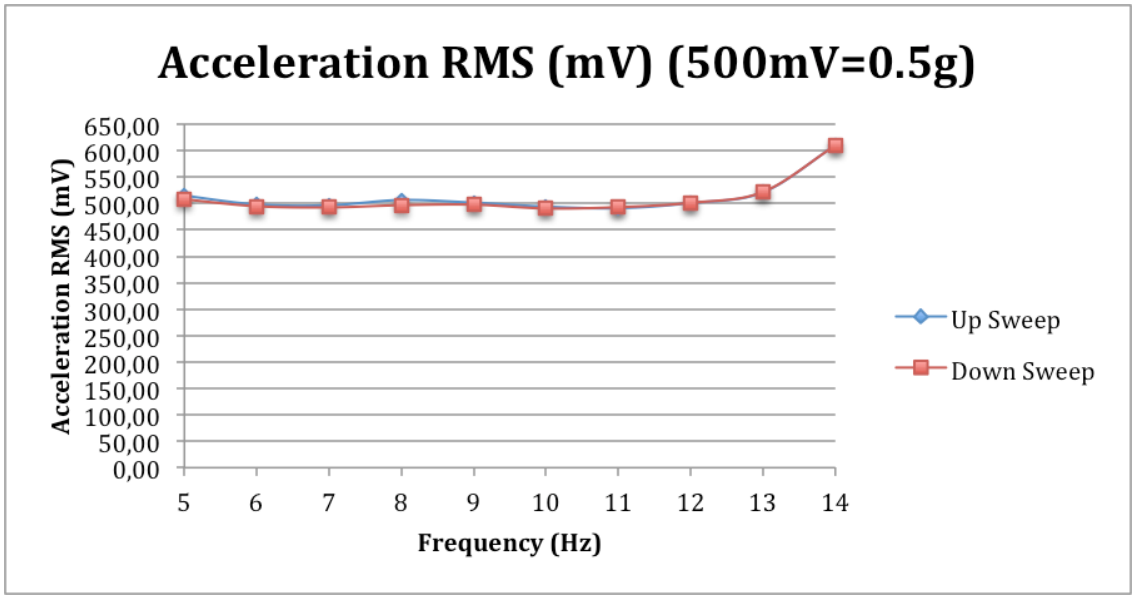

Figure 69: Acceleration RMS plot of test number 4

The acceleration RMS values can be seen in Table 61 for the different frequency values of test number 4.

Table 61: Acceleration RMS values of test number 4

Frequency (Hz)	Acceleration RMS (mV)
5	514.25
6	498.25
7	496.50
8	506.50
9	501.50
10	494.00
11	491.00
12	500.75
13	521.25
14	610.00
13	522.00
12	501.25
11	493.00
10	490.50
9	497.75
8	496.75
7	492.50
6	494.75
5	507.75

Figure 70 presents the output RMS voltage for test number 4.

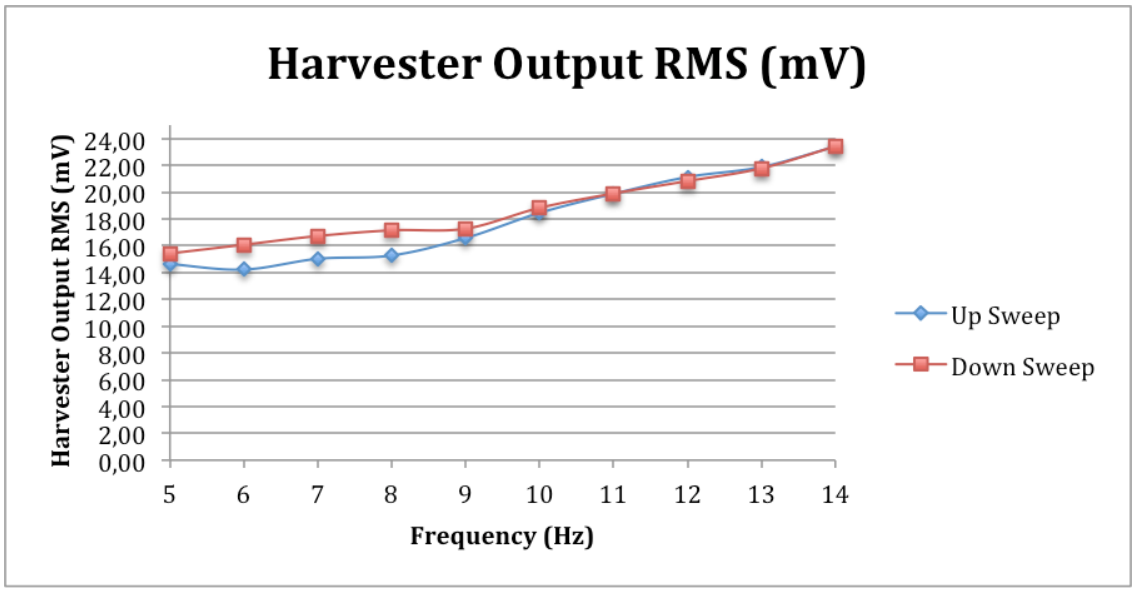

Figure 70: Output RMS voltage plot of test number 4

Table 62 includes the output RMS voltage values of test number 4.

Table 62: Output RMS voltage values of test number 4

Frequency (Hz)	Harvester Output RMS (mV)
5	14.60
6	14.23
7	15.03
8	15.28
9	16.58
10	18.45
11	19.88
12	21.13
13	21.88
14	23.40
13	21.78
12	20.83
11	19.90
10	18.83
9	17.28
8	17.15
7	16.73
6	16.08
5	15.43

- **Test Number 5**

This was the first test using the harvester base v1.2.4, in which the springs did not present spring-magnet contact, and also the first test in which the results obtained looked promising. Four measurements were normally considered for each test frequency and the final acceleration and harvester output value were obtained as the average of these four values. The main characteristics of this test are:

- Shaker clamped to vibrations table in two points
- Long leg L-Section attached to shaker's base
- Accelerometer attached to base of the shaker
- Frequencies from 5Hz to 21Hz in intervals of 1Hz up-sweep
- Ambient noise of 2.63mV RMS in the harvester

- Almost constant 0.5g up to 14Hz and non-constant g from 14 Hz to 21Hz
- Horizontal configuration
- Mass of magnetic cart 76 grams

The problems encountered during this test included:

- The voltage measuring probe was broken, even if proper results were obtained
- The acceleration wasn't kept constant

Figure 71 presents the acceleration RMS values for the interval of frequencies of the test.

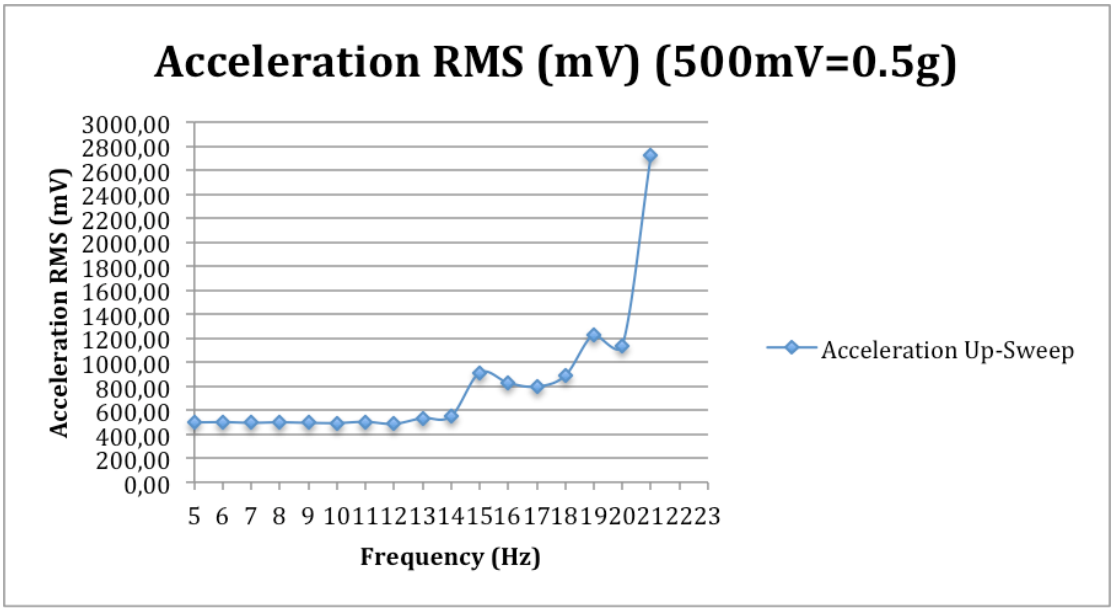

Figure 71: Acceleration RMS plot of test number 5

Note that the acceleration RMS values were kept almost constant around 500mV up to 14Hz (550mV) and increased substantially from 14Hz to 21Hz. The test was not run up to 25Hz due to the violent movement of the harvester, which could possibly break the device. The acceleration RMS values of test number 5 can also be seen in Table 63.

Table 63: Acceleration RMS values of test number 5

Frequency (Hz)	Acceleration RMS (mV)
5	496.50
6	500.50
7	494.67
8	499.00
9	494.50
10	492.50
11	503.00
12	486.00
13	534.00
14	550.00
15	912.00
16	828.00
17	796.00
18	889.00
19	1230.00
20	1140.00
21	2720.00

Figure 72 shows the output RMS voltage obtained in test number 5. The ambient noise is not considered in the results although its value was mentioned at the beginning of this test (2.63mV).

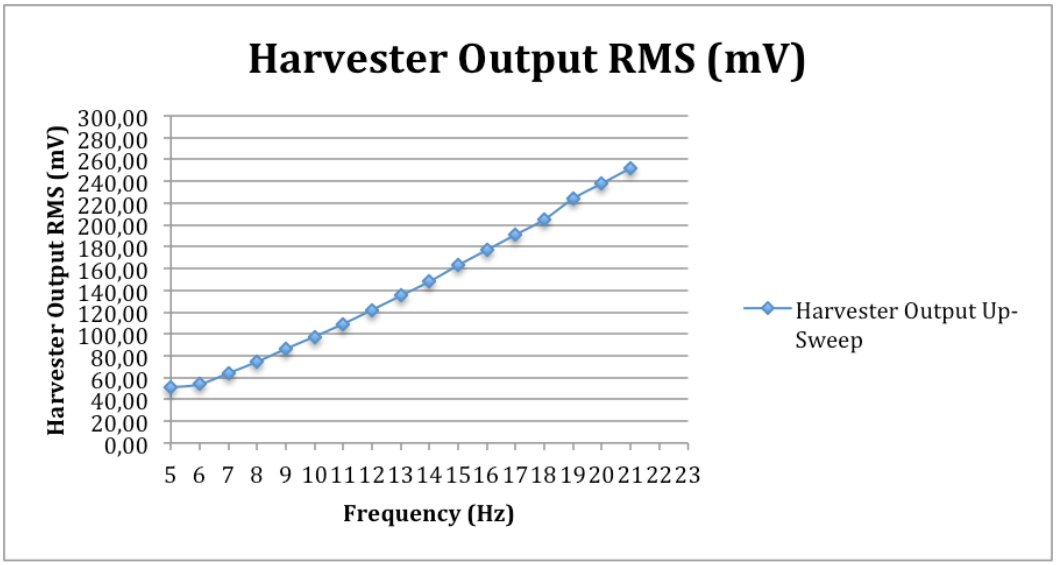

Figure 72: Output RMS voltage plot of test number 5

The output RMS voltage of the harvester increases almost linearly with an increase of frequency reaching a maximum value of 252mV at the maximum test frequency of 21Hz. It was noticed during this test that for a constant frequency value, an increase of acceleration did not imply an increase in harvester output voltage. Instead, the harvester output value was constant. Table 64 includes the output RMS voltage values of test number 5.

Table 64: Output RMS voltage values of test number 5

Frequency (Hz)	Harvester Output RMS (mV)
5	50.75
6	53.90
7	64.00
8	74.48
9	86.28
10	97.55
11	109.25
12	122.00
13	135.00
14	148.00
15	163.00
16	177.00
17	191.00
18	205.00
19	224.00
20	238.00
21	252.00

The acceleration (Channel 1 RMS) and harvester output (Channel 2 RMS) waves for 5-10Hz can be seen in Figure 73.

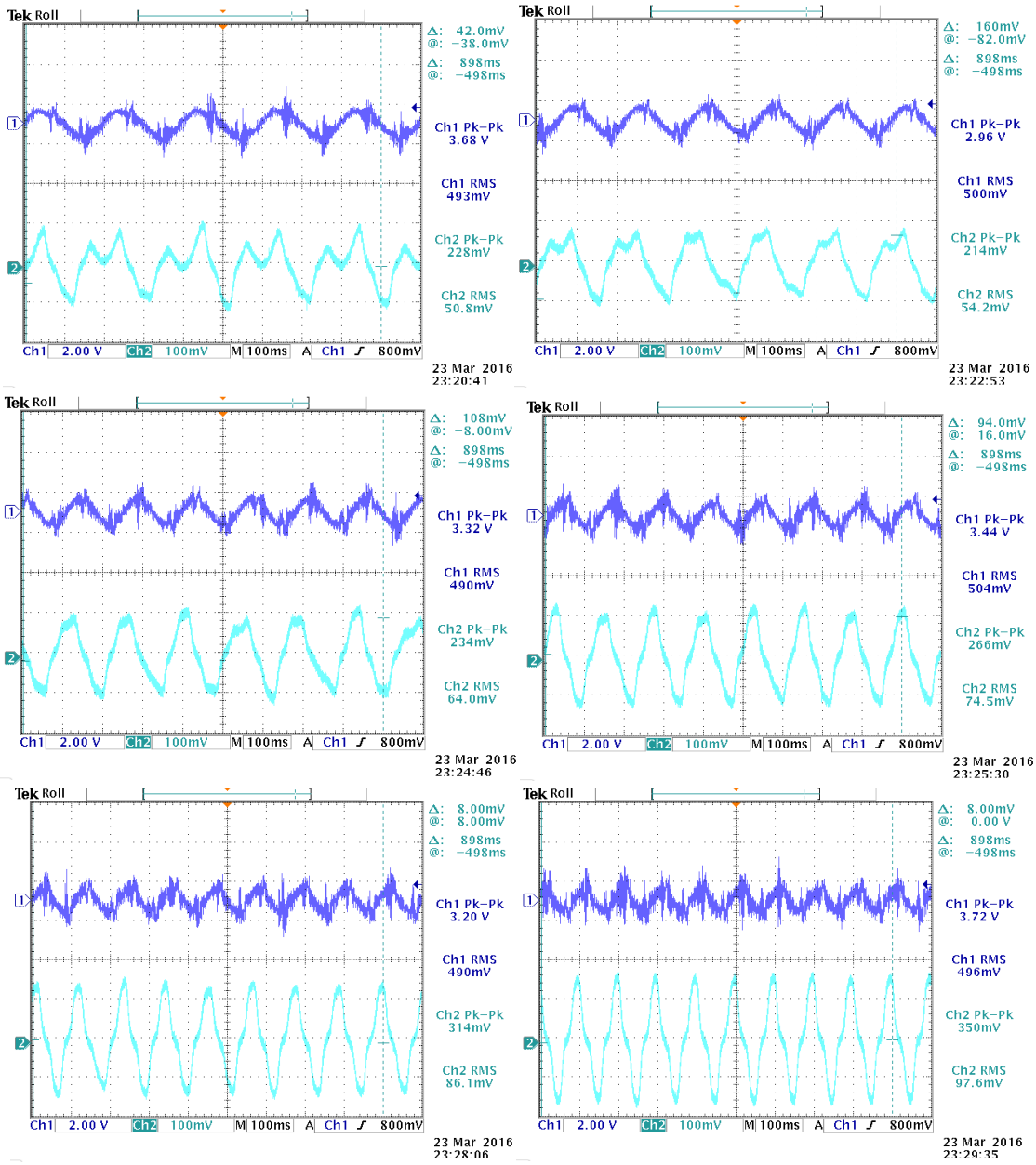

Figure 73: Acceleration and harvester output waves for 5-10Hz in test number 5

It can be seen in Figure 73 that for 5Hz-8Hz the harvester output curves are not symmetric whereas for 9Hz and 10Hz the curves are symmetric. The explanation for this phenomenon is that for low frequencies the harvester magnetic cart does not bounce with the springs at both sides of the harvester cart or if it does, it does not bounce with the same velocity. The symmetry appears gradually with the frequency increase until the magnetic cart

bounces against both sets of springs. The same shape of the curves at 9-10Hz is repeated in the curves up to 21Hz. It is also interesting to repeat that only the RMS values are considered in this study and not the peak-to-peak values.

The probe used in this test was still defective but fortunately the broken internal connection might have been properly working during the test and so proper voltage values were obtained.

- **Test Number 6**

In this new test the acceleration was kept constant at 0.5g from 5Hz to 20Hz. The test stopped at 20 Hz instead of continuing until 25Hz because one of the cables of the harvester broke. Four measurements were normally considered for each test frequency and the final acceleration and harvester output value were obtained as the average of these four values. The main characteristics of this test are:

- Shaker clamped to vibrations table in two points
- Long leg L-Section attached to shaker's base
- Accelerometer also attached to harvester's base
- Frequencies from 5Hz to 20Hz in intervals of 1Hz up-sweep
- Ambient noise of 2.16mV RMS in the harvester
- Almost constant 0.5g up to 20Hz
- Horizontal configuration
- Mass of magnetic cart 76 grams

Figure 74 presents the acceleration RMS values for the interval of frequencies of test 6.

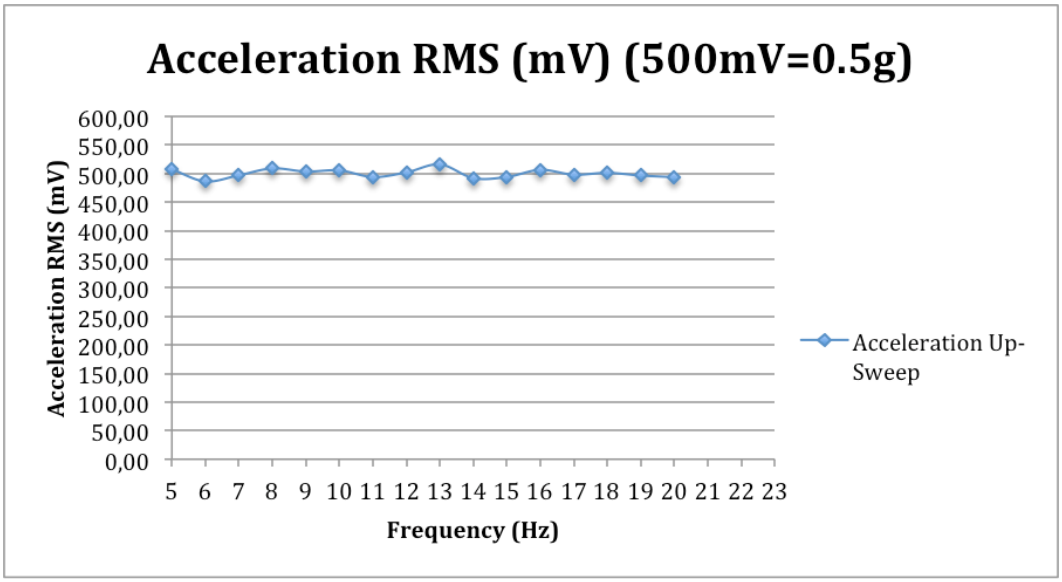

Figure 74: Acceleration RMS plot of test number 6

The acceleration RMS values of test number 6 can also be seen in Table 65.

Table 65: Acceleration RMS values of test number 6

Frequency (Hz)	Acceleration RMS (mV)
5	507.25
6	486.25
7	497.00
8	509.00
9	503.50
10	505.50
11	494.00
12	502.00
13	516.00
14	492.00
15	494.00
16	506.50
17	498.00
18	501.25
19	496.50
20	493.75

Figure 75 shows the output RMS voltage obtained in test number 6. The ambient noise is not considered in the results although its value was mentioned at the beginning of this test (2.16mV).

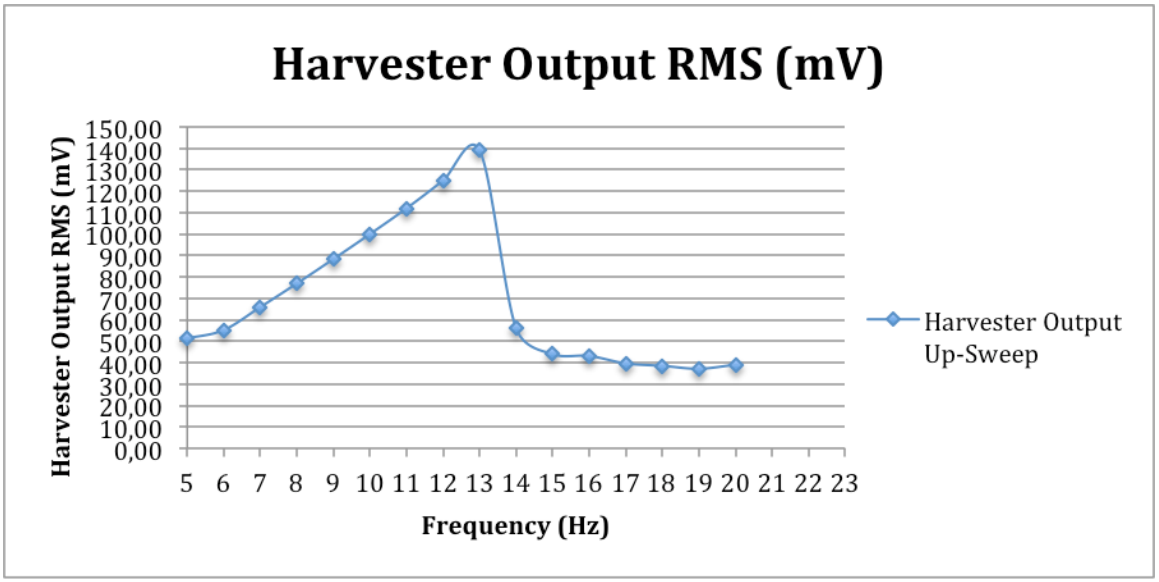

Figure 75: Output RMS voltage plot of test number 6

The output RMS voltage of the harvester increases almost linearly with an increase of frequency reaching a maximum value of 139mV at 13Hz. Then the output voltage suddenly drops until the final frequency value of 20Hz. Table 66 includes the output RMS voltage values of test number 6.

Table 66: Output RMS values of test number 6

Frequency (Hz)	Harvester Output RMS (mV)
5	51.13
6	55.23
7	65.93
8	76.95
9	88.35
10	100.00
11	112.00
12	125.00
13	139.00
14	56.00
15	44.00
16	43.13
17	39.63
18	38.50
19	37.15
20	39.03

The acceleration and harvester output waves for 5-10Hz can be seen in Figure 76.

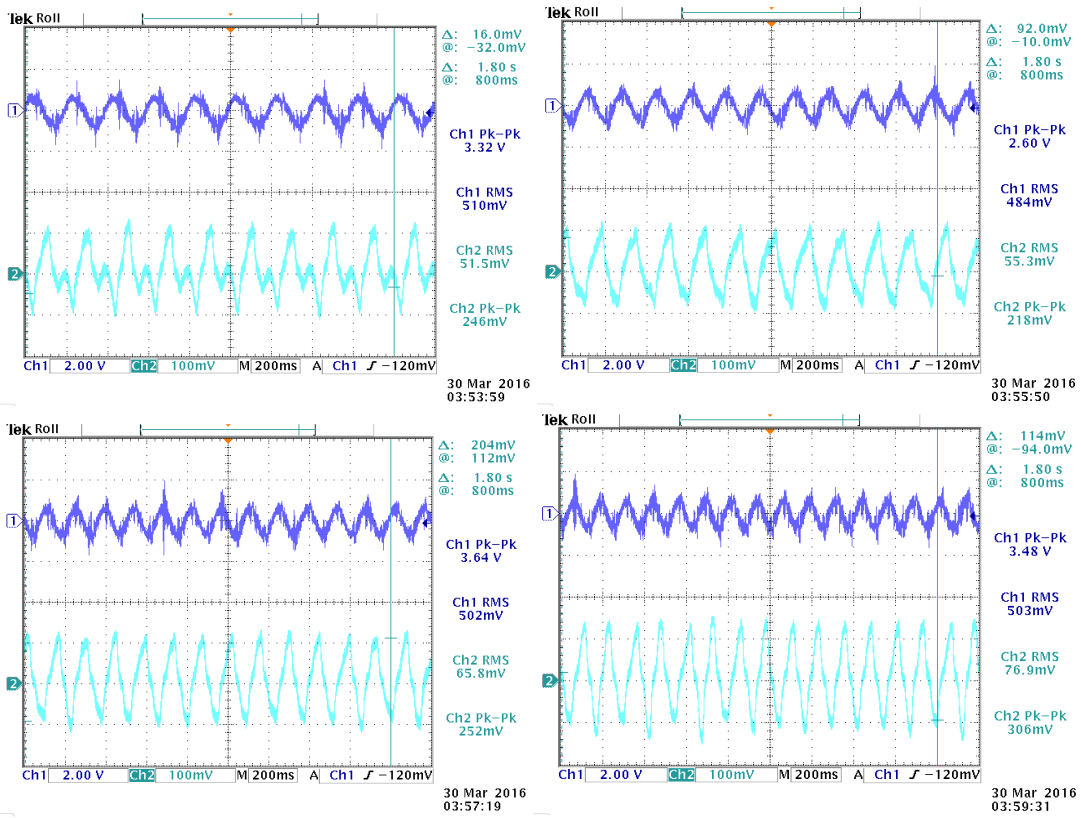

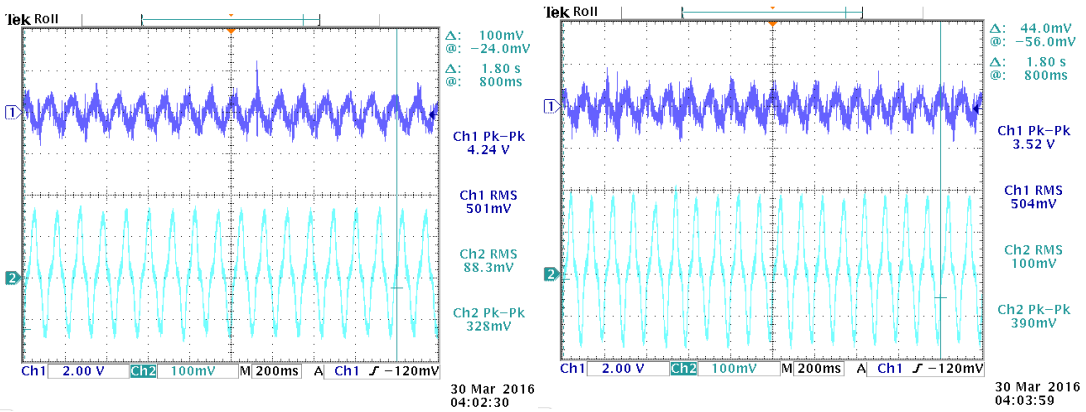

Figure 76: Acceleration and harvester output waves for 5-10Hz in test number 6

As in test number 5, the harvester output curves (Channel 2 RMS) are not symmetric for 5Hz 8Hz and become symmetric for 9Hz and 10Hz. The same shape of the curves at 9-10Hz is repeated up to 13Hz, where the output voltage peak is obtained. The acceleration and harvester output waves for 13-20Hz can be seen in Figure 77.

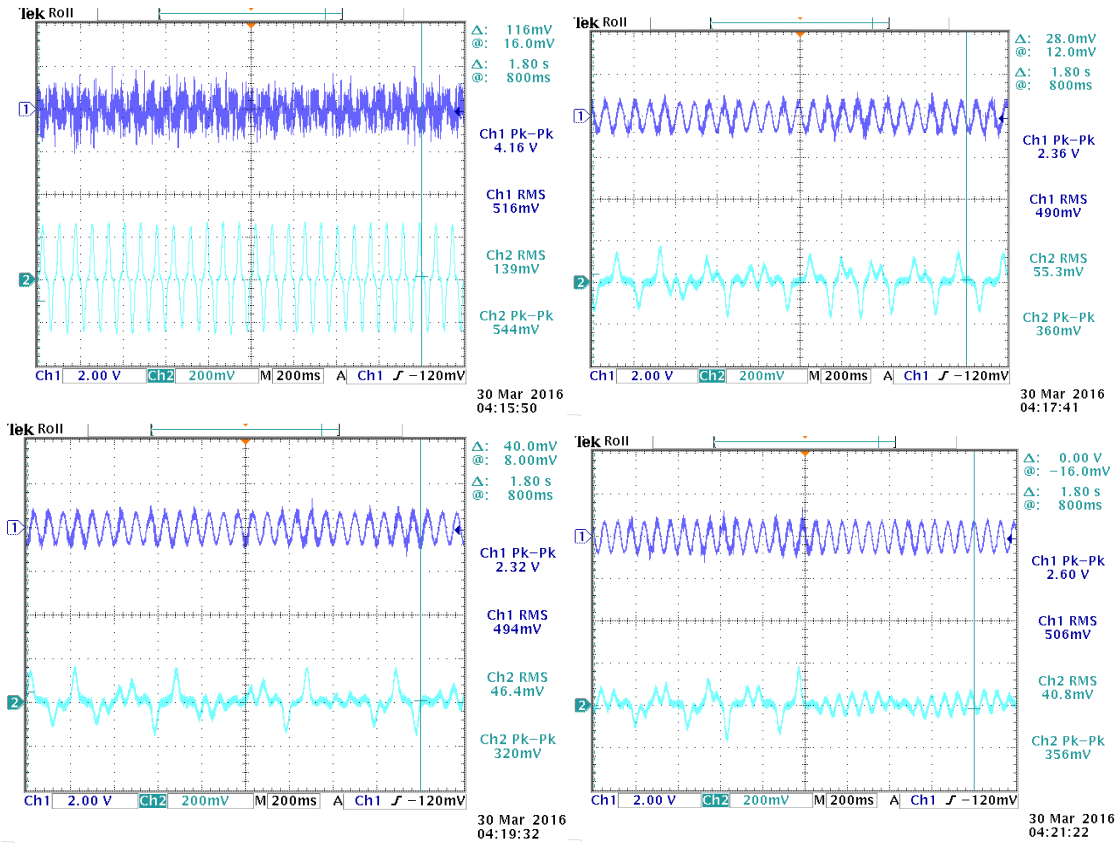

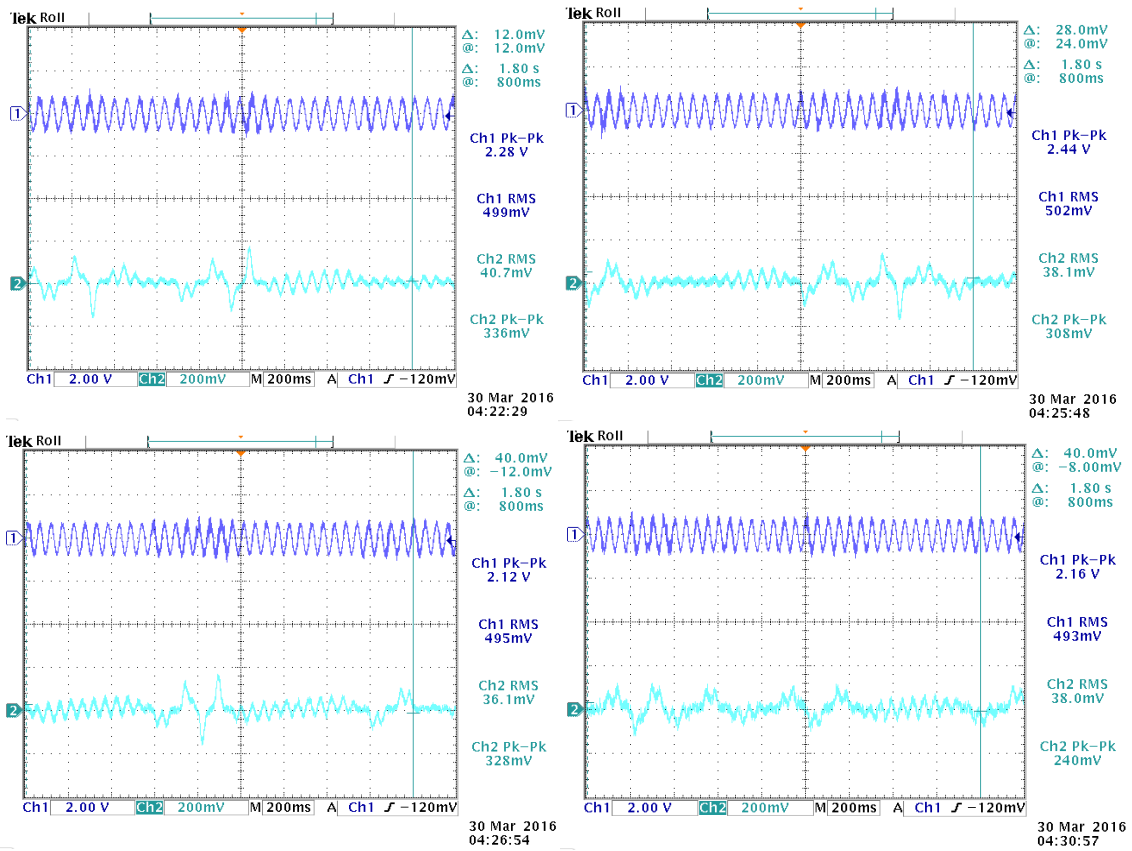

Figure 77: Acceleration and harvester output waves for 13-20Hz in test number 6

Note how for 13Hz the harvester output wave (Channel 2 RMS) is symmetric with peaks both up and down. From 14Hz to 20Hz the number of peaks decrease, as each peak corresponds to an impact against the springs. The curves stop being repetitive and become somehow random.

Appendix 4: 3D Printed Harvester Bases

This appendix includes detailed information about all the 3D printed harvester bases that were manufactured during the thesis work.

3D Printed Harvester Base v1.0

The main 3D printing characteristics of base v1.0 are included in Table 67.

Table 67: Harvester base v1.0 3D printing characteristics

Printing Features	Harvester base v1.0
3D printer model	Makerbot replicator 2
3D printer cost ($)	2500
Printing mass including raft or brim (g)	10.14
Additional components (raft of brim)	Raft
Final mass (g)	7
Material	HIPS
Material cost ($/Kg)	24.95
Total cost ($)	0.25
Printing quality	Low
Design defects	• Tolerance of lateral slots too small (0.12”x0.12”) • Wrong distance between holes for 3D printed layer
First component set-up time (min)	8
Printing time (min)	36
Total time (min)	44
Manufacturing defects	• Lateral displacement of the initial base layers • Filling of lower base holes • Need to clean holes with cutter • Misalignment of base holes due to cutting operation • Minimum layering gaps in the base

3D Printed Harvester Base v1.1

The dimensions of v1.0 were modified to solve the design defects of that base, this is, the distance between the holes to attach the 3D printed layer and the dimensions of the lateral slots to insert the rail. After these modifications the 3D printed layer could be perfectly

bolted but the lateral holes ended up being too big, not allowing a perfect tightness. The metallic rail was tested in this base, inserting it via the lateral slot and bolting it via the five holes in the base. Base v1.1was printed in low quality, and because of this, the holes in the base were not perfectly formed and they had to be finished with a cutter. This operation slightly modified the tolerance of the holes and when the bolts were screwed, only 4 out of the possible 5 bolts could be fitted into the rail. Figure 78 shows the 3D printed harvester base v1.1 (the severe layering default is easily perceptible in it).

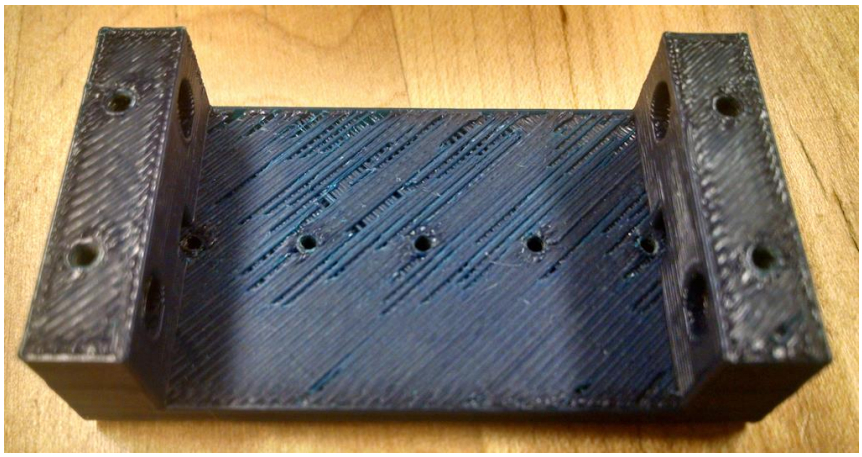

Figure 78: 3D printed harvester base v1.1

The main printing aspects of this component can be seen in Table 68.

Table 68: Harvester base v1.1 3D printing characteristics

Printing Features	Harvester base v1.1
3D printer model	Makerbot replicator 2
3D printer cost ($)	2500
Printing mass including raft or brim (g)	9.77
Additional components (raft of brim)	Raft
Final mass (g)	6
Material	HIPS
Material cost ($/Kg)	24.95
Total cost ($)	0.24
Printing quality	Low
Design defects	• Tolerance of lateral slot too big(0.136”x0.125”)
First component set-up time (min)	8
Printing time (min)	36
Total time (min)	44
Manufacturing defects	• Lateral displacement of the initial base layers • Filling of lower base holes • Need to clean holes with cutter • Misalignment of base holes due to cutting operation • Severe layering gaps in the base

3D Printed Harvester Base v1.2.0

The harvester base v1.2.0 corresponds to a minor modification of v1.1 regarding the dimensions of the lateral slots, which were set to an average value between base v1.0 and v1.1. The 3D printer was in this case modified (with respect to v1.0 and v1.1) with the intention of improving the quality of the model and to verify if this new printer could improve the aesthetics and performance of the component. This time the five bolts in the base could be attached to the rail although the laterals of the base still presented some layering gaps and the base holes still needed to be improved using a cutter. Figure 79 shows the 3D printed harvester base v1.2.0.

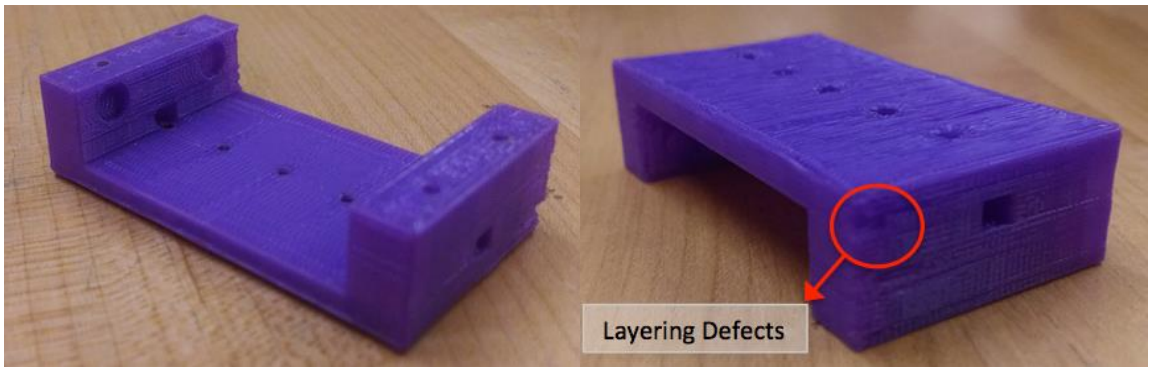

Figure 79: 3D printed harvester base v1.2.0

Table 69 presents the principal printing aspects of base v1.2.0.

Table 69: Harvester base v1.2.0 3D printing characteristics

Printing Features	Harvester base v1.2.0
3D printer model	Makerbot replicator 5th generation
3D printer cost ($)	2900
Printing mass including raft or brim (g)	9.77
Additional components (raft of brim)	Raft
Final mass (g)	6
Material	HIPS
Material cost ($/Kg)	24.95
Total cost ($)	0.24
Printing quality	Low
Design defects	• None. Dimensions of lateral slot 0.128”x0.1225”
First component set-up time (min)	8
Printing time (min)	50
Total time (min)	58
Manufacturing defects	• Slight filling of lower base holes • Need to clean holes with cutter • Slight misalignment of base holes due to cutting operation • Severe layering gaps in the laterals

3D Printed Harvester Base v1.2.1

Due to the presence of manufacturing defaults regardless of the printer used, it was decided to select a new printer model and improve the printing quality, while maintaining the

dimensions. These modifications would allow for a better performance of the component and also for a higher density, while taking more time to print the same component.

When 3D printing in low quality, the raft is printed in lower quality and density compared to the component, and both parts can be normally detached from each other with a minor operation (a knife can be used for this purpose). When 3D printing in higher quality, even if the quality and density of the raft are of a lower quality than the component, they still present high quality and density and therefore its removal from the part turns out to be very difficult. This fact was learnt after 3D printing the harvester base v1.2.1 in high quality using HIPS. In this case the raft and the harvester base were almost melted together and a sander was used to separate them, resulting in an improper visual impact.

Table 70 presents the principal printing aspects of base v1.2.1.

Table 70: Harvester base v1.2.1 3D printing characteristics

Printing Features	Harvester base v1.2.1
3D printer model	Lulzbot TAZ 5
3D printer cost ($)	2200
Printing mass including raft or brim (g)	9
Additional components (raft of brim)	Raft
Final mass (g)	6
Material	HIPS
Material cost ($/Kg)	24.95
Total cost ($)	0.22
Printing quality	High Detail
Design defects	• None. Dimensions of lateral slot 0.128”x0.1225”
First component set-up time (min)	8
Printing time (min)	92
Total time (min)	100
Manufacturing defects	• Raft completely melted with base of component • Impossible to detach • Sanding operation worsen things

3D Printed Harvester Base v1.2.2

The material selected was then changed from HIPS to ABS basing this decision upon their thermal properties. HIPS components solidify slower than ABS and then by the time the component is being 3D printed, the raft has not yet solidified and can melt to the component. ABS is supposed to solidify faster and it is thought that by the time the component starts printing, the raft will already be solid, not having time to melt within the harvester's base.

This new ABS base presented very good quality and the raft wasn't completely melted into the component. Minor cutting operations were needed to separate the raft and the base and so it was believed that the material choice was ideal. Table 71 presents the principal printing aspects of base v1.2.2.

Table 71: Harvester base v1.2.2 3D printing characteristics

Printing Features	Harvester base v1.2.2
3D printer model	Lulzbot TAZ 5
3D printer cost ($)	2200
Printing mass including raft or brim (g)	9
Additional components (raft of brim)	Raft
Final mass (g)	6
Material	Blue ABS
Material cost ($/Kg)	29
Total cost ($)	0.26
Printing quality	High Detail
Design defects	• None. Dimensions of lateral slot 0.128"x0.1225"
First component set-up time (min)	8
Printing time (min)	92
Total time (min)	100
Manufacturing defects	• Raft slightly melted with base of component • Simple cutter operation to separate it

3D Printed Harvester Base v1.2.3

A second base (v1.2.3) using the same parameters and material was also 3D printed and this time the raft and the base were completely melted together. Table 72 presents the principal printing aspects of base v1.2.3.

Table 72: Harvester base v1.2.3 3D printing characteristics

Printing Features	Harvester base v1.2.3
3D printer model	Lulzbot TAZ 5
3D printer cost ($)	2200
Printing mass including raft or brim (g)	9
Additional components (raft of brim)	Raft
Final mass (g)	6
Material	Blue ABS
Material cost ($/Kg)	29
Total cost ($)	0.26
Printing quality	High Detail
Design defects	• None. Dimensions of lateral slot 0.128”x0.1225”
First component set-up time (min)	8
Printing time (min)	92
Total time (min)	100
Manufacturing defects	• Raft completely melted with base of component. • Difficult cutter operation to separate it.

The conclusion extracted from this was that in fact the melting process between the raft and the base didn’t depend as much on the thermal properties of the materials as on the time in between the end of the printing process and the separation operation of the raft and the base. The more time past from the end of the 3D printing process the more attached both components became and the more difficult it became to separate them.

3D Printed Harvester Base v1.2.4

After the positive outcome of the harvester base v1.2.3 it was decided to run a new printing test without a raft, due to the problems that a high quality raft introduced in the

separation and cleaning operations. To do this, the pre-established parameters in the Lulbotz TAZ 5 3D printer were selected, using ABS as printing material. These configuration values differed from those in v1.2.3, including changes in the bed temperature and the ventilation of the printer. Some of the tolerances of the base were affected because of the new set-up due to a melting problem. This issue consisted of a melt of the initial 3D printed layers, increasing the initial dimensions (length and width) of the base and decreasing its total height. Because of this matter the tolerance between the top holes of the harvester's base (where the 3D printed layer is bolted) and the height of the holes of the base (where the rail is attached) were modified. Some minor manufacturing errors that didn't affect the global assembly were observed after the assembly of this harvester.

- Due to the change in tolerance between the top holes of the harvester's base, when the 3D printed layer was installed on the base, it presented some curvature. Figure 80 shows the curvature of the layer when bolted to the base.

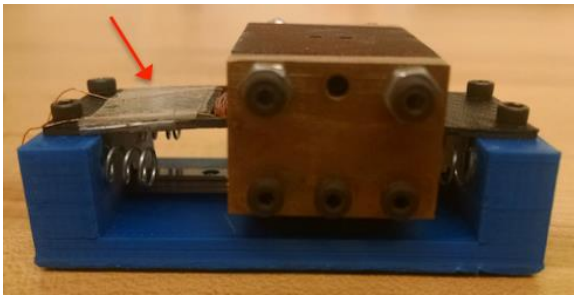

Figure 80: Curvature of the 3D printed layer installed in the harvester base v1.2.4

- The change in height of the holes of the base worsened the installation of the head of the fasteners inside and completely covered by the base. Figure 81 presents the slightly protruding head of the fasteners bolted to the base.

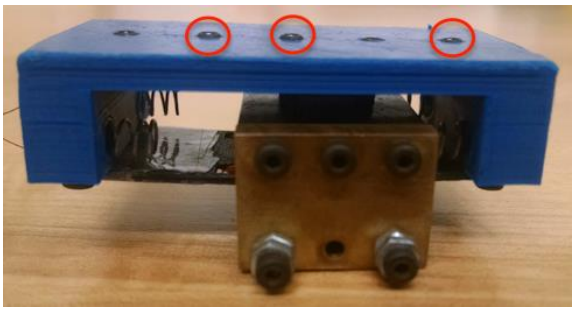

Figure 81: Problematic with head of fasteners in the harvester base v1.2.4

Table 73 presents the principal printing aspects of base v1.2.4.

Table 73: Harvester base v1.2.4 3D printing characteristics

Printing Features	Harvester base v1.2.4
3D printer model	Lulzbot TAZ 5
3D printer cost ($)	2200
Printing mass including raft or brim (g)	8
Additional components (raft of brim)	-
Final mass (g)	6
Material	Blue ABS
Material cost ($/Kg)	29
Total cost ($)	0.23
Printing quality	Pre-established parameters
Design defects	• Wrong tolerance in the top holes of the harvester's base • Incorrect height of the holes of the base • Wrong height of spring holes causing spring-magnet contact
First component set-up time (min)	8
Printing time (min)	73
Total time (min)	81
Manufacturing defects	• Component melted to base of printer • Minor cutter cleaning operation.

3D Printed Harvester Base v1.3

Harvester base v1.3 intended to solve the magnetic contact problem of base v1.2.4. To do that, the holes of the base where the springs are installed were lowered 0.02". After

mounting new springs in this base it was noticed that the contact had been substantially reduced but not cancelled. Also minor buckling was observed in base v1.3.

Table 74 presents the principal printing aspects of base v1.3.

Table 74: Harvester base v1.3 3D printing characteristics

Printing Features	Harvester base v1.3
3D printer model	Lulzbot TAZ 5
3D printer cost ($)	2200
Printing mass including raft or brim (g)	8
Additional components (raft of brim)	-
Final mass (g)	6
Material	Blue ABS
Material cost ($/Kg)	29
Total cost ($)	0.23
Printing quality	Pre-established parameters
Design defects	• Wrong tolerance in the top holes of the harvester's base • Incorrect height of the holes of the base • Minimum spring-magnet contact
First component set-up time (min)	8
Printing time (min)	73
Total time (min)	81
Manufacturing defects	• Component melted to base of printer • Minor cutter cleaning operation • Slight buckling in one of the lower corners

3D Printed Harvester Base v1.4

Harvester base v1.4 was created to solve the design defects of base v1.3. In this base, the holes of the base where the springs are installed were lowered 0.01" more, the holes of the base where the 3D printed layer is installed were separated for a better tolerance and the total height of the part was increased. Also the quality of the print was modified back to high quality and a brim was added to avoid buckling.

3D Printed Harvester Base v3.0.0

The harvester base v3.0.0 was an initial test in low quality to allow understanding how this new base might work. Figure 82 shows the 3D printed harvester base v3.0.0 including its severe layering defects.

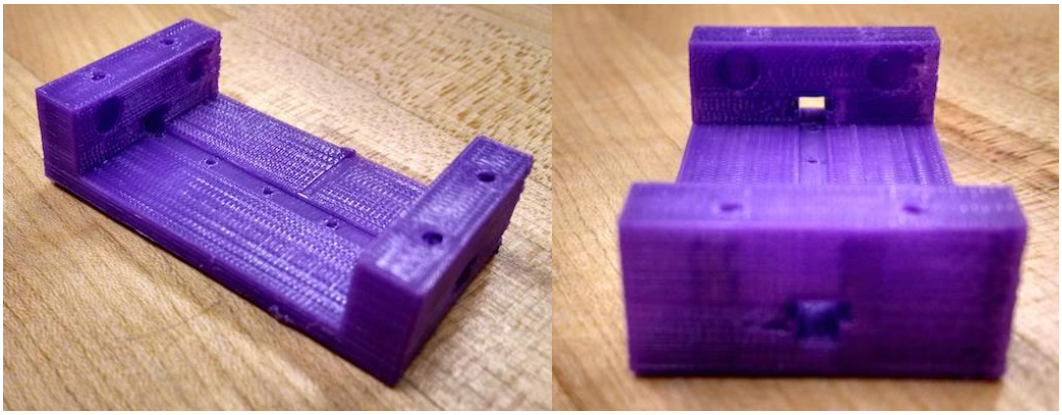

Figure 82: 3D printed harvester base v3.0.0

Table 75 presents the principal printing aspects of base v3.0.0.

Table 75: Harvester base v3.0.0 3D printing characteristics

Printing Features	Harvester base v3.0.0
3D printer model	Makerbot replicator 5th generation
3D printer cost ($)	2900
Printing mass including raft or brim (g)	9
Additional components (raft of brim)	Raft
Final mass (g)	6
Material	HIPS
Material cost ($/Kg)	24.95
Total cost ($)	0.22
Printing quality	Low
Design defects	• Initial test to check dimensions of rail hole
First component set-up time (min)	8
Printing time (min)	73
Total time (min)	81
Manufacturing defects	• Filling of base holes • Multiple and severe layering problem

3D Printed Harvester Base v3.0.1

The base v3.0.1 is the improved quality version of base v3.0.0. In this case the pre-defined parameters of the printer were selected for ABS, and the use of a raft was neglected. The same design defects as in base v1.3 were here obtained. Also due to the printing parameters the same manufacturing defects as in base v1.2.4 occurred. After this base was obtained it was decided to stop using the pre-established parameters of the Lulzbot TAZ 5 printer because this option should be used for quick prints but not for high detail and tolerance operations. Figure 83 shows the 3D printed harvester base v3.0.1.

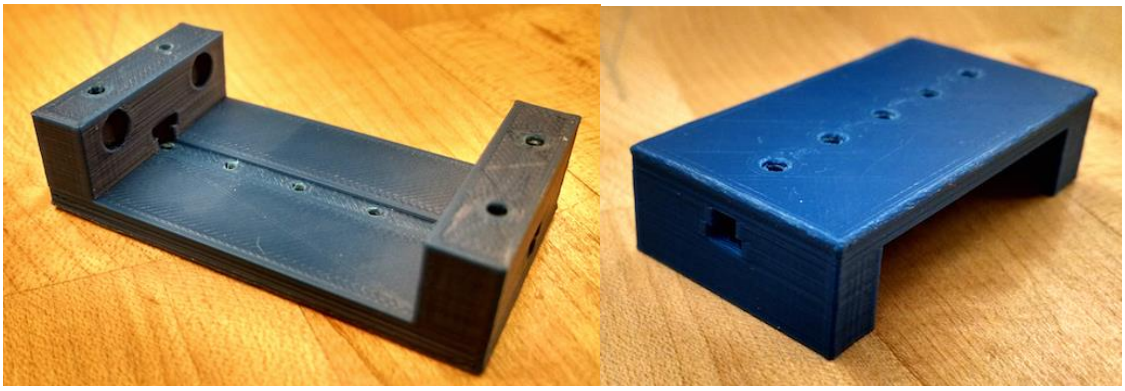

Figure 83: 3D printed harvester base v3.0.1

Table 76 presents the principal printing aspects of base v3.0.1.

Table 76: Harvester base v3.0.1 3D printing characteristics

Printing Features	Harvester base v3.0.1
3D printer model	Lulzbot TAZ 5
3D printer cost ($)	2200
Printing mass including raft or brim (g)	8
Additional components (raft of brim)	-
Final mass (g)	6
Material	Blue ABS
Material cost ($/Kg)	29
Total cost ($)	0.23
Printing quality	Pre-established parameters
Design defects	• Wrong tolerance in the top holes of the harvester's base • Incorrect height of the holes of the base • Minimum spring-magnet contact
First component set-up time (min)	8
Printing time (min)	73
Total time (min)	81
Manufacturing defects	• Component melted to base of printer • Minor cutter cleaning operation.

3D Printed Harvester Base v3.0.2

Base v3.0.2 consisted of an attempt to try a different material to manufacture the harvester base. The new material is called PET and presented really good density, external tolerances, and finishing characteristics although it wasn't a good selection for internal holes or complex geometry (PET tends to melt and fill holes). The 3D printing quality was modified to high detail. Figure 84 shows the 3D printed harvester base v3.0.2.

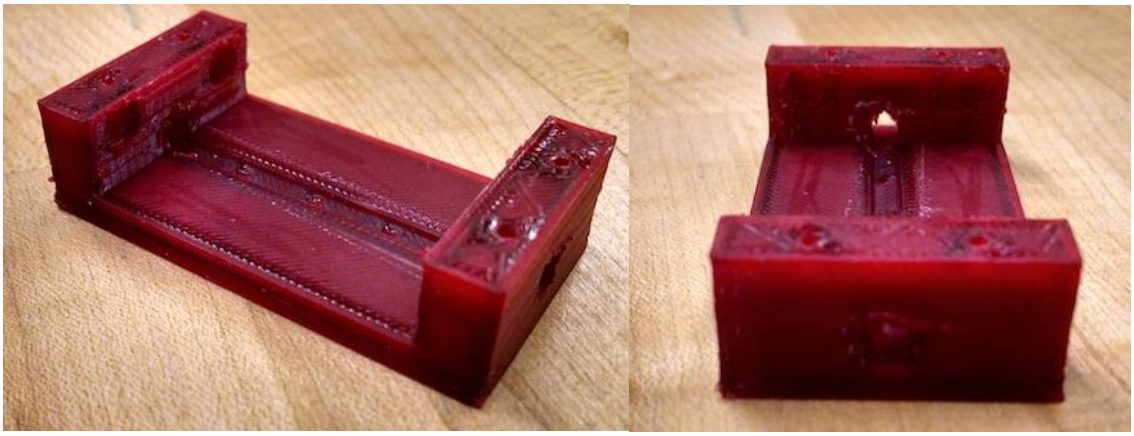

Figure 84: 3D printed harvester base v3.0.2

Table 77 presents the principal printing aspects of base v3.0.2.

Table 77: Harvester base v3.0.2 3D printing characteristics

Printing Features	Harvester base v3.0.2
3D printer model	Lulzbot TAZ 5
3D printer cost ($)	2200
Printing mass including raft or brim (g)	13
Additional components (raft of brim)	-
Final mass (g)	13
Material	PET
Material cost ($/Kg)	48
Total cost ($)	0.62
Printing quality	High Detail
Design defects	• Wrong tolerance in the top holes of the harvester's base • Incorrect height of the holes of the base • Minimum spring-magnet contact
First component set-up time (min)	8
Printing time (min)	76
Total time (min)	84
Manufacturing defects	• Filled holes due to new properties of the material

3D Printed Harvester Base v3.1.0

The manufacturing and design defects of the previous base were solved in base v3.1.0. The quality used was high detail and a brim was added to the manufacturing process. The 3D printed harvester base v3.1.0 can be seen in Figure 85.

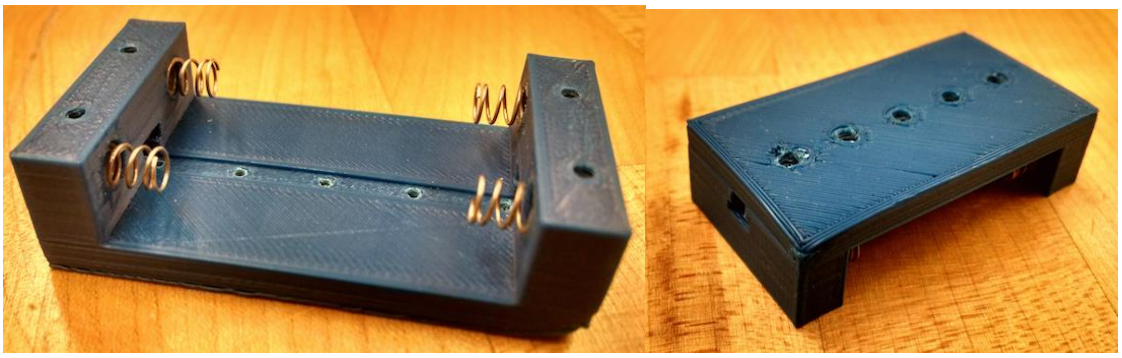

Figure 85: 3D printed harvester base v3.1.0

Table 78 presents the principal printing aspects of base v3.1.0.

Table 78: Harvester base v3.1.0 3D printing characteristics

Printing Features	Harvester base v3.1.0
3D printer model	Lulzbot TAZ 5
3D printer cost ($)	2200
Printing mass including raft or brim (g)	9
Additional components (raft of brim)	Brim
Final mass (g)	7
Material	Blue ABS
Material cost ($/Kg)	29
Total cost ($)	0.26
Printing quality	High Detail
Design defects	• None
First component set-up time (min)	8
Printing time (min)	76
Total time (min)	84
Manufacturing defects	• Buckling in one of the lower corners.

3D Printed Harvester Base v3.1.1

A second copy of the previous base was done using a different and cheaper brand of ABS. This base was denominated v3.1.1. The buckling was reduced this time although minor layering gaps and minor tolerance reduction were noticed.

Appendix 5: 3D Printed Layer

This appendix includes detailed information about all the 3D printed layers that were manufactured during the thesis work.

3D Printed Layer v1.0

The design dimensions of the 3D printed layer v1.0 duplicated those of the 3D printed layer included in the original springless vibration energy harvester. Figure 86 shows a design drawing of this component.

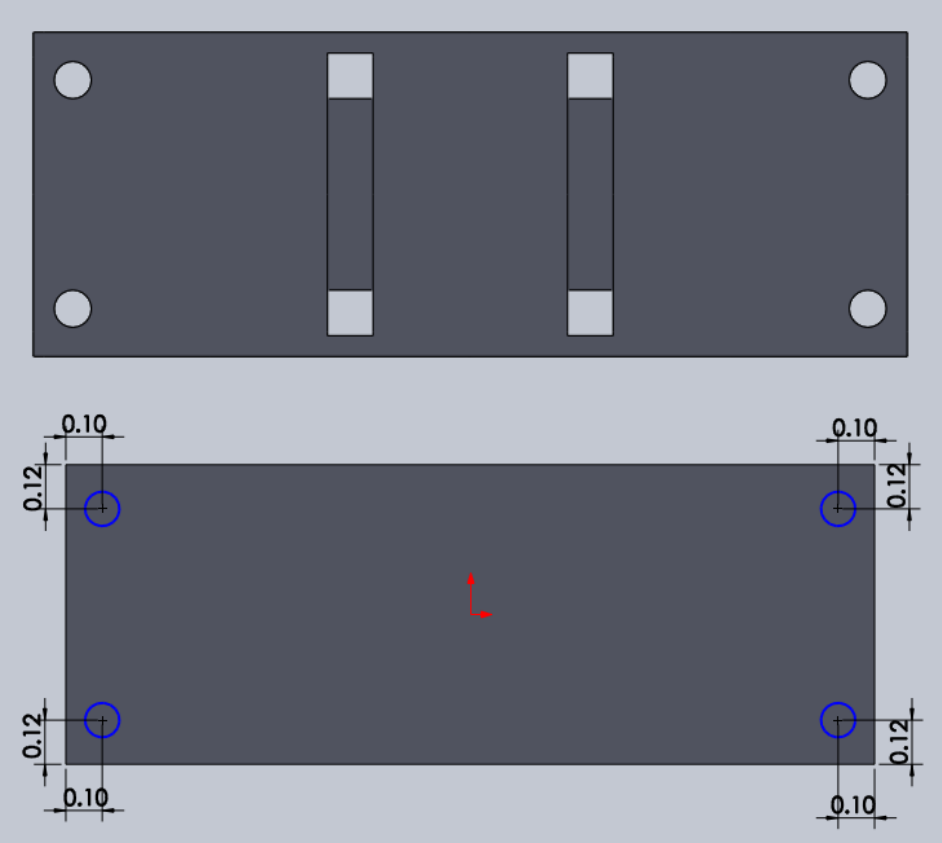

Figure 86: Top view and dimensions of design drawing of 3D printed layer v1.0

The manufacturing characteristics of the 3D printed layer v1.0 can be seen in Table 79.

Table 79: 3D printing characteristics of 3D printed layer v1.0

Printing Features	3D Printed Layer v1.0
3D printer model	Makerbot replicator 2
3D printer cost ($)	2500
Printing mass including raft or brim (g)	3.3
Additional components (raft of brim)	Brim
Final mass (g)	1
Material	PLA
Material cost ($/Kg)	48
Total cost ($)	0.16
Printing quality	Low
Design defects	• Holes in the layer needed to be modified to adapt to new harvester bases
First component set-up time (min)	8
Printing time (min)	10
Total time (min)	18
Manufacturing defects	• None

3D Printed Layer v1.1

The 3D printed layer v1.1 solved some minor dimensional problems concerning the position of the holes in the 3D printed layer v1.0. No manufacturing defects were observed. Although the manufacturing process was viable, the original 3D printed layer was used for the tests. Figure 87 shows the dimension of the 3D printed layer v1.1.

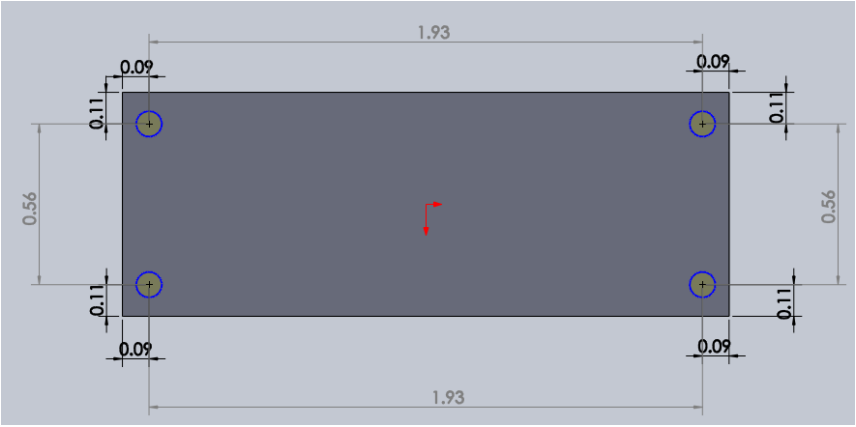

Figure 87: Dimensions of 3D printed layer v1.1

The 3D printed layer v1.1 can be seen in Figure 88.

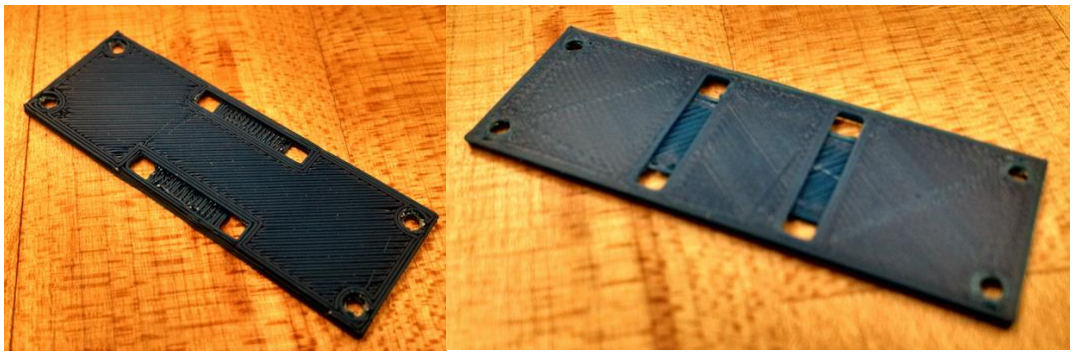

Figure 88: 3D printed layer v1.0

The manufacturing characteristics of the 3D printed layer v1.1 can be seen in Table 80.

Table 80: 3D printing characteristics of 3D printed layer v1.1

Printing Features	3D Printed Layer v1.1
3D printer model	Lulzbot TAZ 5
3D printer cost ($)	2200
Printing mass including raft or brim (g)	3
Additional components (raft of brim)	Brim
Final mass (g)	1
Material	Blue ABS
Material cost ($/Kg)	29
Total cost ($)	0.09
Printing quality	High Detail
Design defects	• None
First component set-up time (min)	8
Printing time (min)	13
Total time (min)	21
Manufacturing defects	• None

Appendix 6: 3D Printed Miniature Linear Guide

This appendix includes detailed information about all the versions of the 3D printed miniature linear guide, including a rail and a guide, that were manufactured during the thesis work. Three versions of the rail were initially designed and can be seen in Figure 89.

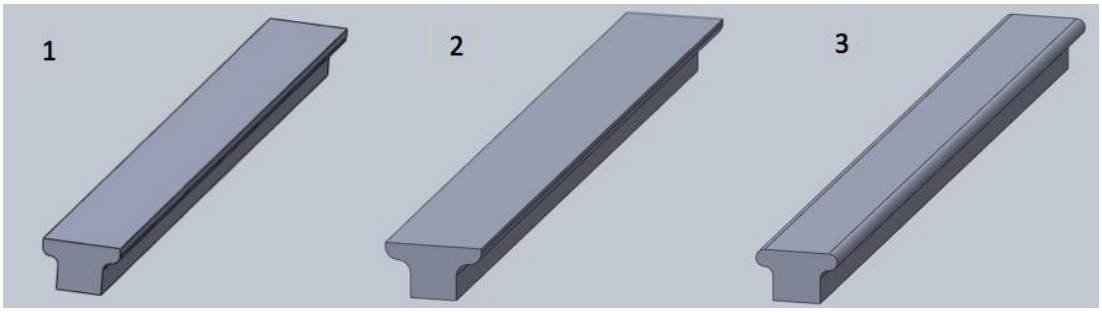

Figure 89: Three designs for the 3D printed harvester rail

Design number 3 (right side image) would be unmanageable to manufacture unless it was 3D printed vertically, which is a very difficult process. Design number 2 (middle image) would have difficulty adapting to a harvester guide due to the reduced height in its protruding part. Then, design 1 (left side image) was considered as the best idea. These harvester rails were denominated as mushroom type rails due to their shape.

Harvester Mushroom Rail v1.0

This rail corresponds to design number 1 of the harvester rail. The 3D printed mushroom rail v1.0 can be identified in Figure 90.

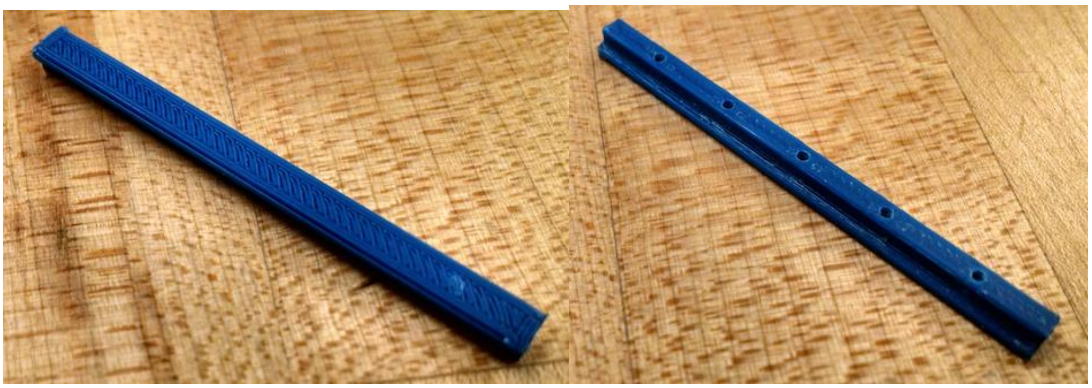

Figure 90: 3D printed mushroom rail v1.0

The manufacturing characteristics of the mushroom rail v1.0 can be seen in Table 81.

Table 81: 3D printing characteristics of harvester mushroom rail v1.0

Printing Features	Mushroom rail v1.0
3D printer model	Lulzbot TAZ 5
3D printer cost ($)	2200
Printing mass including raft or brim (g)	1
Additional components (raft of brim)	Brim
Final mass (g)	1
Material	Blue ABS
Material cost ($/Kg)	29
Total cost ($)	0.03
Printing quality	High Detail
Design defects	• Holes for fasteners in the lower side too deep
First component set-up time (min)	8
Printing time (min)	10
Total time (min)	18
Manufacturing defects	• None

Following the same design process done for the harvester rail, three designs for the harvester guide were created. Each one of the guides was generated to adapt each one of the harvester rails. The selection of design number 1 for the harvester rail concluded with the parallel selection of design number 1 for the harvester guide. The initial guides included a gap where the rail is inserted as well as two additional holes in the upper face of the guide to

attach it to the magnetic cart of the harvester. Figure 91 presents the sketch of the three initial designs.

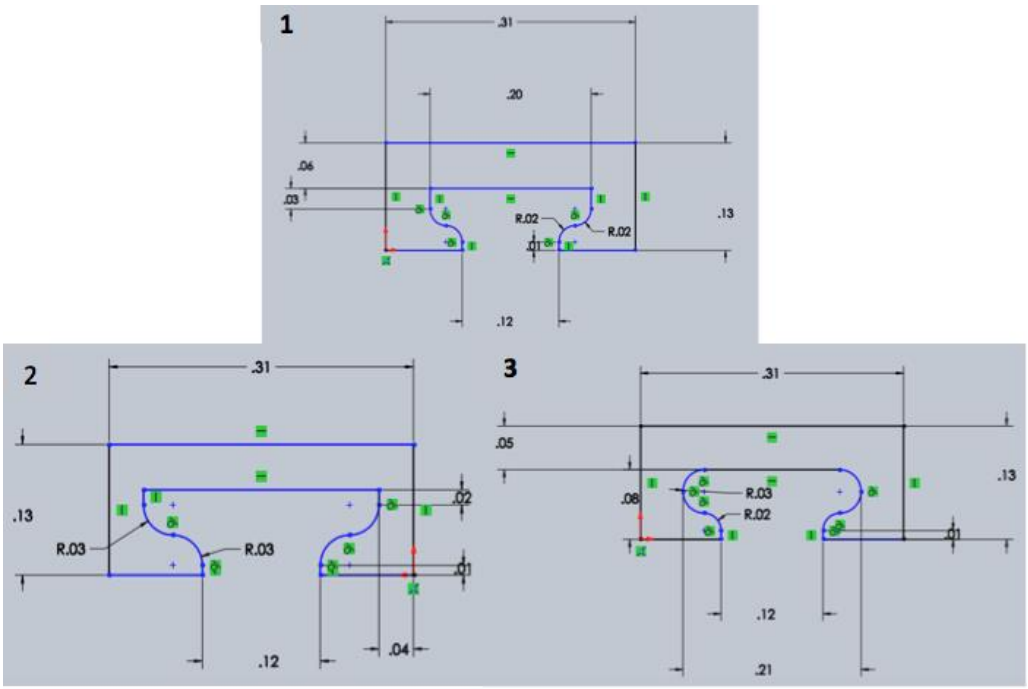

Figure 91: Initial designs for the 3D printed guide of the harvester

Harvester Guide v1.0

An isometric view with the global dimensions of the harvester guide 1.0 can be seen in Figure 92.

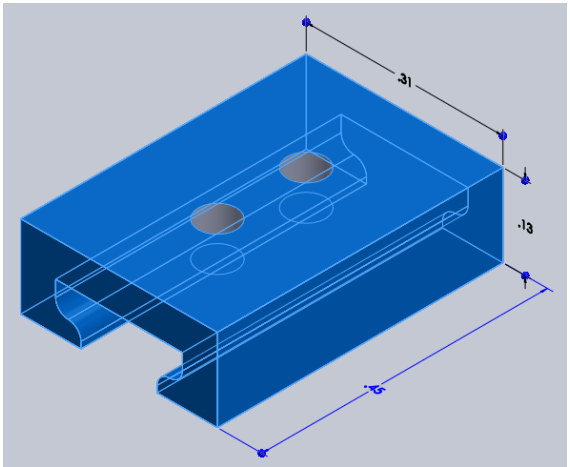

Figure 92: Global dimensions of harvester guide v1.0

An iterative process was done on design number 1, which was denominated as harvester guide v1.0, to obtain the perfect dimensions of the rail gap to adapt to the mushroom rail v1.1 and to the rest of components of the harvester. The 3D printed harvester guide v1.0 can be seen in Figure 93.

Figure 93: 3D printed harvester guide v1.0

The manufacturing characteristics of harvester guide v1.0 can be seen in Table 82.

Table 82: 3D printing characteristics of harvester guide v1.0

Printing Features	Harvester guide v1.0
3D printer model	Lulzbot TAZ 5
3D printer cost ($)	2200
Printing mass including raft or brim (g)	1
Additional components (raft of brim)	Brim
Final mass (g)	1
Material	PLA
Material cost ($/Kg)	48
Total cost ($)	0.05
Printing quality	High Detail
Design defects	• Need to increase the height of the rail gap and reduce its initial width
First component set-up time (min)	8
Printing time (min)	15
Total time (min)	23
Manufacturing defects	• Small amount of material near the upper holes that limit the movement

The tolerances of the rail gap in this guide model were not big enough to fit the rail. The next iteration tried to solve this problem by increasing the length of one of the rail gap dimensions from 0.025” to 0.035” while maintaining the global height of the guide (0.13”) and by decreasing the initial width of it (from 0.12” to 0.115”) to better adapt to the male component. Regarding the holes located in the upper side of the guide, the manufacturing process allocated some extra material around them, limiting the rail/guide movement.

Harvester Guide v1.1

A sketch with the dimensions of the rail gap in the harvester guide v1.1 can be seen in Figure 94.

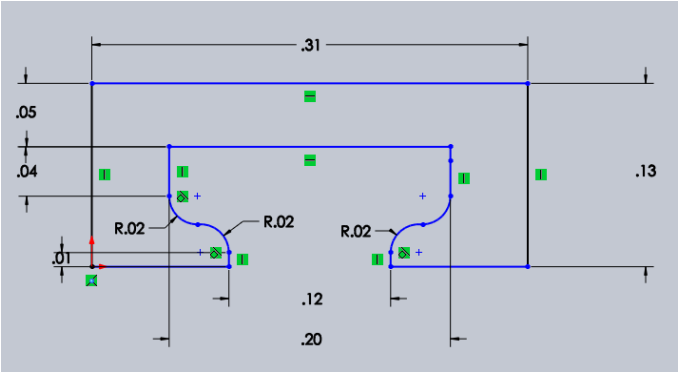

Figure 94: Design of rail gap for harvester guide v1.1

The manufacturing characteristics of the harvester guide v1.1 can be seen in Table 83.

Table 83: 3D printing characteristics of harvester guide v1.1

Printing Features	Harvester guide v1.1
3D printer model	Lulzbot TAZ 5
3D printer cost ($)	2200
Printing mass including raft or brim (g)	1
Additional components (raft of brim)	Brim
Final mass (g)	1
Material	PLA
Material cost ($/Kg)	48
Total cost ($)	0.05
Printing quality	High Detail
Design defects	• Need to increase the height of the rail gap
First component set-up time (min)	8
Printing time (min)	15
Total time (min)	23
Manufacturing defects	• Small amount of material near the upper holes that limit the movement

Harvester Guide v1.2

Harvester guide v1.2 intended to modify the height problem of v1.1 by increasing the length of one of the rail gap dimensions from 0.035” to 0.04” while maintaining the global height of the guide (0.13”). A sketch with the dimensions of the new rail gap can be seen in Figure 95.

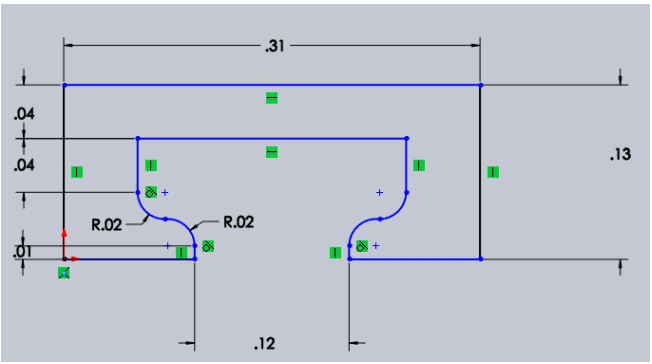

Figure 95: Design of rail gap for harvester guide v1.2

The manufacturing characteristics of the harvester guide v1.2 can be seen in Table 84.

Table 84: 3D printing characteristics of harvester guide v1.2

Printing Features	Harvester guide v1.2
3D printer model	Lulzbot TAZ 5
3D printer cost ($)	2200
Printing mass including raft or brim (g)	1
Additional components (raft of brim)	Brim
Final mass (g)	1
Material	PLA
Material cost ($/Kg)	48
Total cost ($)	0.05
Printing quality	High Detail
Design defects	• None
First component set-up time (min)	8
Printing time (min)	15
Total time (min)	23
Manufacturing defects	• Small amount of material near the upper holes that limit the movement

Harvester Guide v1.3

The design of harvester guide v1.3 deleted the holes located in the upper side of the guide while maintaining the dimensions of v1.2. The manufacturing characteristics of the harvester guide v1.3 can be seen in Table 85.

Table 85: 3D printing characteristics of harvester guide v1.3

Printing Features	Harvester guide v1.3
3D printer model	Lulzbot TAZ 5
3D printer cost ($)	2200
Printing mass including raft or brim (g)	1
Additional components (raft of brim)	Brim
Final mass (g)	1
Material	PLA
Material cost ($/Kg)	48
Total cost ($)	0.05
Printing quality	High Detail
Design defects	• Need to increase the height of the rail gap
First component set-up time (min)	8
Printing time (min)	15
Total time (min)	23
Manufacturing defects	• None

Harvester Guide v1.4

The difference between v1.3 and v1.4 consists of a variation in length of one of the rail gap dimensions from 0.40” to 0.45” while maintaining the global height of the guide. Figure 96 shows a sketch with the dimensions of this new rail gap.

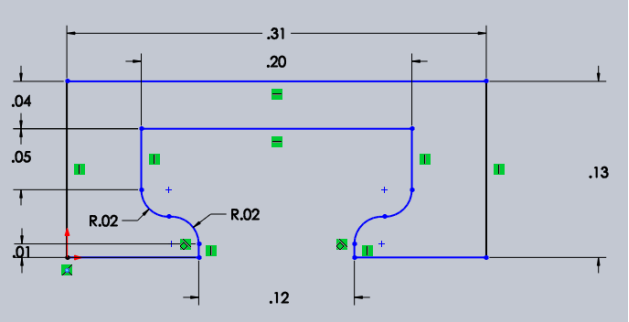

Figure 96: Design of rail gap for harvester guide v1.4

The manufacturing characteristics of the harvester guide v1.4 can be seen in Table 86.

Table 86: 3D printing characteristics of harvester guide v1.4

Printing Features	Harvester guide v1.4
3D printer model	Lulzbot TAZ 5
3D printer cost ($)	2200
Printing mass including raft or brim (g)	1
Additional components (raft of brim)	Brim
Final mass (g)	1
Material	PLA
Material cost ($/Kg)	48
Total cost ($)	0.05
Printing quality	High Detail
Design defects	• Need to increase the width of the rail gap
First component set-up time (min)	8
Printing time (min)	15
Total time (min)	23
Manufacturing defects	• None

Harvester Guide v1.5

The difference between v1.4 and v1.5 consists of a variation in total width of the rail gap from 0.2” to 0.205” while maintaining the global width of the guide. Figure 97 shows a sketch with the dimensions of this new rail gap.

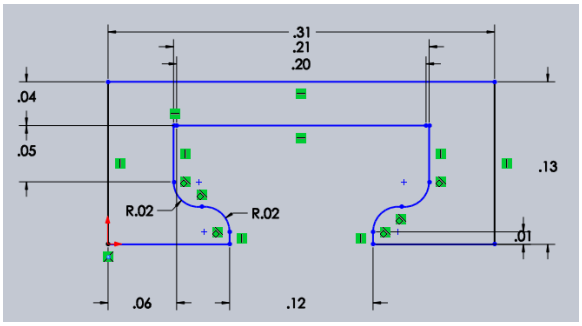

Figure 97: Design of rail gap for harvester guide v1.5

The manufacturing characteristics of the harvester guide v1.5 can be seen in Table 87.

Table 87: 3D printing characteristics of harvester guide v1.5

Printing Features	Harvester guide v1.5
3D printer model	Lulzbot TAZ 5
3D printer cost ($)	2200
Printing mass including raft or brim (g)	1
Additional components (raft of brim)	Brim
Final mass (g)	1
Material	PLA
Material cost ($/Kg)	48
Total cost ($)	0.05
Printing quality	High Detail
Design defects	• None
First component set-up time (min)	8
Printing time (min)	15
Total time (min)	23
Manufacturing defects	• None

Harvester Guide v1.6

This new guide pretended to check if with the evolution of the dimensions from v1.0 to v1.5, the fact of adding back two holes to the upper side of the guide, did not add this time any manufacturing defects. The dimensions of this guide are identical to those of v1.5. The manufacturing characteristics of the harvester guide v1.6 can be seen in Table 88.

Table 88: 3D printing characteristics of harvester guide v1.6

Printing Features	Harvester guide v1.6
3D printer model	Lulzbot TAZ 5
3D printer cost ($)	2200
Printing mass including raft or brim (g)	1
Additional components (raft of brim)	Brim
Final mass (g)	1
Material	PLA
Material cost ($/Kg)	48
Total cost ($)	0.05
Printing quality	High Detail
Design defects	• None
First component set-up time (min)	8
Printing time (min)	15
Total time (min)	23
Manufacturing defects	• Small amount of material near the upper holes that limit the movement

Harvester Guide v2.0

Using the design of the harvester guide v1.5 as departure point, the guide design was modified to include the necessary components of the magnetic cart, this is, magnets, steel plates and bolts. Figure 98 shows the design of the harvester guide v2.0.

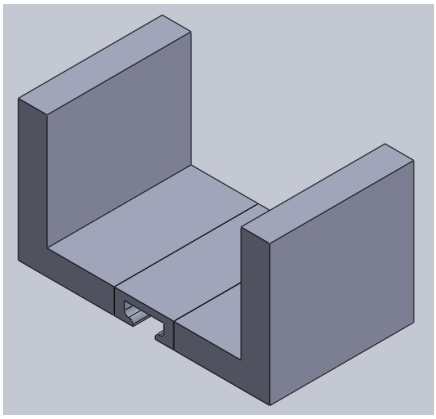

Figure 98: Design of harvester guide v2.0

Two versions of harvester base v2.0 were necessary because in the first attempt (harvester guide v2.0.0) a wrong face was selected as the base for the manufacturing process. In this initial operation the component was printed with the rail gap in a horizontal position, which concluded with the wrong forming of rail gap due to presence of internal material filaments. The second operation (harvester guide v2.0.1) positioned the rail gap in a vertical direction, improving its tolerance, dimensions and finishing. Figure 99 presents the 3D printed guide v2.0.1.

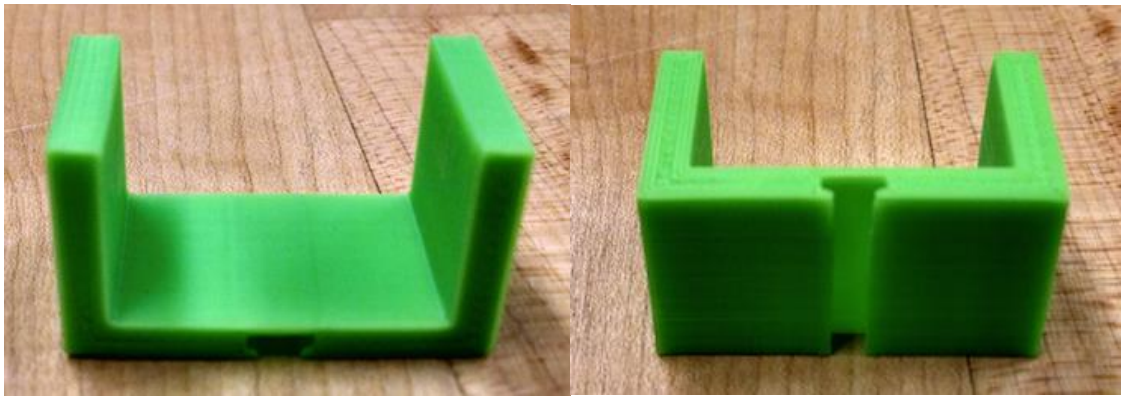

Figure 99: 3D printed harvester guide v2.0.1

The manufacturing characteristics of the harvester guide v2.0.0 and v2.0.1 can be seen in Table 89 and Table 90 respectively.

Table 89: 3D printing characteristics of harvester guide v2.0.0

Printing Features	Harvester guide v2.0.0
3D printer model	Lulzbot TAZ 5
3D printer cost ($)	2200
Printing mass including raft or brim (g)	4
Additional components (raft of brim)	Brim
Final mass (g)	3
Material	Green ABS
Material cost ($/Kg)	19.47
Total cost ($)	0.08
Printing quality	High Detail
Design defects	• Wrong internal dimensions
First component set-up time (min)	8
Printing time (min)	50
Total time (min)	58
Manufacturing defects	• Printing in horizontal direction instead of vertical direction • Wrong forming of rail cavity due to presence of internal material filaments

Table 90: 3D printing characteristics of harvester guide v2.0.1

Printing Features	Harvester guide v2.0.1
3D printer model	Lulzbot TAZ 5
3D printer cost ($)	2200
Printing mass including raft or brim (g)	4
Additional components (raft of brim)	Brim
Final mass (g)	3
Material	Green ABS
Material cost ($/Kg)	19.47
Total cost ($)	0.08
Printing quality	High Detail
Design defects	• Wrong internal dimensions
First component set-up time (min)	8
Printing time (min)	50
Total time (min)	58
Manufacturing defects	• None

Harvester Guide v2.1

The harvester guide v2.1 added lateral holes to the harvester guide v2.0 at both sides of the guide to attach the steel components of the harvester magnetic cart. The internal length, height and width of this guide also differ from v2.0 to adapt to the steel pieces from the original springless vibration energy harvester. The manufacturing characteristics of the harvester guide v2.1 can be seen in Table 91.

Table 91: 3D printing characteristics of harvester guide v2.1

Printing Features	Harvester guide v2.1
3D printer model	Lulzbot TAZ 5
3D printer cost ($)	2200
Printing mass including raft or brim (g)	5
Additional components (raft of brim)	Brim
Final mass (g)	4
Material	Green ABS
Material cost ($/Kg)	19.47
Total cost ($)	0.10
Printing quality	High Detail
Design defects	• Wrong internal width • Wrong height of first row of holes
First component set-up time (min)	8
Printing time (min)	52
Total time (min)	60
Manufacturing defects	• None

Harvester Guide v2.2

The internal width of harvester guide v2.1 was reduced from 1.06” to 1.045” to better adapt the metallic components and to reduce bending when the magnetic cart was assembled. The manufacturing characteristics of the harvester guide v2.2 can be seen in Table 92.

Table 92: 3D printing characteristics of harvester guide v2.2

Printing Features	Harvester guide v2.2
3D printer model	Lulzbot TAZ 5
3D printer cost ($)	2200
Printing mass including raft or brim (g)	5
Additional components (raft of brim)	Brim
Final mass (g)	4
Material	Green ABS
Material cost ($/Kg)	19.47
Total cost ($)	0.10
Printing quality	High Detail
Design defects	• Wrong height of first row of holes
First component set-up time (min)	8
Printing time (min)	52
Total time (min)	60
Manufacturing defects	• None

Harvester Guide v2.3

Harvester guide v2.3 included a new modification with respect to harvester guide v2.2 consisting on decreasing the height of the initial row of holes from 0.22” to 0.213”. This version of the guide was the one used to assemble the magnetic cart installed in the low cost harvester.

Appendix 7: 3D Printed Steel Plates

3D Printed Steel Plates v1.0

The manufacturing characteristics of the 3D printed steel plates v1.0 can be seen in Table 93.

Table 93: 3D printing characteristics of steel plates v1.0

Printing Features	Small steel plate v1.0	Big steel plate v1.0
3D printer model	Lulzbot TAZ 5	Lulzbot TAZ 5
3D printer cost ($)	2200	2200
Printing mass including raft or brim (g)	2	3
Additional components (raft of brim)	Brim	Brim
Final mass (g)	2	3
Material	Green ABS	Green ABS
Material cost ($/Kg)	19.47	19.47
Total cost ($)	0.04	0.06
Printing quality	High Detail	High Detail
Design defects	• Wrong distance between holes • Small hole diameter	• Wrong distance between holes • Small hole diameter • Wrong distance between holes and upper part of component
First component set-up time (min)	8	8
Printing time (min)	21	27
Total time (min)	29	35
Manufacturing defects	• Non ferromagnetic material	• Non ferromagnetic material

3D Printed Steel Plates v1.1

The design defects of v1.0 were corrected in v1.1. The diameter of the holes was increased to 0.08” and the distances between holes were equaled to those of the harvester guide v2.3. The manufacturing characteristics of the 3D printed steel plates v1.1.0 can be seen in Table 94.

Table 94: 3D printing characteristics of steel plates v1.1.0

Printing Features	Small steel plate v1.1.0	Big steel plate v1.1.0
3D printer model	Lulzbot TAZ 5	Lulzbot TAZ 5
3D printer cost ($)	2200	2200
Printing mass including raft or brim (g)	2	3
Additional components (raft of brim)	Brim	Brim
Final mass (g)	2	3
Material	Green ABS	Green ABS
Material cost ($/Kg)	19.47	19.47
Total cost ($)	0.04	0.06
Printing quality	High Detail	High Detail
Design defects	• None	• None
First component set-up time (min)	8	8
Printing time (min)	20	27
Total time (min)	28	35
Manufacturing defects	• Non ferromagnetic material	• Non ferromagnetic material

Using the steel plates v1.1.0 and the harvester guide v2.3 a magnetic cart was built.

Pictures of this magnetic cart can be seen in Figure 100.

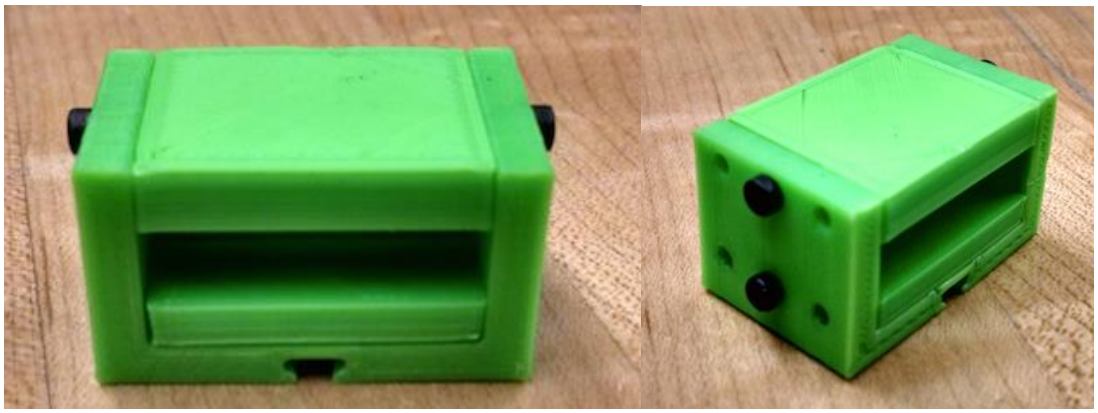

Figure 100: Magnetic cart assembled using steel plates v1.1.0 and guide v2.3

Appendix 8: Cost Analysis

Harvester Base

A cost analysis was carried out for the 3D printing process of the harvester base v1.4, compared to the traditional manufacturing of the base of the springless vibration energy harvester. Table 95 presents the pecuniary and temporal characteristics of the traditional manufacturing of the harvester base using a mill.

Table 95: Time and cost analysis of the traditional manufacturing process of the metallic harvester base

	Traditional Manufacturing		
	Value	Cost	Time
Initial Investment ($)	-	25000	-
Aluminum 6061 Price ($/ft)*	-	2.11	-
Aluminum 6061 (g)	17.82	-	-
Aluminum 6061Total Price ($)	-	0.422	-
Lexan Unitary Price ($/inch)*	-	5.06	-
Lexan Mass (g)	4.18	-	-
Lexan Total Price ($)	-	0.14	-
Unitary Machining Operator Price ($/hour)	-	18	-
Manufacturing Time (min)	-	-	360*
Assembly Time (min)	-	-	9
Total Operator Time (min)	-	-	369
Total Operator Cost ($)	-	110.7	-
Final Base Mass (g)	22	-	-
Total Time (min)	-	-	369
Total Cost per Component ($)	-	111.26	-
Total Cost With Initial Investment ($)	-	25111.26	-

NOTE: the total manufacturing time was estimated using expert machinist advice. The shape of aluminum considered was 3/16” thick, 1.25” wide and 1/2'sheet. Instead of Lexan, a similar material was used. This material is impact resistant Styrene square sheet with dimensions 6”x6” and 0.5” thick.

The total time and cost were calculated as:

$$\boldsymbol{Total\ time\ (min) = Manufacturing\ Time\ (min) + Assembly\ Time\ (min)}$$

$$\boldsymbol{Total\ cost}\ (\$) = \frac{\boldsymbol{Total\ Operator\ Time\ (min) \times Unitary\ Machining\ Operator\ Price\ (\$/hour)}}{\boldsymbol{60}} + \boldsymbol{Material\ Cost}\ (\$)$$

Table 96 presents the pecuniary and temporal characteristics of the 3D printing process of harvester base v1.4.

Table 96: Time and cost analysis of the 3D printing process of the harvester base v1.4

	3D Printing Base v1.4		
	Value	Cost	Time
Initial Investment ($)	-	2200	-
Set-up Time (min)	-	-	8
Blue ABS Unitary Price ($/kg)	-	29	-
Blue ABS Mass (g)	9	-	-
Blue ABS Total Price ($)	-	0.26	-
Unitary Machining Operator Price ($/hour)	-	18	-
Manufacturing Time (min)	-	-	76
Assembly Time (min)	-	-	9
Total Operator Time (min)	-	-	93
Total Operator Cost ($)	-	27.9	-
Final Base Mass (g)	7	-	-
Total Time (min)	-	-	93
Total cost per component ($)	-	28.16	-
Total cost with initial investment ($)	-	2228.16	-

Where the total time and cost were calculated as:

$$\boldsymbol{Total\ Time\ (min) = Manufacturing\ Time\ (min) + Assembly\ Time\ (min) + Setup\ Time\ (min)}$$

$$\boldsymbol{Total\ cost}\ (\$) = \frac{\boldsymbol{Total\ Operator\ Time\ (min) \times Unitary\ Machining\ Operator\ Price\ (\$/hour)}}{\boldsymbol{60}} + \boldsymbol{Material\ Cost}\ (\$)$$

It can be seen in the previous tables that the cost of traditional manufacturing is almost 4 times as expensive as the 3D printing. In terms of time, traditional manufacturing is also almost 4 times as long as the 3D printing. Then it can be concluded that replacing traditional construction processes by rapid prototyping, 3D printing in particular, is a very rentable time and moneywise manufacturing alteration.

Miniature Linear Guide

Cost analysis shows that comparing the original miniature linear guide (metallic rail and guide) by the 3D printed mushroom rail and the guide, a savings of $55 is obtained. This is considering the price of the metallic miniature linear guide, which is $80. The manufacturing and shipping times of the miniature linear guide are not known. The time and cost analysis of the 3D printing manufacturing process to obtain the mushroom rail v1.1 can be seen in Table 97.

Table 97: 3D printing time and cost analysis of mushroom rail v1.1

	3D Printing Mushroom Rail v1.1		
	Value	Cost	Time
Initial Investment ($)	-	2200	-
Set-up Time (min)	-	-	8
Green ABS Unitary Price ($/kg)	-	19.47	-
Green ABS Mass (g)	1	-	-
Green ABS Total Price ($)	-	0.02	-
Unitary Machining Operator Price ($/hour)	-	18	-
Manufacturing Time (min)	-	-	15
Total Operator Time (min)	-	-	23
Total Operator Cost ($)	-	6.9	-
Final Base Mass (g)	1	-	-
Total Time (min)	-	-	23
Total cost per component ($)	-	6.92	-
Total cost with initial investment ($)	-	2206.92	-

The time and cost analysis of the 3D printing manufacturing process to obtain the guide v2.3 can be seen in Table 98.

Table 98: 3D printing time and cost analysis of guide v2.3

	3D Printing Guide v2.3		
	Value	Cost	Time
Initial Investment ($)	-	2200	-
Set-up Time (min)	-	-	8
Green ABS Unitary Price ($/kg)	-	19.47	-
Green ABS Mass (g)	5	-	-
Green ABS Total Price ($)	-	0.10	-
Unitary Machining Operator Price ($/hour)	-	18	-
Manufacturing Time (min)	-	-	52
Total Operator Time (min)	-	-	60
Total Operator Cost ($)	-	18	-
Final Base Mass (g)	4	-	-
Total Time (min)	-	-	60
Total cost per component ($)	-	18.10	-
Total cost with initial investment ($)	-	2218.10	-

Where the total time and cost were calculated as:

$$\boldsymbol{Total\ Time}\ (\boldsymbol{min}) = \boldsymbol{Manufacturing\ Time}\ (\boldsymbol{min}) + \boldsymbol{Setup\ Time}\ (\boldsymbol{min})$$

$$\boldsymbol{Total\ cost}\ (\$) = \frac{\boldsymbol{Total\ Operator\ Time}\ (\boldsymbol{min}) \times \textbf{Unitary Machining Operator Price}\ (\$/\textbf{hour})}{\mathbf{60}} + \boldsymbol{Material\ Cost}\ (\$)$$

Then combining the time and cost of the mushroom rail v1.1 and the guide v2.3, the final cost and time of the 3D printed miniature linear guide can be obtained. These values can be seen in Table 99.

Table 99: Time and cost analysis of 3D printed miniature linear guide

	3D Printed Miniature Linear Guide
Total Time (min)	83
Total cost per component ($)	25.02

These results show that from a pure economic perspective, 3D printing the miniature linear guide can save around $55. Considering production time, the advantage of 3D printing these components is incommensurable because just the shipping period of a metallic miniature linear guide can be higher than a week.

Steel Plates

The total cost and time of manufacturing the big and small steel plates will be analyzed altogether. Table 100 shows the estimated cost and time analysis for traditional manufacturing the steel plates.

Table 100: Traditional manufacturing time and cost of steel plates

	Traditional Manufacturing		
	Value	Cost	Time
Initial Investment ($)	-	25000	-
1215 Carbon Steel Price ($/ft)*	-	12.05	-
1215 Carbon Steel Mass (g)	41	-	-
1215 Carbon Steel Total Price ($)	-	1.00	-
Unitary Machining Operator Price ($/hour)	-	18	-
Manufacturing Time (min)	-	-	600*
Total Operator Time (min)	-	-	600
Total Operator Cost ($)	-	180	-
Final Base Mass (g)	41	-	-
Total Time (min)	-	-	369
Total Cost per Component ($)	-	181.00	-
Total Cost With Initial Investment ($)	-	25181.00	-

NOTE: the total manufacturing time was estimated using expert machinist advice. The shape of steel considered is a 1” square bar (around 12 steel parts can be obtained per feet of this material).

The total time and cost were calculated as:

$$\boldsymbol{Total\ time}\ (\boldsymbol{min}) = \boldsymbol{Manufacturing\ Time}\ (\boldsymbol{min})$$

$$\boldsymbol{Total\ cost}\ (\$) = \frac{\boldsymbol{Total\ Operator\ Time}\ (\boldsymbol{min}) \times \textbf{Unitary Machining Operator Price}\ (\$/\textbf{hour})}{\textbf{60}} + \boldsymbol{Material\ Cost}\ (\$)$$

The time and cost analysis of the 3D printing manufacturing process to obtain the steel plates v1.1.1 can be seen in Table 101.

Table 101: 3D printing time and cost of steel plates v1.1.1

	3D Printing Steel Plates v1.1.1		
	Value	Cost	Time
Initial Investment ($)	-	2200	-
Set-up Time (min)	-	-	16
Magnetic Iron PLA Unitary Price ($/kg)	-	69.98	-
Magnetic Iron PLA Mass (g)	11	-	-
Magnetic Iron PLA Total Price ($)	-	0.77	-
Unitary Machining Operator Price ($/hour)	-	18	-
Manufacturing Time (min)	-	-	60
Total Operator Time (min)	-	-	76
Total Operator Cost ($)	-	22.8	-
Final Parts Mass (g)	11	-	-
Total Time (min)	-	-	76
Total cost per component ($)	-	23.57	-
Total cost with initial investment ($)	-	2223.57	-

Where the total time and cost were calculated as:

$$\boldsymbol{Total\ Time}\ (\boldsymbol{min}) = \boldsymbol{Manufacturing\ Time}\ (\boldsymbol{min}) + \boldsymbol{Setup\ Time}\ (\boldsymbol{min})$$

$$\boldsymbol{Total\ cost}\ (\$) = \frac{\boldsymbol{Total\ Operator\ Time}\ (\boldsymbol{min}) \times \textbf{Unitary Machining Operator Price}\ (\$/\textbf{hour})}{\textbf{60}} + \boldsymbol{Material\ Cost}\ (\$)$$

Regarding the economic aspect, traditional manufacturing the steel plates cost almost 8 times more than 3D printing them. In terms of time traditional manufacturing the steel plates takes almost 5 times more than 3D printing them.

Fully 3D Printed Harvester

Some assumptions were considered when generating the cost of the fully 3D printed harvesters:

- The price of the coil wrapped around the 3D printed layer is neglected
- The cost and time of the 3D printed layer v1.1 is used even if this is not the component used during the tests. Similar values can be expected for the original 3D printed layer
- The maximum possible number of bolts is used even if some of them are not used in the construction and testing
- Springs v2 were purchased in packs of 6 at $5.01

Also, the unitary price of the bolts used in the assembly of the fully 3D printed harvesters can be seen in Table 102.

Table 102: Unitary price of bolts used in fully 3D printed harvesters

	Thread	Box price ($)	Amount	Unitary price ($)
Base bolts	#0-80	3.24	50	0.0648
3D printed layer bolts	#2-56	6.52	100	0.0652
Guide bolts	#1-72	4.4	50	0.088

References

[1] F. Cottone. Introduction to Vibration Energy Harvesting. NiPS Energy Harvesting Summer School August 1-5, 2011.

[2] Z. Li, L. Zuo, G. Luhrs, L. Lin, and Y. -X Qin. Electromagnetic Energy-Harvesting Shock Absorbers: Design, Modeling, and Road Tests. IEEE TRANSACTIONS ON VEHICULAR TECHNOLOGY, VOL. 62, NO. 3, MARCH 2013.

[3] P. Glynne-Jones, M.J. Tudor, S.P. Beeby and N.M. White. An electromagnetic, vibration-powered generator for intelligent sensor systems. Sensors and Actuators, A 110, (2004), pp. 344–349.

[4] B. -C Lee and G. -S Chung. Frequency tuning design for vibration-driven electromagnetic energy harvester. ET Renew. Power Gener., 2015, Vol. 9, Iss. 7, pp. 801–808.

[5] J. T. Cheung, Childress, E. F. III Childress. Ocean Wave Energy Harvesting Devices. Contract No. HRO01 1-06-C-0030, April 2007.

[6] X. Tang and L. Zuo. Simultaneous energy harvesting and vibration control of structures with tuned mass dampers. Journal of Intelligent Material Systems and Structures 23(18), pp. 2117-2127.

[7] Eric Carl Dierks. Design of an Electromagnetic Vibration Energy Harvester for Structural Health Monitoring of Bridges Employing Wireless Sensor Networks. 2011.

[8] F. U. Khan and I. Ahmad. Vibration-based Electromagnetic type Energy Harvester for Bridge Monitoring Sensor Application. IEEE, 2014.

[9] C.R. Saha, T. O'Donnell, N. Wang and P. McCloskey. Electromagnetic generator for harvesting energy from human motion. Sensors and Actuators, A 147 (2008), pp. 248–253.

[10] H. Liu, S.Gudla, F. A.Hassani, C. H.Heng, Y.Lian and C. Lee. Investigation of the Nonlinear Electromagnetic Energy Harvesters From Hand Shaking. IEEE SENSORS JOURNAL, VOL. 15, NO. 4, APRIL 2015, pp 2356-2364.

[11] M. A. Halim and J. Y. Park. Modeling and experiment of a handy motion driven, frequency up-converting electromagnetic energy harvester using transverse impact by spherical ball. Sensors and Actuators A 229 (2015), pp. 50–58.

[12] E. Shahhaidar, B. Padasdao, R. Romine, C. Stickley and O. Boric-Lubecke. Piezoelectric and Electromagnetic Respiratory Effort Energy Harvesters. 35th Annual International Conference of the IEEE EMBS Osaka, Japan, 3 - 7 July, 2013.

[13] W. Chen, Y. Cao and J. Xie. Piezoelectric and electromagnetic hybrid energy harvester for powering wireless sensor nodes in smart grid. Journal of Mechanical Science and Technology, 29 (10) (2015), pp. 4313-4318.

[14] P. Li, S. Gao, H. Cai and L. Wu. Theoretical analysis and experimental study for nonlinear hybrid piezoelectric and electromagnetic energy harvester. Microsyst. Technol.

[15] J. Qiu, X. Liu, H. Chen, X. Xu, Y. Wen, and P. Li. A Low-Frequency Resonant Electromagnetic Vibration Energy Harvester Employing the Halbach Arrays for Intelligent Wireless Sensor Networks. IEEE TRANSACTIONS ON MAGNETICS, VOL. 51, NO. 11, NOVEMBER 2015.

[16] D. Mallicka and S. Roy. An Electrically Tunable Low Frequency Electromagnetic Energy Harvester. Procedia Engineering, 87 (2014), pp. 771 – 774.

[17] J. Ding, V. R. Challa, M. G. Prasad and F. T. Fisher. Vibration Energy Harvesting and Its Application for Nano- and Microrobotics. Y. Guo (ed.). *Selected Topics in Micro/Nano-Robotics for Biomedical Applications.*

[18] L. Wang and F. G. Yuan. Vibration energy harvesting by magnetostrictive material. Smart Mater. Struct. 17 (2008)(14pp)

[19] L. Wang. Vibration Energy Harvesting by Magnetostrictive Material for Powering Wireless Sensors. 2007, thesis dissertation.

[20] F.Khan, F. Sassani and B. Stoeber. Nonlinear behavior of membrane type electromagnetic energy harvester under harmonic and random vibrations. Microsyst. Technol. (2014) 20, pp. 1323–1335.

[21] P. Patel and M. B.Khamesee. Electromagnetic micro energy harvester for human locomotion. Microsyst. Technol., (2013) 19, pp. 1357–1363.

[22] B. S. Joyce. Development of an Electromagnetic Energy Harvester for Monitoring Wind Turbine Blades. December 12, 2011.

[23] G. Hatipoglua and H. Urey. FR4-based electromagnetic energy harvester for wireless tyre sensor nodes. Procedia Chemistry 1, (2009), pp. 1211–1214.

[24] X. Wu and D. -W. Lee. An electromagnetic energy harvesting device based on high efficiency windmill structure for wireless forest fire monitoring application. Sensors and Actuators A 219 (2014), pp. 73–79.

[25] S. Moss, J. McLeod, I. Powlesland and S.Galea. Bi-axial Vibration Energy Harvesting. July 2012.

[26] S.P. Beeby1, R.N. Torah1, M.J. Tudor1, T. O'Donnell2 and S. Roy. Wireless sensor system powered by an electromagnetic vibration energy harvester. Measurement + Control Vol 41/4 May 2008, pp. 109-113.

[27] L. Tang, Y. Yang, and C.Kiong So. Broadband Vibration Energy Harvesting Techniques. N. Elvin and A. Erturk (eds.). *Advances in Energy Harvesting Methods*.

[28] B. L. Ooi, J. M. Gilbert, A. Rashid and A. Aziz. Switching damping for a frequency-tunable electromagnetic energy harvester. Sensors and Actuators A 234 (2015), pp. 311–320.

[29] P. D. Mitcheson, T. T. Toh, K. H. Wong, S. G. Burrow and A. S. Holmes. Tuning the Resonant Frequency and Damping of an Electromagnetic Energy Harvester Using Power Electronics. IEEE TRANSACTIONS ON CIRCUITS AND SYSTEMS—II: EXPRESS BRIEFS, VOL. 58, NO. 12, DECEMBER 2011.

[30] B. –C. Lee and G. –S. Chung. Frequency tuning design for vibration-driven electromagnetic energy harvester. IET Renew. Power Gener., 2015, Vol. 9, Iss. 7, pp. 801–808.

[31] H. Liu, Y. Qian, N. Wang and C. Lee. An In-Plane Approximated Nonlinear MEMS Electromagnetic Energy Harvester. JOURNAL OF MICROELECTROMECHANICAL SYSTEMS, VOL. 23, NO. 3, JUNE 2014.

[32] M. S. M. Soliman, E. M. Abdel-Rahman, E. F. El-Saadany, and R. R. Mansour. A wideband vibration-based energy harvester. J. Micromech. Microeng., vol. 18, no. 11, p. 115021, 2008.

[33] M. Bendame. Springless Electromagnetic Vibration Energy Harvesters.

[34] D. S. Nguyen, E. Halvorsen, G. U. Jensen, and A. Vogl. Fabrication and characterization of a wideband MEMS energy harvester utilizing nonlinear springs. J. Micromech. Microeng., vol. 20, no. 12, p. 125009, 2010.

[35] A. Riduan, M. Foisala, C. Hongb and G. –S. Chung. Multi-frequency electromagnetic energy harvester using a magnetic spring cantilever. Sensors and Actuators A 182 (2012), pp. 106–113.

[36] P. Wang, K. Tanaka, S. Sugiyama, X. Dai, X. Zhao and J. Liu. A micro electromagnetic low level vibration energy harvester based on MEMS technology. Microsyst. Technol. (2009) 15, pp. 941–951.

[37] J. Chen, D. Chen, T. Yuan and X. Chen. A multi-frequency sandwich type electromagnetic vibration energy harvester. APPLIED PHYSICS LETTERS 100, 213509 (2012).

[38] M. Han, Z. Li, X. Sun and H. Zhang. Analysis of an in-plane electromagnetic energy harvester with integrated magnet array. Sensors and Actuators A 219 (2014), pp. 38–46.

[39] M. Han, G. Qiu, W. Liu, B. Meng, X. –S. Zhang, and H. Zhang. Note: A cubic electromagnetic harvester that convert vibration energy from all directions. Review of Scientific Instruments 85, 2014.

[40] T. Shirai, Y. Wakasa, T. Nakagawa, K. Nomura, and H. Yagyu. Electromagnetic Energy Harvester With High Efficiency Using Micro-machining Si Springs. MEMS 2014, San Francisco, CA, USA, January 26 - 30, 2014.

[41] P.Poddera, A.Amannb and S. Roy. FR4 based bistable electromagnetic vibration energy harvester. Procedia Engineering 87 (2014), pp. 767 – 770.

[42] N. G. Elvin and A. A. Elvin. An experimentally validated electromagnetic energy harvester. Journal of Sound and Vibration 330 (2011), pp. 2314–2324.

[43] C.B.Williams, C.Shearwood, M.A.Harradine, P.H. Mellor, T.S.Birch and R.B.Yates. Development of an electromagnetic micro-generator. IEE Proc.-Circuits Devices Syst., Vol 148, No. 6, December 2001.

[44] Q. Zhang and E. S. Kim. Microfabricated Electromagnetic Energy Harvesters With Magnet and Coil Arrays Suspended by Silicon Springs. IEEE Sensors Journal, Vol. 16, No. 3, FEBRUARY 1, 2016, pp. 634-641.

[45] X. Liu, J. Qiu, H. Chen, X. Xu, Y. Wen, and P. Li. Design and Optimization of an Electromagnetic Vibration Energy Harvester Using Dual Halbach Arrays. IEEE TRANSACTIONS ON MAGNETICS, VOL. 51, NO. 11, NOVEMBER 2015.

[46] D. Zhu, S. Beeby, J. Tudor and N. Harris. Increasing output power of electromagnetic vibration energy harvesters using improved Halbach arrays. Sensors and Actuators A 203 (2013), pp. 11–19.

[47] S. E. Jo, M. S. Kim and Y. J. Kim. Electromagnetic human vibration energy harvester comprising planar coils. ELECTRONICS LETTERS 5th July 2012 Vol. 48 No. 14.

[48] M. Yilmaz, B. A. Tunkar, S. Park, K.Elrayes, M. A. E. Mahmoud, E. Abdel-Rahman, and M.Yavuz. High-efficiency passive full wave rectification for electromagnetic harvesters. JOURNAL OF APPLIED PHYSICS 116, 134902 (2014) , pp 1-8.

[49] M.Zucca and O.Bottauscio . Hysteretic Modeling of Electrical Micro-Power Generators Based on Villari Effect . IEEE TRANSACTIONS ON MAGNETICS, VOL. 48, NO. 11, NOVEMBER 2012. Pp 3092-3095.

[50] M.A. Halim and J.Y. Park. Optimization of a Human-Limb Driven, Frequency Up-Converting Electromagnetic Energy Harvester for Power Enhancement. Transducers 2015, Anchorage, Alaska, USA, June 21-25, 2015.